Effects of Curing Agents and Drilling Methods on CAF Formation in Halogen-Free Laminates

by

Lok Si Chan

A thesis
presented to the University of Waterloo
in fulfillment of the
thesis requirement for the degree of
Master of Applied Science
in
Mechanical Engineering

Waterloo, Ontario, Canada, 2011

AUTHOR'S DECLARATION

I hereby declare that I am the sole author of this thesis. This is a true copy of the thesis, including any required final revisions, as accepted by my examiners.

I understand that my thesis may be made electronically available to the public.

Abstract

Increasing demands for more reliability and functionalities in electronic devices have pushed the electronics industry to adopt newly developed materials and reduce interconnect sizes and spacing. These adaptations have led to concerns of reliability failures caused by conductive anodic filament formation (CAF). CAF is a conductive copper-containing salt that forms via an electrochemical process. It is initiated at the anode and grows along the epoxy/glass interface to the cathode, and once CAF reaches the cathode a short circuit will occur.

The objective of this research is to evaluate and compare the effects of curing agents (DICY vs. phenolic-cured epoxy) and drilling methods (laser vs. mechanical drilling) on CAF formation using an insulation resistance test at 85 ºC, relative humidity of 85%, and a voltage gradient of 0.4V/μm.

Time-to-failure for DICY-cured and phenolic-cured epoxy with laser drilled microvias and mechanically drilled vias were determined using the insulation resistance test. The failed coupons were cross-sectioned and examined using a Scanning Electron Microscope equipped with Energy-dispersive X-ray spectroscopy to verify the existence of CAF. Weibull analysis was used to compare the reliability and identify the failure modes of the failed coupons.

Test results show that DICY-cured epoxy is a better CAF resistant material than phenolic-cured epoxy. It is believed that the brittleness of phenolic-cured material might enhance the damage to the epoxy/glass fiber interface during drilling; and hence, facilitate subsequent CAF formation.

The study also shows that laser drilled microvias are less prone to CAF formation than mechanically drilled vias, because there is less mechanical damage and lower glass fiber content. Finally, using Weibull analysis, it is determined that laser drilled microvias experienced infant-mortality failure, whereas mechanically drilled vias exhibited a wear-out type failure.

Acknowledgements

First and foremost I offer my sincerest gratitude to my supervisors, Dr. Laura Turbini and Dr. Y. Norman Zhou, for their kindness, patient, encouragement, guidance, support, time, and generosity from the initial NSERC application to the final edition of this thesis.

I am also heartily thankful and will treasure my friendship with the great people, Andrew Michael, Andrew Ryzynski, Bev Christian, Darryl Bake, Deepchand Ramjattan, Gus Rinella, Irina Romanova, Ryan Hu, and Valente Buendia, who I have worked with at Research In Motion. These amazing people have spent their time, provided guidance and assistance when I most needed them during the two years of my research.

Last but not least, I would like to thank the other staff members from the Materials Interconnect Lab at Research In Motion, and the members at the Centre for Advanced Materials Joining (CAMJ) at the University of Waterloo for all their contributions to this project.

Financial contributions to this research projects from both the Natural Science and Engineering Research Council of Canada (NSERC) Industrial Postgraduate Scholarship and Research in Motion Ltd. are acknowledged.

Table of Contents

Chapter 3 Experimental Procedures

Chapter 4 Results

List of Figures

Chapter 1 Introduction

Chapter 2 Literature Review

Chapter 3 Experimental Procedures

Chapter 4 Results

Chapter 5 Discussion and Conclusion

List of Tables

Chapter 1 Introduction

Chapter 2 Literature Review

Chapter 3 Experimental Procedures

Chapter 4 Results

Chapter 5 Discussion and Conclusion

List of Acronyms

a.k.a…….	Also known as
AC……...	Alternating current
BMDV….....	Buried mechanically drilled vias
BT…….....	Bismaleimide triazine
CALCE….....	Center for Advanced Life Cycle Engineering
CAF…….	Conductive anodic filament
cdf…….....	Cumulative distribution function
CE…….....	Cyanate esters
CTE…….	Coefficient of thermal expansion
DC…….....	Direct current
DICY…….....	Dicyandiamide
EDX…….	Energy-dispersive X-ray spectroscopy
EU……	European Union
FTIR……	Fourier transform infrared spectroscopy (FTIR)
HAST…….....	Highly accelerated stress test
HDI…….....	High density interconnect
HF……	Halogen-free
H-H…….....	Hole-to-hole
H-L…….....	Hole-to-line
IST……...	Interconnect Stress Test
LC……	Linear circuit
LF……	Lead-free
L-H…….....	Line-to-hole
L-L……...	Line-to-line
MTTF…….....	Mean-time-to-failure
MR……...	Median rank
OEM……	Original equipment manufacturer
PBBs……	Polybrominated biphenyls
PBDEs…….	Polybrominated diphenyl ether
PCB…….	Printed circuit board
PTH…….....	Plated through hole
PWB……	Printed wiring boards
RH……...	Relative humidity
RoHS……...	Restriction of Hazardous Substances
SAC…….....	Sn-Ag-Cu
SEM…….....	Scanning Electron Microscopy
SLDM…….....	Surface laser drilled microvias
SQUID…….	Superconducting quantum interference device
t_B…….	Bias time
t_M……	Measurement time
TBBA……...	Tetrabromobisphenol A
TEM…….	Transmission Electron Microscopy
T_g……..	Glass transition temperature

THB……. Temperature, humidity, bias
UV ……... Ultra violet

Chapter 1

Introduction

This chapter will briefly introduce the current trends in the electronics industry, the process of manufacturing printed circuit boards (PCBs), the interconnect drilling methods, and a short introduction to conductive anodic filament (CAF). Finally, the objective of this research will be stated.

1.1 Current trend in the electronic industry

The electronics industry is a fast-paced and highly competitive industry. Customers are always demanding lighter weight, more reliability, higher speed, more functionalities, but less environmental impact from their devices. In order to fulfill these demands, electronic industries have been emphasizing the development of lightweight and environmentally friendly materials that are water/chemical resistant and have better thermal, mechanical, and electrical properties in highly compact circuitry.

A few approaches such as lead-free (LF) soldering, the substitution of halogen-free (HF) flame retardant materials for brominated PCBs, and minimizing conductor size and spacing have been used. Unfortunately, these supposedly "green" products are not always that "green" and possess reliability issues such as delamination, warpage, cracked solder joints, and conductive anodic filament formation (CAF) which end up destroying products and wasting materials.

Since 1 July 2006, the European Union (EU) has implemented the Restriction of Hazardous Substances (RoHS) Directive [1, 2] to restrict the use of six hazardous materials; namely lead (Pb), mercury (Hg), cadmium (Cd), hexavalent chromium (Cr(VI)), polybrominated biphenyls (PBBs), and polybrominated diphenyl ethers (PBDEs). The first restriction eliminated the use of lead-containing solder (eg. SnPb) in the affected electronic products. [3] This solder is being replaced by lead-free solder such as Sn-Ag-Cu alloys (SAC).

Unfortunately, this new LF soldering process is controversial as it requires a higher processing temperature which raises concerns about the reliability of devices. [4]

Moreover, several studies [5, 6] have shown that there is little or no benefit to the environment by switching to LF soldering.

Due to the concern of releasing toxic chemicals such as dioxins and furans during improper incineration of bromine-contained materials (eg. PBBs and PBDEs), many companies have voluntarily chosen to adopt the use of halogen-free (HF) epoxy. [3]

In fact, on the IPC website, it has claimed that there is rarely any hazardous PBBs or PBDEs used in electronic products nowadays. Most of the bromine-containing PCBs contain some other effective bromine-contained flame retardant materials such as tetrabromobisphenol-A (TBBPA) that has insignificant impact on health and environment. [7, 8] Nonetheless, in order to be perceived as a "green" company, Greenpeace (www.greenpeace.org/international) has pushed some large electronic companies to substitute traditional brominated flame retardants with HF flame retardants in PCBs.

The commonly used HF materials are metal hydroxides such as aluminum and magnesium hydroxides and/or phosphorus doped or nitrogen doped epoxy. [9] These newly developed materials are required to have good thermal stability, in order to sustain the high processing temperatures during LF soldering. Sometimes SiO_2 is added to the epoxy to reduce the thermal expansion during the soldering process. [10]

Finally, in order to fulfill the market demands for a device that could achieve many tasks, the circuitry design must be more compact and sophisticated. Some of the methods include the reduction in the size of interconnects and the spacing between conductors, and the fabrication of thinner laminates at the same time as increasing the layer count (defined by the number of copper layers in a PCB), etc.

Traditionally, the interconnects were achieved by mechanical drilling; however, as the size of vias has become so small, a more precise and efficient drilling method is required. For example, the IPC Technology Roadmap has projected the size of a via will be reduced to 100 μm and hole-to-hole distance to 250 μm by 2012/2016. [11] A promising solution using laser drilling has been proven to be cost effective at high via count and provides precise and good quality microvias down to 50 μm. However, there is a little understanding how this new processing method will affect the reliability of PCBs.

In summary, due to environmental concerns, lead-free soldering and halogen-free materials have been widely adopted. Moreover, laser drilling is becoming popular for producing precise and high quality microvias for high density circuitry. Nonetheless, studies are necessary to evaluate the reliability of PCBs due to the adoption of these new processing, materials, and drilling methods.

1.2 PCB manufacturing process

The PCB manufacturing process is a repetitive process that requires lamination, patterning, drilling, and copper deposition. First, B-stage resin (a.k.a prepreg, which is a partially cured epoxy layer) is formed. This step requires a mixture of epoxy resin (A-stage) that contains additives such as curing agents, flame retardants, and woven glass fibers with coupling agents for better binding of glass fibers to epoxy. [12, 13]

Once the prepreg is cured, copper foil is laid on top of the prepreg and laminated at an elevated temperature to form a C-stage resin which is also called the core laminate of a PCB. The copper foil is patterned using photo-resist material, which is a process known as the subtractive method. After exposure to UV light (200 – 500 nm), the copper that is covered with photo-resist will be protected from the subsequent etching solution and the copper that does not have photo-resist applied will be etched away. [14]

Holes are then drilled through the copper/laminate mechanically or using a laser. These holes are made conductive by plating copper using an electroless process, followed by electroplating of Cu. [15]

The lamination, patterning, drilling, and copper deposition steps are repeated in order to make a multi-layer PCB. Once all the layers are formed, a solder mask is then applied to protect the copper traces on the PCB from oxidation, contamination, and other physical damage. Figure 1-1 illustrates the general structural components such as patterned copper, solder mask, laminate and drilled holes in a PCB. [12]

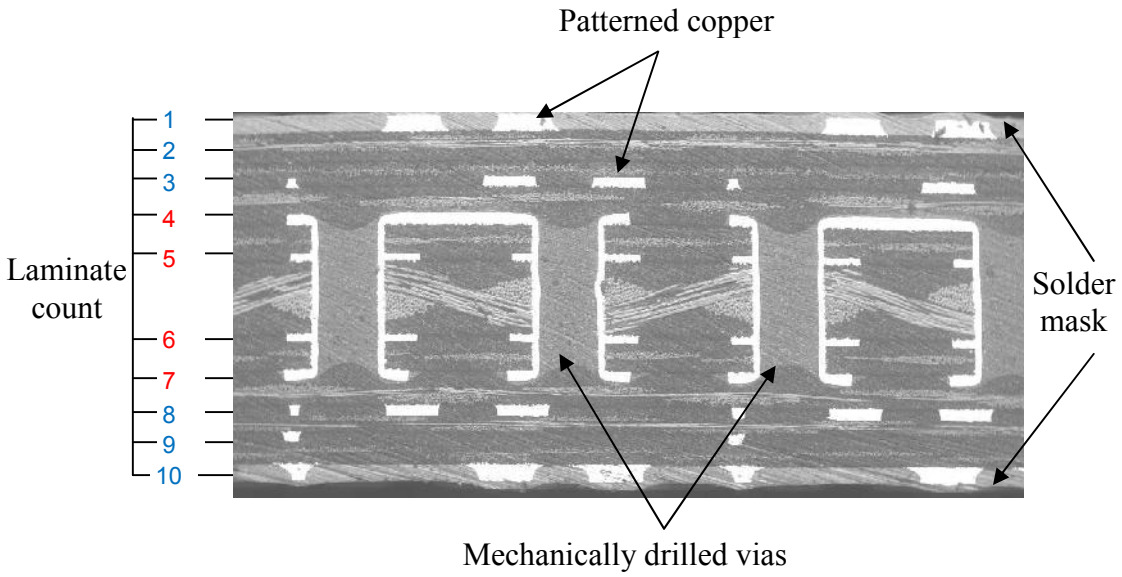

Figure 1-1: SEM image of PCB cross-section showing the patterned copper, solder mask, drilled holes, and laminate count.

1.3 PCB laminate materials

A smart selection of PCB laminate materials is important as it has a huge impact on the reliability, performance, cost, and environment. In general, materials with good process capability, low CTE mismatch, high T_g, low dielectric constant, and high CAF resistance are desired. In this section, some laminate materials such as epoxy resins, glass fibers, curing agents, and flame retardants are briefly introduced.

1.3.1 Epoxy resin and glass fibers

Epoxy resin and glass fibers are the main components in PCBs. A double-side board usually contains 41-48% of resin, and 50-70% for multi-layer boards. In other words, percentage wise there is usually less glass fiber content in a multi-layer board. [11]

Epoxy resin serves as a binder to hold the reinforcements (resin and glass fibers) together and impart important electrical properties (eg. low-dielectric constant) in PCBs. Ideally, the epoxy materials should be available and easy to process. Moreover, because of the high soldering temperature, glass transition temperature (T_g) in the range of 180-190 °C is now commonly used. [12]

Traditionally, brominated FR-4 epoxy was widely used because it provides excellent adhesion, good thermal stability, low processing temperature, and low cost. [16]

E-glass fiber contains silica, calcium oxide, alumina, boron oxide, and alkaline oxides and is the most common glass fiber used in electronic devices, due to its better electrical insulation and water resistance properties. However, for advanced electronic equipment, D-glass and S-glass are used due to their lower dielectric constant and dielectric loss in comparison with E-glass. [13]

There are also different styles of glass fibers (eg. 106, 1080, 7628 etc.), and the higher the style number, the thicker the glass fibers. [12] These glass fibers are woven in the warp and fill directions that are perpendicular to one another with warp in the same direction as the weaving direction. [17] Knots that contain both warp and fill glass fibers have a higher glass density, and therefore, are harder to drill.

1.3.2 Curing agents

A proper selection of curing agent is critical because it controls the cross-linking of the epoxy matrix. As lead-free soldering becomes the prominent method in manufacturing electronic devices; [18] PCB materials with better heat resistance, dimensional stability, electrical insulation, and chemical/moisture resistance are favored.

Ehrler et al. concluded at the 2005 EIPC conference that traditional brominated FR-4 boards cured by dicyandiamide (DICY) could not be used for lead-free soldering. [19] Instead, phenolic-cured resins should be used in PCBs due to better heat resistance (high T_g) and less water absorption. [18]

The low water absorption in phenolic-cured epoxy is due to the non-polar ring structures as shown in Figure 1-2a. This non-polar structure of phenolic-cured epoxy helps to reduce water absorption in comparison with the strong polar aliphatic alkyl bond structure of the DICY-cured epoxy as shown in Figure 1-2b. Because of the better heat resistance and water resistance properties, phenolic-cured epoxies are hypothesized to be less susceptible to CAF formation. [20]

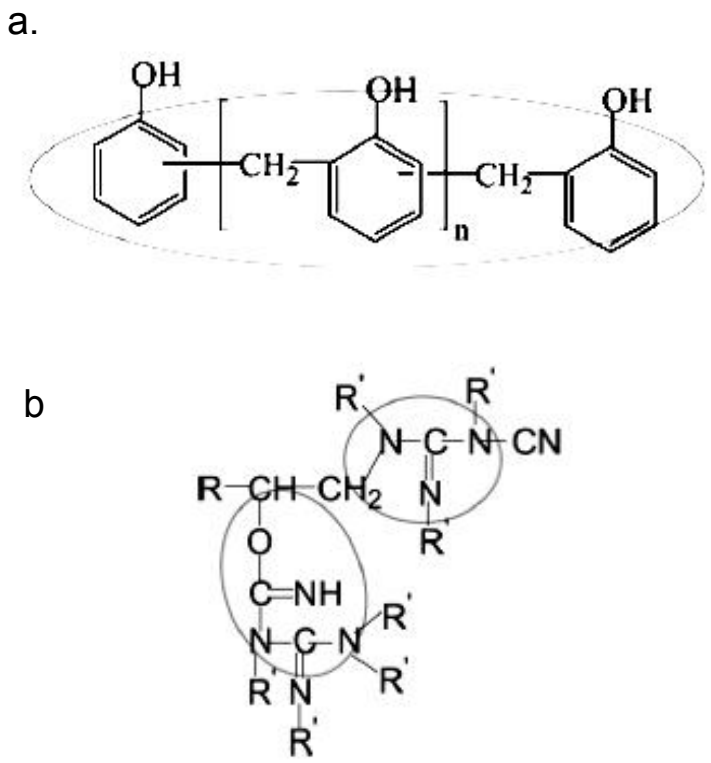

Figure 1-2: (a) non-polar ring structure of phenolic-cured epoxy and (b) strong polar aliphatic alkyl bond structure of the DICY-cured epoxy [20]

However, there are still some disadvantages that need to be overcome during the phenolic curing process. For example, during the curing process of novolac hexamine, volatiles such as water and ammonia compounds may be released, leading to the formation of microvoids. [18] Moreover, it is also known that phenolic-cured PCBs are more brittle and harder to process than dicyanamide-cured (DICY-cured) epoxy; therefore, manufacturing costs increase. [18, 21]

1.3.3 Flame retardants

Even though brominated epoxy has flame retardant properties, it is being replaced by halogen-free (HF) materials due to concerns about toxins released upon combustion. Current HF materials usually contain phosphorus- or nitrogen-doped epoxy and/or metal hydroxide fillers such as aluminum and magnesium hydroxides. [9]

Phosphorous doped epoxy utilizes a char formation mechanism to reduce temperature upon burning by acting as an insulation layer. [22] Liu's study showed that the higher percentage of phosphorous in epoxy, the higher the flame resistance. [23]

On the other hand, the major flame retardant mechanism for metal hydroxides works via endothermic reactions that release water molecules upon heating through the following reactions. [22, 24]

$$2Al(OH)_3 \text{ ---> } Al_2O_3 + 3H_2O \quad \text{.....(1.1)}$$

$$Mg(OH)_2 \text{ ---> } MgO + H_2O \quad \text{.....(1.2)}$$

1.3.4 Others

In addition to the mentioned components in laminates, other materials such as accelerators, coupling agents, and fillers are required but in relatively smaller amounts. For example, the accelerators (eg. organophosphine and imidazole) are used to reduce curing temperature, control the cross-linking density, and increase reaction rate.

Coupling agents such as organosilanes are important as they assist the bonding between the epoxy resin and glass fibers, so that local stresses can be transferred across the composite. Finally, fillers such as aluminum silicate and silicon dioxide help to reduce thermal expansion during the soldering process. [21]

1.4 Interconnect drilling methods

IPC projected a roadmap for mechanical drilling that predicts via size, aspect ratio, via pitch, and hole-to-hole spacing to be 100 µm, 18:1, 350 µm, and 250 µm, respectively by 2012/2016 as shown in Table 1-1. [11] Unfortunately, even with advances in mechanical drilling, there are still some limitations in using mechanical drilling to achieve these targets. For example,

1. Hole diameter is limited to 100 µm or higher.
2. Hole diameter has to be equal to or greater than 200 µm in order to be cost effective. [25]
3. It is impossible to drill blind vias (exposed on only one side of a PCB) when dielectric thickness is equal to or less than 50 µm.

Table 1-1: IPC roadmap for mechanical drilling [11]

Via size	Aspect ratio	Via pitch	Hole-to-hole spacing
100 µm	18:1	350 µm	250 µm

Because of these limitations in mechanically drilling small vias and the demand for higher speed and more functionality in electronic devices, a newly developed high density interconnect technology (HDI) using laser drilling is becoming popular. [12] HDI technologies can achieve superior signal integrity and increase the integrated circuit density by applying a laser beam to drill microvias in thinner dielectric laminates that are usually located on the top few layers of a multi-layer PCB.

There are two main types of laser drilling methods: UV and CO_2 laser drilling. If high quality vias are required in PCB designs, UV laser drilling is more favorable than CO_2 laser drilling. However, the disadvantage of UV drilling is the slower drilling rate relative to that of a CO_2 laser and the UV method creates tapered vias. This slow UV drilling increases production costs. [26, 27]

Nonetheless, there are still some challenges to laser drilling. For example, it is difficult to drill anisotropic materials, to clean the microvias, and to electroplate Cu on the vias after drilling. [28] Only a limited number of researchers [29] have studied the effects of laser drilling on CAF formation. Hypothetically, laser drilled microvias should be less susceptible to CAF formation due to minimal damage to the glass fibers.

1.5 Conductive anodic filament formation (CAF)

CAF is an electrochemically induced failure mode in which a conductive copper-containing salt grows from the anode to the cathode along the epoxy/glass interface. Several studies [16, 30-35] have shown that increasing temperature, relative humidity, and voltage gradient promote CAF formation.

CAF formation could become a serious reliability concern in electronic devices, as

1. Lead-free soldering process increases the reflow temperature.
2. The thermal and mechanical properties of the newly developed halogen-free flame retardants and curing systems are not well characterized in relation to CAF formation.

3. The introduction of laser drilling technology has not been studied fully relative to CAF.

1.6 Objective

There are two objectives in this research:

1. To evaluate and compare the effect of DICY- vs. phenolic-cured epoxy on the rate of CAF formation.
2. To compare the rate of CAF formation using laser drilled microvias vs. mechanically drilled vias under the same voltage gradient condition.

1.7 Summary

Chapter 1 has briefly introduced how the demands for environmental friendly, high speed, and reliable products lead to the study of CAF formation. The next chapter will introduce the details about the history of CAF; examples of CAF induced catastrophic failures, composition of CAF and the formation mechanisms, CAF detection methods, time-to-failure models, factors that affects CAF formation, and CAF resistance materials etc.

Chapter 2

Literature Review

This chapter will briefly introduce the history of CAF discovery, the catastrophic failure caused by CAF, the study of the chemical composition and microstructure of CAF, and the two step mechanism and time-to-failure models developed to understand CAF formation. Subsequently, a description of current testing method and techniques for detecting and verifying CAF formation, followed by the limitations of these techniques will be discussed. Finally, material related factors such as curing agents and glass fibers, and processing related factors such as humidity, temperature, and PCB drilling methods on the effect of CAF formation will be summarized.

2.1 Brief history of CAF discovery

Since the discovery of CAF by researchers at AT&T Bell Laboratory and Der Marderosian at Raytheon in 1976, many studies have been done to understand the mechanisms of CAF formation, the composition and spatial distribution of CAF, the factors affecting CAF formation, and to search for CAF resistance materials.

At Bell Labs, Boddy, Delaney, and Lahti *et al.* [36] identified two types of substrate-related failures: through-substrate shorts and sub-surface shorts that caused sudden loss of insulation resistance. Moreover, they also discovered covercoat-related and interface related failures. These failure modes were found using a wide range of test conditions (35 - 95 °C, 25 - 95% RH, and up to 400 V bias voltage).

Through-substrate shorts were caused by the formation of conductive corrosion products between the conductors on opposite side of the substrate. On the other hand, sub-surface shorts involved the accumulation of conductive materials along the glass fibers between the conductors on the same side of the substrate.

The through-substrate shorts dominated only at temperatures and relative humidities (RH) above 75 °C and 85% RH respectively; whereas, the sub-surface failure mode was prevalent at temperatures and RHs below 75 °C and 85% RH. Nonetheless, the researchers predicted that the sub-surface failure mode would not be a problem under

normal use conditions (25 – 35 °C, 40 – 60% RH) as the mean service life would be measured in tens of years. [36]

The covercoat-related failures were related to the dendritic growth that initiated from the cathode to the anode through copper migration process in the bulk of the covercoat material. Moreover, they also found another mechanism for the covercoat-related failure that was caused by a highly localized anodic reaction which produced an eruption at the covercoat surface. [36]

Interface-related failures were found at the interface between covercoat and substrate. This failure mode was believed to be related to a high contamination level prior to covercoat application. [36]

The same year, Der Mardeosian [32] found a new failure mode while studying measling. He compared the effect of 100 V AC, 100 V DC, and no voltage on the reliability of PCBs at 65 °C and 95% RH. He found a failure mode termed "punch thru" occurred only when 100 V DC was applied from an anode copper track (+) to a cathode ground plane (-). He concluded that this failure was caused by an electrochemically initiated metal migration. Moreover, he also proposed the following reaction:

$$3Cu + 3H_2O = CuO_{(anode)} + Cu(OH)_{2\,(anode)} + 2H_{2\,(cathode)} + Cu_{(cathode)} \quad \text{.....(2.1)}$$

to explain his observation of the conductive CuO compound formed along the glass fibers from anode to cathode that "blew out" the epoxy and fibers glass. [32]

In 1979, Lando, Mitchell, and Welsher *et al.* from Bell Labs first used the term – conductive anodic filament (CAF) – to describe the failure modes associated with permanent or intermittent loss of insulation resistance (IR) inside a PCB. The study also proposed a mechanism for CAF formation and compared the effects of test configurations (line-to-line, line-to-hole, and hole-to-hole) on IR readings. [33] Details of the mechanism and test configuration can be found in Section 2.4 and Section 2.9.2.3.

2.2 Example of catastrophic failure caused by CAF

CAF was originally discovered in an experimental setting; however, there was also real life evidence of catastrophic failures caused by CAF. For example, in military hardware, shown in Figure 2-1, a failure caused by CAF was found between the inner power plane (+20 V) and the component through hole pin (-20 V) with a separation of 125 µm. (Once CAF bridges the conductor spacing, it will create a short circuit because CAF is a semiconductive salt.) The epoxy in this example, melted as the filament released a high current when the bridging occurred. [31, 37, 38, 39]

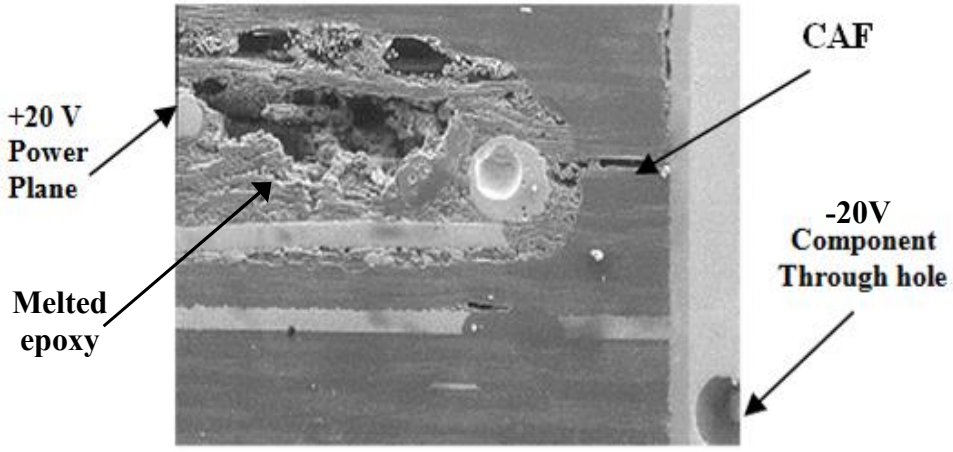

Figure 2-1: Catastrophic failure caused by CAF grows from [38]

2.3 Microstructure and chemical compositions of CAF

Ready and Stock *et al.* studied the microstructure and chemical compositions of CAF using Scanning Electron Microscopy (SEM) equipped with energy dispersive X-ray analysis (EDX). In addition, they also determined the spatial distribution of the amount of CAF emanating from the anode. [40]

In Ready and Stock's study, they found at the anode that copper dissolved and formed CAF which they identified as a chloride containing semi-conductive salt. [40] The chloride was believed to come from the epichlorohydrin (C_3H_5OCl) used during the epoxy manufacturing process. [41] Through serial sectioning, the researchers observed that the highest percentage of CAF was found within the epoxy near the anode (Figure

2-2 a), but as the distance increased from the anode, the quantity of CAF decreased and was mostly confined to the surface of epoxy/glass interfaces (Figure 2-2 b). [40]

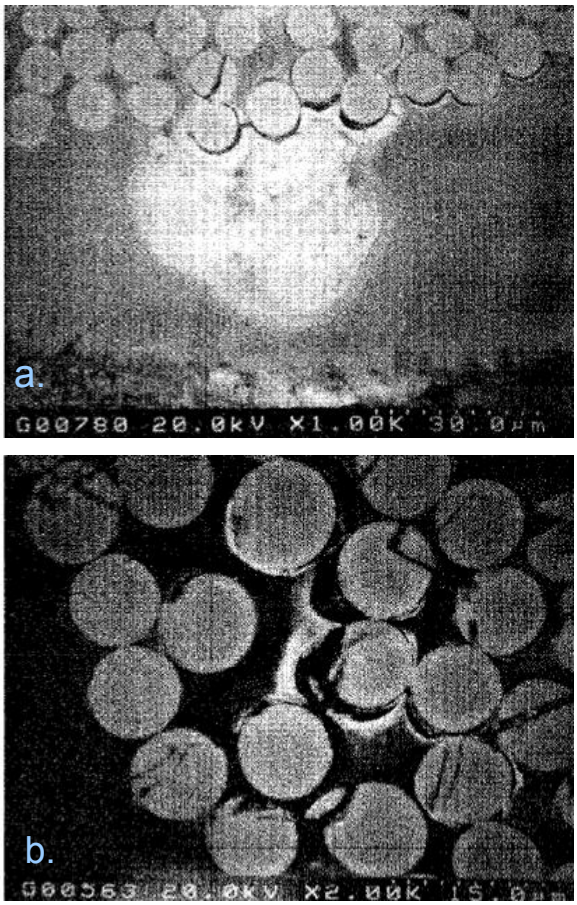

Figure 2-2: (a). CAF found at 50 µm away from anode and (b). at the end of the anode [40]

During additional research using Transmission Electron Microscopy (TEM), Ready and Turbini were able to show CAF formed during a temperature-humidity-bias (THB) test corresponded to a synthetic atacamite $2CuCl_2 \cdot 5Cu(OH)_2 \cdot H_2O$ in the powder diffraction database (1971). [31] Recently, the x-ray diffraction database for atacamite has been updated and the original structure ($2CuCl_2 \cdot 5Cu(OH)_2 \cdot H_2O$) was replaced with $3Cu(OH)_2 \cdot CuCl_2$. [35]

In nature, atacamite is a mineral which displays a slender, striated, and acicular to fibrous rhombic or orthorhombic crystal structure and appears in various shades of green, usually dark. [31] Interestingly, atacamite was also discovered to be contained in the jaws of the marine bloodworm Glycera dibranchiata. [42, 43]

2.4 Mechanism for CAF formation

In 1979, Lando *et al.* suggested a two step model to describe the CAF formation. The first step was determined to be related to the physical degradation of the epoxy/glass interface, and then followed by the electrochemical process in the second step. [33] During the electrochemical process, CAF will grow from the anode to the cathode along the epoxy/glass interface as shown in Figure 2-3.

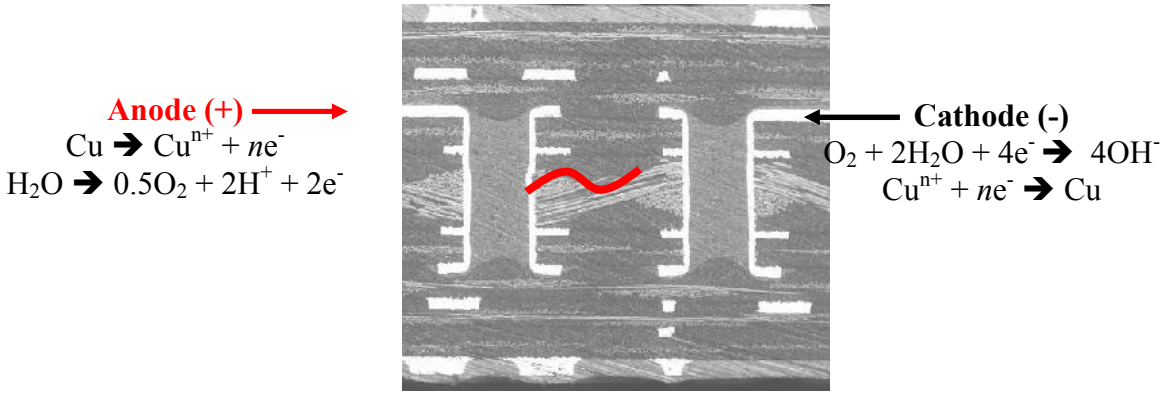

Figure 2-3: CAF grows from the anode to the cathode along the epoxy/glass interface

2.4.1 First step: physical degradation of the epoxy/glass interface

The first step was a rate limiting step, and it was believed to be reversible because the insulation resistance of the test coupon could return after baking and drying. [44] This step involved the physical degradation of the resin/glass bond, and this debonding would provide an easy path for electrodeposition of CAF while humidity was provided. In addition, this degradation could be enhanced through mechanical stress caused by handling/transporting the materials, thermal stress during soldering process [30], and hydrolysis of the silane glass finish. [33]

2.4.2 Second step: electrochemical reaction

The second step was found to be irreversible, and it required DC voltage to act as a driving force for the electrochemical reactions. [32] Lahti *et al.* described CAF as growing in a random direction at the beginning, but eventually preferentially growing toward the cathode.

[45] This directional preference could be explained by the voltage gradients between the two oppositely charged electrodes.

At the anode, water is oxidized to form hydrogen ions (H^+) and oxygen. At the cathode, water reacts with oxygen and is reduced to hydroxide ions (OH^-). The proposed reactions

At the anode are:

$$Cu \rightarrow Cu^{n+} + ne^- \quad \text{.....(2.2)}$$

$$H_2O \rightarrow 0.5O_2 + 2H^+ + 2e^- \quad \text{.....(2.3)}$$

At the cathode are:

$$O_2 + 2H_2O + 4e^- \rightarrow 4OH^- \quad \text{.....(2.4)}$$

$$Cu^{n+} + ne^- \rightarrow Cu \quad \text{.....(2.5)}$$

The reason why CAF forms from the acidic anode was explained by studying the Pourbaix Diagram for the copper-chloride system. As shown in Figure 2-4, [46] CAF with the chemical formula of $3Cu(OH)_2{\cdot}CuCl_2$ or $2Cu_2(OH)_3Cl$ is insoluble at pH below 4; [33] therefore; CAF grows from the anode. CAF formation is different from another failure mode named dendritic growth which involves the migration of Cu ions toward the cathode where it plates out producing localised sites in the form of needles or spikes. [47, 48]

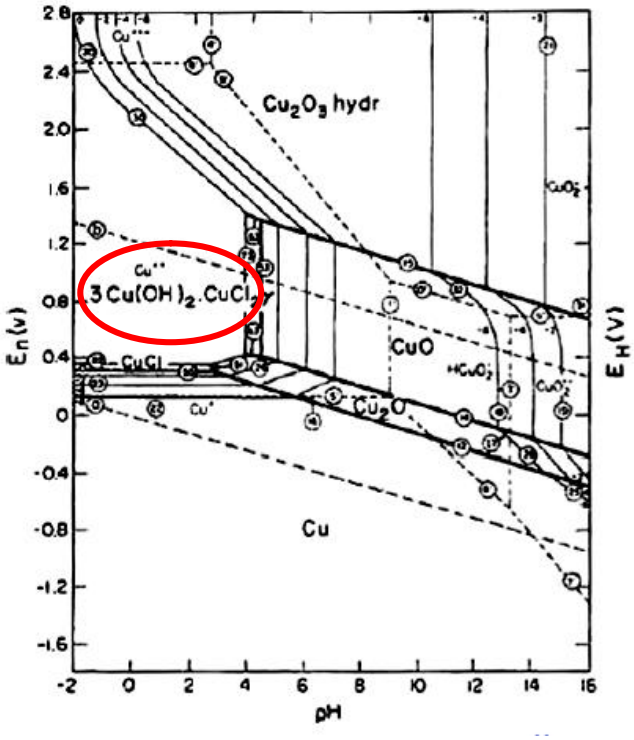

Figure 2-4: Pourbaix diagram of copper-chloride-water system [46]

2.5 Humidity threshold for CAF formation

In 1989, Augis and Mitchell *et al.* had suggested "the existence of a relative humidity threshold, below which no significant filament growth was expected". The proposed threshold humidity was based on the three pieces of evidence that were observed prior to 1985. [16]

The first observation was the contradictory results that the numbers of failures predicted from the linear acceleration factors model were more than the actual number of failures observed in the field. For example, one of the AT&T products was predicted to have a 6% dropout rate after five years of usage, but this failure rate was observed to be less in reality than the predicted percentage.

The second observation indicated that there was no difference in failures caused by CAF using materials that have been used in the field for years or the newly manufactured boards. The third observation was that while running PCBs at step stress tests, aging the material at moderate stress before testing actually resulted in slower degradation at high stress. For example, the boards pre-conditioned at a temperature of 65 °C and RH of 60% before testing at 65 °C and RH of 80% actually had a longer mean time-to-failure than the boards without pre-conditioning. [16]

These three observations suggested that there was a humidity threshold below which catastrophic failures would likely not be caused by CAF. In other words, the evidence suggested that CAF would not be a reliability issue if the humidity of the operating environment was well controlled. Augis *et al.* proposed the existence of threshold humidity that could be quantified by a formula, [16]

$$RH = \exp\left[\frac{2.3975 + \ln(c) + 10484/T - 1.52\ln(V)}{5.47}\right] \quad \text{.....(2.6)}$$

where c is the ratio of the rate constants (k_1/k_2) in the kinetic model shown in Figure 2-5. [16]. The model demonstrates that at a low relative humidity, k_1 is less than k_2 which decreases in proportion to RH to the fifth power. And hence, CAF is depleted by the higher rate of formation (k_2) of the innocuous trapped chlorine compounds (A_3). [16]

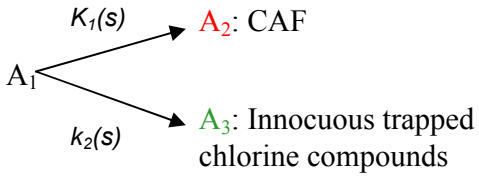

Figure 2-5: Kinetic models for CAF formation for modeling the threshold humidity [16]

Aguis had mentioned that this model might not be sufficient to explain the complex issue for CAF formation. Subsequent study done by Caputo and Turbini *et al.* have proven that there is no physical evidence for any "harmless chloride compounds" found in failed samples, so the kinetic model as shown in Figure 2-5 is invalid; instead the kinetic model shown in Figure 2-6 should be the appropriate explanation for CAF formation. [35]

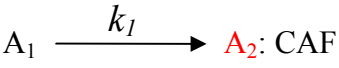

Figure 2-6: Model for CAF formation [35]

2.6 Mean-time-to-failure models

Several studies [30, 31, and 35] have found that the higher the temperature, RH, and bias voltage the shorter the mean-time-to-failure (MTTF) for CAF formation. Researchers (Welsher, Mitchell, Pecht *et al.*) have proposed a few models/formulas to predict the time-to-failure as a function of temperature, RH, bias voltage, and shape of conductors etc.

Welsher *et al.* investigated the effect of temperature (in the range of 50 to 100 °C) on MTTF using different materials at 95% RH and 200V DC bias. Their studies showed that MTTF and temperature followed the Arrhenius behaviour with an activation energy of 1 eV and were materials dependent. In addition, by doing a linear regression analysis with variables of temperature and RH, they suggested the following [49]

$$MTTF = a(H)^b \exp (E_A/RT) \text{.....} (2.7)$$

where H and T are relative humidity and temperature in Kelvin, a and b are material dependent, and E_A is the activation energy determined by best-of-fit data. Finally, they also modeled the effect of conductor spacing and bias voltage into the expression for MTTF and concluded that MTTF followed the L^2/V relationship (L is conductor spacing, and V is the bias voltage). In summary, an expression for MTTF was proposed as [49]

$$MTTF = a(H)^b \exp (E_A/RT) + d(L^2/V) \text{……..} (2.8)$$

Mitchell and Welsher then conducted more experiments to include the effect of conductor orientations (H-H, H-L, L-H, and L-L) on MTTF. The modified equation was determined to be

$$MTTF = \alpha \cdot (1 + \beta \cdot L^n/V) \cdot H^\gamma \cdot \exp [E_A / (R \cdot T)] \text{…….} (2.9)$$

where α and β are material-dependent factors, γ is a humidity-dependent factor, and n is the geometry factor based on the conductor configuration. Ready's work showed that the spacing/voltage relationship for the H-H configuration was L^4 / V^2. [31]

Pecht at CALCE also proposed a time-to-failure model for predicting the time-to-failure between two closely positioned conductors. The model was

$$t_f = \frac{a \cdot f \cdot (1000 \cdot L_{eff})^n}{V^m \cdot (M - M_t)} \quad \text{.....(2.10)}$$

where t_f is the time-to-failure, a is an acceleration factor, f is a multilayer correction factor, L_{eff} is the spacing between conductors, n is the geometry acceleration factor, V is the voltage bias applied between conductors, m is the voltage acceleration factor, M is the percentage moisture absorbed by the substrate, and M_t is a threshold moisture content. [50]

Time-to-failure is an important parameter to determine reliability relative to CAF formation for PCBs; however, researchers have found that there was a variation in the mean time-to-failure for different lots of the same testing material. For example, Lahti *et al.* observed that there were one or two orders of magnitude variation in mean time-to-failure during a THB test. They suggested that this variation could be caused by process chemistry and lamination parameters for the test coupons. [45] Using the two step model, Lando *et al.* explained that the activation energy of the debonding process was the cause for the variation.

Lando *et al.* suggested that the variation in activation energies depends on the integrity of the resin/glass interface. For example, if the materials were defective before testing, it required lower activation energy, and hence, time-to-failure decreased. On the other hand, if the materials had good adhesion between glass fibers and epoxy, the time-to-failure would be longer because substantial hydrolysis would be required before the electrochemical process (step two of the model) took place. [33]

2.7 CAF detection methods

2.7.1 Test coupon design

There are a few CAF test board designs in today's market, and some of the popular designs suggested by IPC for PTH-PTH testing are shown in Figure 2-7. The possible site and orientation for CAF formation are highlighted in red. The in-line PTH-PTH design indicates

that holes are in-line with glass fiber direction, and the staggered PTH-PTH design has the closest PTH-PTH spacing in a diagonal direction. [51]

There are two rows of 42 signal-1 vias intermeshed with three rows of 42 signals-2 vias in the in-line PTH-PTH design. This will allow a total of 168 possible sites for CAF formation. The staggered PTH-PTH design has three rows of 26 signal-1 vias intermeshed with four rows of 27 signal-2 vias for a total of 312 possible sites for CAF formation. It should also be noted that the PTH-PTH spacing is smaller in the in-line direction than in the staggered direction. [51]

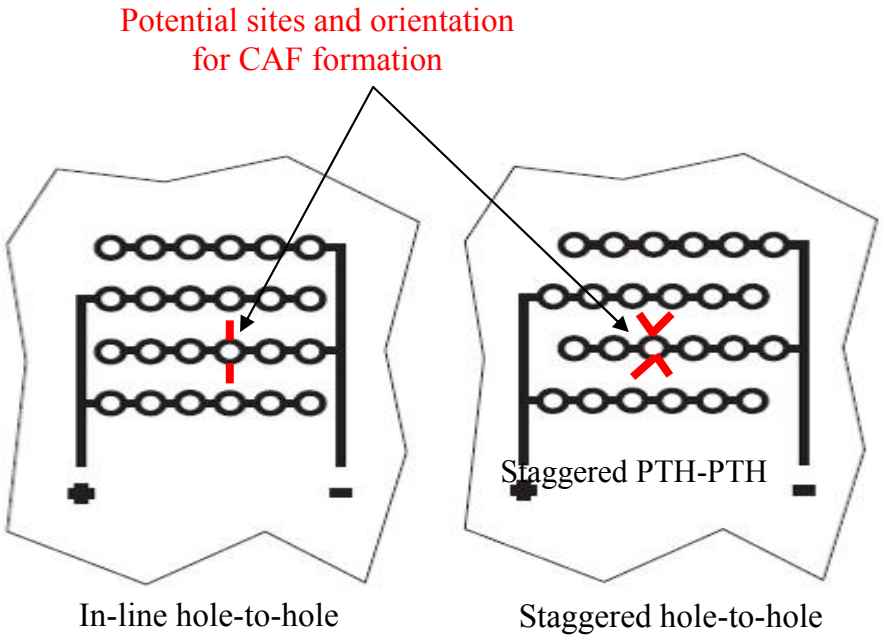

Figure 2-7: Spacing design for PTH-PTH recommended by IPC standard [51]

2.7.2 CAF test equipment

An IPC committee has published a standard CAF test for the industry to follow. The test method is IPC-TM-650, test method 2.6.25 [51] which was originally developed by Sun Microsystems. [52] The manual describes the procedures and lists the equipment needed for the CAF test, i.e. environmental chamber, power supply, current limiting resistors, mega-ohm meter, and connecting wires.[51, 53] This test requires at least 25 test coupons to be tested in order to obtain statistical results.

The parameters for using the environmental chamber are 65 ± 2 °C (149 ± 3.6 °F) or 85 ± 2 °C (185 ± 3.6 °F) and 87 +3/-2% relative humidity. [51] While using an environmental chamber, the prevention of condensation is paramount because if water condenses on the

samples, corrosion and erroneous readings can occur. One of the strategies is to maintain the uniformity of airflow inside the chamber. For example, the placement of the test coupons should allow air to flow freely on both sides of a test coupon and the wirings should not obstruct the airflow.

CAF is an electrochemically created salt which requires bias voltage; therefore, a DC power supply is needed. Moreover, in order to prevent catastrophic failure, a current limiting resistor between 1 to 10 M ohms is required. [53]

Another important piece of equipment is the resistance measuring equipment (mega-ohm meter) which is usually connected with a switch system, and it has to be capable of working in a range up to 10^{12} ohms and capable of yielding an accuracy of ± 5% at 10^{10} ohms with an applied voltage of 100 ± 2 VDC. The meter-switch system is used to turn on one measurement at a time with a measurement stabilization time of 20 seconds. If there are a large number of samples, the total measurement time will be lengthy. [53]

2.7.3 CAF test procedures

Before running a CAF test, an electrical continuity test has to be taken to identify shorts and open circuits. The samples need to be cleaned before wiring. When samples are ready, they are placed into the environmental chamber for pre-conditioning for 96 hours at minimum of 23 °C and 50% RH with free airflow. [51] The testing cycle (bias voltage supplied) and the measurement cycle (switch system activated) running with a data collection program are initiated.

2.7.4 Bias voltage time

CAF formation requires a bias voltage, but when the IR measurement is taken, the bias voltage is terminated. Traditionally, the bias voltage was supplied for 24 hours and then followed by resistance measurement. Studies done by Ready and Turbini demonstrated that CAF formation was not detected electrically during a surface insulation resistance test (SIR) with daily or even hourly measurement. [54]

The SIR test is used to monitor the changes of resistance due to conductive ions between anode and cathode at an elevated temperature and high relative humidity. SIR testing is widely used in the industry to detect the potential ionic contamination on the PCB during the fabrication process. [55]

2.7.5 *A novel test circuit*

As mentioned, the daily and hourly testing was insufficient to measure CAF formation electrically; a more sensitive test setup and a shorter bias time between measurements were needed.

R. Nickel *et al.* have developed a "linear circuit" (LC) to overcome the challenges for detecting dendrite or CAF formation, and preventing catastrophic failures by terminating power to a particular test coupon once IR drops dramatically. This technique allows the preservation of the dendrite or CAF for further analysis. [47]

Because of the high voltage required for CAF initiation and formation (Figure 2-8a), a switching system was required to switch the power supply for the measurement phase that required a low voltage supply (Figure 2-8b). The low voltage supply was required to avoid damage to the operational amplifier in the LC, which is limited to 10-15V.

Using this technique, Ready and Turbini *et al.* were able to detect CAF electrically and identify CAF dissolution phenomenon that was believed to be responsible for the increased in resistance during the measurement phase (low power supply) when the high power supply was temporarily disconnected. [47]

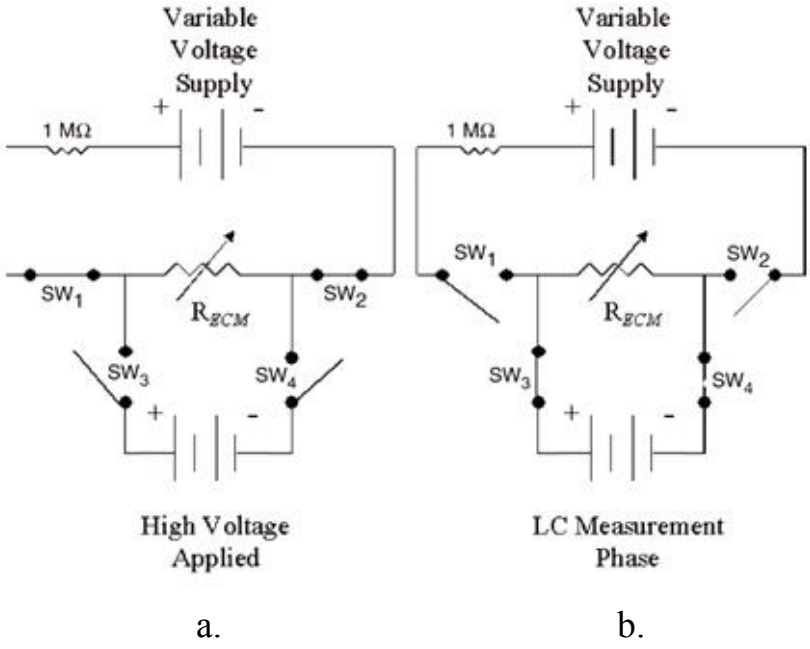

a. b.

Figure 2-8: Switching system for the LC. (a). At high bias supply state, (b). At low voltage measurement stage [47]

2.8 CAF failures verification techniques

Once the CAF test terminated, the failed coupons needed to be examined to find out the root causes of insulation resistance loss. The failure analysis required the identification of failure sites and the confirmation of chemical compositions if possible. The most commonly used technique is the use of an electrical test to identify the CAF site when resistance goes below a certain value. For CAF the electrical failure is followed by cross-sectioning and SEM-EDX analysis. The drawbacks of this technique include the following:

1. It requires a clear circuit layout.
2. The surfaces of the test coupons have to have minimum contamination and be debris free.

Recently, Pecht *et al.* at CALCE (Center for Advanced Life Cycle Engineering) have applied a new technology called superconducting quantum interference device (SQUID) that can overcome the drawbacks of currently used CAF identification techniques.

SQUID is a relatively new non-destructive magnetic field imaging technique that can map out the current distribution in a device. [56] Roger's study has shown that this technique could identify CAF and was able to overcome the problems encountered in the electrical test. [57]

For example, this technique can detect a low current leakage that forms between a power and a ground plane that could not be achieved using the present SIR test. Moreover, the low voltage and current can prevent damage to the fragile filament. Nonetheless, the drawbacks of SQUID are the cost and the small working distance (~ 100 μm) between the detector and the shorted sites; therefore, if there are any tall components above the shorted sites, the technique will be improper. [57]

2.9 Factors that affect CAF formation

2.9.1 Material related factors

2.9.1.1 Curing agents (dicyandiamide vs. phenolic)

In the present study, there are two main types of curing systems being examined: dicyandiamide-cured (DICY) and phenolic-cured (PN) epoxy. Traditionally, DICY-cured materials were more popular because of lower cost, less brittle nature, better process-ability and good adhesive properties. Unfortunately, due to the strong polar aliphatic alkyl bond in

the DICY-cured epoxy, it is less heat and water resistance; and hence, suspected to be more prone to CAF formation.

Because of the need for better thermal properties required for lead-free soldering, original equipment manufacturers (OEMs) have been encouraged to use the PN-cured epoxies that have higher heat resistance, lower water absorption, and presumably better CAF resistance. However, PN-cured materials are more expensive, brittle and harder to process.

Peng *et al.* have determined the glass transition temperature (T_g), time to delamination at 288 °C (T_{288}), and water absorption using two different PN-cured and two different DICY-cured materials. Test results verified that both PN-cured materials have higher T_d (360 and 364 °C vs. 340 and 310 °C), higher T_{288} (above 70 minutes vs. less than 6 minutes), and lower water absorption (0.61% and 0.74% vs. 1.02% and 1.21% of moisture absorption) than both DICY-cured materials. Table 2-1 compares some more material properties of DICY- and PN-cured materials. [20]

Table 2-1: Material properties comparison for DICY- and PN-cured epoxy [20]

	DICY	PN
Current market share	>90 percent	<10 percent
Process friendliness	Excellent	Poor
Thermal properties		
T_g	Fair	Fair
T260	Poor (10 min)	Good (>30 min)
Physical properties		
CTE	Fair	Fair
Adhesion	Excellent	Poor
Robustness	Excellent	Brittle
Reliability		
Humidity resistance	Poor	Excellent
CAF	Poor	Excellent
Thermal cycle test	Fair	Fair

Bergum compared a non-DICY FR-4 laminate to four other commercial materials which claim to be CAF resistant materials with improved glass finishes and epoxy. He concluded that glass finishes did not have as significant an effect on preventing CAF formation as non-DICY cured epoxy, because the non-DICY-cured laminate was the best CAF resistance

material over a period of 1,000 hours at 85 ˚C and 85% RH. [58] Unfortunately, his paper did not mention the curing agent that was used for his non-DICY samples.

2.9.1.2 Glass fibers distance and orientation

The distance between the glass fibers was proven by Johander *et al* to have a significant effect on CAF formation, while the distance between vias was maintained constant. Their study showed that when the distance between glass fibers was 570 µm, the resistance dropped one additional order of magnitude in comparing to 880 µm that ran parallel to the direction of CAF formation. They concluded that the drop in resistance was related to the higher glass fibers density because of the smaller distance between glass fibers. The higher the density means the more possible locations for CAF formation. [59]

Karavakis *et al.* showed that via-to-glass fiber direction has a significant effect on CAF formation regardless of via-to-via distance. For example, the IR measurement was lower for the vias in the fill direction than the warp direction. [17]

2.9.2 Processing related factors

2.9.2.1 Humidity

Water molecules are usually absorbed through the surface and subsequently diffuse into the epoxy. Under humid condition, water molecules diffuse into PCBs and cause swelling of the epoxy resin. The swelling induces the stress on the glass/epoxy interface and water molecules provide an aqueous medium for ions to migrate in the presence of a bias voltage. [60]

As mentioned, CAF is formed by an electrochemical reaction that produces electrolytes from water and other dissolved materials; therefore, it becomes apparent that the higher the relative humidity the faster failures occur (shorter MTTF).

Rudra *et al.* studied the effect of humidity during tests using traditional FR-4 PCBs at 70 °C and RH of 70% and 85% for different spacing. The MTTF was shorter for boards exposed to the higher RH (85%) and/or smaller spacing between conductors. [30]

2.9.2.2 Conductor spacing/bias voltage /voltage gradient

Cohn et al. found that the smaller spacing appears to have a faster drop in insulation resistance for either laser or mechanical drilling when a fixed voltage was applied. For

example, all test coupons failed before 400 hours at a PTH-to-PTH spacing of 100 µm but no drop in insulation even after 1000 hours of testing when the spacing was 200 µm. [29] On the other hand, by fixing the spacing between the conductors and varying the voltage bias, Rudra et al. has demonstrated the higher the bias supplied, the lower the MTTF. [30] These experiments illustrate that the higher the voltage gradient, the faster the CAF formation.

Even though it is desired to test all possible spacings that can be manufactured today, researchers (Rogers, Parry, and Caputo *et al.*) have suggested a minimum spacing that could be used for CAF test. For example, Rogers and Pecht at CALCE have claimed that, below a minimum spacing of 100 µm, premature failure would occur at 85 °C and a RH of 85%, as specified in the IPC-TM-650 method 2.6.25. [61]

On the other hand, Parry and Caputo *et al.* suggested a minimum edge-to-edge spacing should be 350 µm in considering the hole-drilling manufacturing tolerance was ±75 µm, and this tolerance should not exceed 20% of the hole-to-hole distance. [37] A recent study done by Caputo and Turbini *et al.* showed that this spacing (350 µm) could lead to premature shorting during a CAF test. This failure was caused by the cracks created during mechanical drilling. They recommended that a hole-to-hole spacing of 500 µm instead of 350 µm should be used. [11]

2.9.2.3 Temperature

2.9.2.3.1 During THB testing

Temperature has an impact on CAF formation and as temperature increases, mean-time-to-failure (MTTF) decreases. Welsher *et al.* has studied the effect of temperature using three generic FR-4 laminates at 95 %RH and 200 V DC over a range of temperature (50 -100 °C). The test results showed that the MTTF followed Arrhenius behavior with an activation energy on the order of 1 eV. [49]

2.9.2.3.2 During lead-free soldering process

The demand for "greener" products led to the implementation of lead-free soldering by July 1, 2006 through the EU Restriction of Hazardous Substances Directive (RoHS). [1, 9, and 62] This practice leads to the increase in reflow temperature because lead-free solders usually have higher melting points (198 °C to 227 °C) than eutectic Sn/Pb solder (m.p. 183 °C).

The higher reflow temperature has led to some manufacturing issues such as board warpage, component failures, delamination, and CAF formation to occur more frequently. For example, studies done by Turbini and Bent *et al.* showed that PCBs processed with water-soluble fluxes (PPG, PEPG, PEPG 26, GLY, OPE, and LAP) had more CAF failures at a reflow peak temperature of 241 °C than 201 °C. [34]

As mentioned, CAF is not a newly discovered failure mode, but it has drawn new attention as lead-free soldering has been implemented. Lead-free soldering requires a higher peak reflow temperature, which increases the stress between the laminates and weakens the bond between the glass/epoxy interfaces. As estimated by Turbini and Bent *et al.* using the thermal strain formula, $\varepsilon = \Delta CTE * \Delta T$, the strain for the e-glass-epoxy system is 22.7% higher at peak reflow temperature of 241 °C than 201 °C. [34]

In order to withstand the higher reflow temperature during lead-free soldering, PCB materials with better thermal stability are required. In general, thermally stable materials which have a higher thermal decomposition temperature (T_d) and higher time to delamination at either 260 or 288 °C (IPC-TM-650) are desired. T_d is usually defined as the temperature at which a 5% weight loss of a polymer occurs. Time to delamination (T_{260} and T_{288}) is defined as the time it takes for delamination to occur for laminate materials heated to 260 and 288 °C respectively. [59]

2.9.2.4 Conductor configuration

As mentioned earlier, test configurations (L-L, L-H, H-L, and H-H) are important in determining the susceptibility of CAF formation in PCBs. Early studies done by Lando *et al.* using FR-4 materials, the frequency of failures was shown to follow the order from the highest to the lowest in the order of H-H > H-L ≈ L-H > L-L (200 µm) > L-L (380 µm) as shown in Figure 2-9. [33] They concluded that the H-H configuration was most susceptible due to the weakening of the glass/epoxy interface during the hole drilling process.

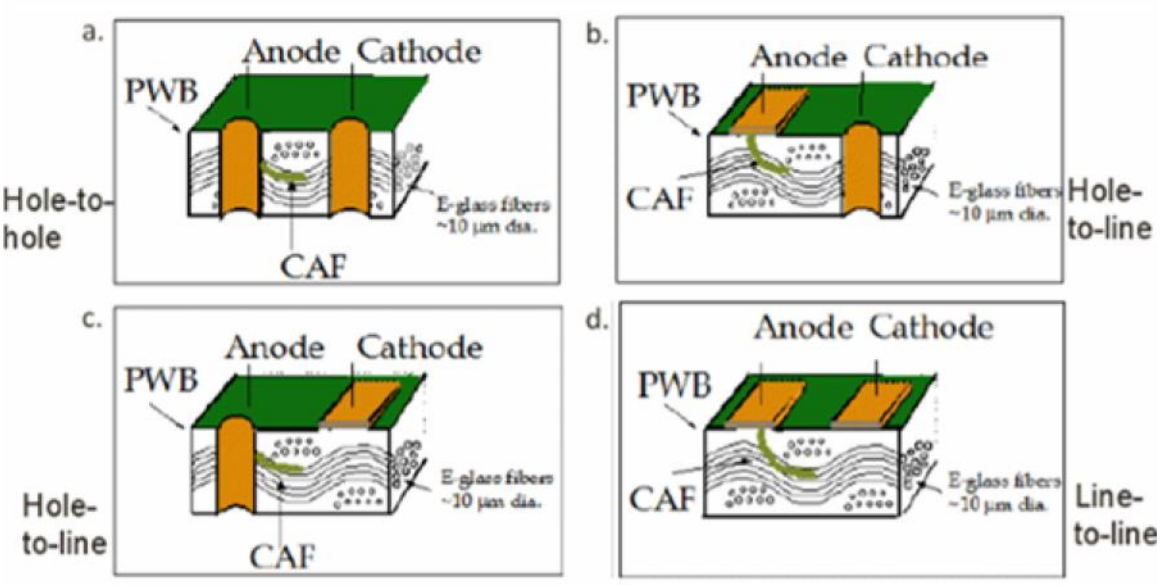

Figure 2-9: Susceptibility of CAF formation in the order of conductor configurations H-H > H-L ≈ L-H > L-L [31 and 37]

2.9.2.5 Drilling methods

There are two main types of interconnect drilling methods: traditional mechanical drilling and recently developed laser drilling methods. Cohn and Kimbara have compared the effects of mechanical and laser drilling on CAF formation using BT epoxy/glass reinforced substrates in a highly accelerated stress test (HAST). [29]

Their study showed that the time for the first insulation resistance loss in mechanically drilled vias increased as the pad-to-pad distance increased. For example, at pad distance of 100 µm, 150 µm, and 200 µm, the time for the first insulation resistance loss were 60 hours, 200 hours, and no resistance lost during the 1000 hours of testing, respectively. On the other hand, there was no insulation resistance drop for laser drilled microvias even with a pad-to-pad distance of 100 µm.

The researchers concluded that mechanical drilling exerted more stress on the epoxy/glass fibers compared to laser drilling; therefore, making it easier for CAF formation. [29] For example, copper wicking could occur during the copper plating process after mechanical drilling as shown in Figure 2-10. Once wicking occurs, copper will migrate along glass fibers during copper deposition, and hence, creates a shorter distance between anode and cathode. [11] In order to reduce CAF formation, drilled holes should be smooth and straight, and there should not be any glass fibers protruding from the hole. [63]

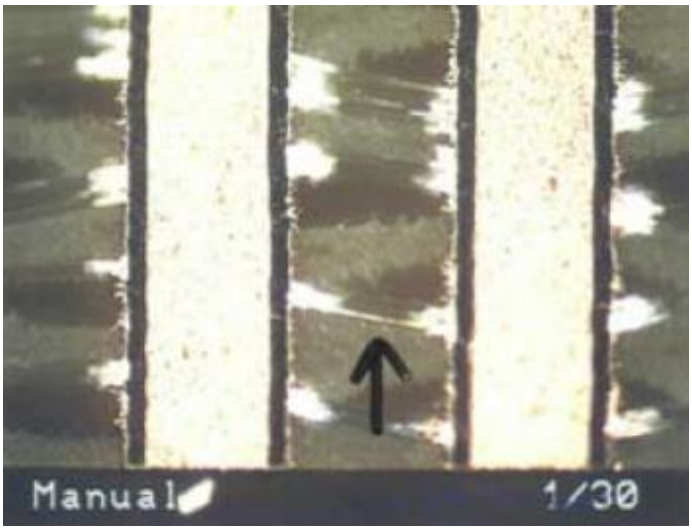

Figure 2-10: Copper wicking due to mechanical drilling [27 and 29]

During mechanical drilling, several factors have to be considered and controlled properly in order to produce good quality vias and thus prevent CAF formation. Of these, only the most significant - drill wear and chip load – are described in this thesis. Adverse control of the process will degrade the quality of mechanical drilling and lead to copper wicking.

Drill bit wear is undesirable but unavoidable during fabrication. Once a drill bit is worn out, it will damage the glass/epoxy interface and promote CAF formation. In general, the less force applied to the board material, the less damage to the material. Unfortunately, statistics show that increasing drill force is required to drill a large number of holes, as traditional drill bits start to wear out after the first 200 holes. Followed by the initial drill wear, a linear increase in wear rate occurs for every 1000 holes. In addition, thicker PCBs will also result in greater drill bit wear.

An optimal chip load, which is the distance traveled by the drill bit into the board in each revolution, is desired. Finally the aspect ratio, defined by the ratio of the board thickness to the via diameter, is also crucial during mechanical drilling. [11]

Developments have been made to reduce drill bit wear and improve drillability. For example, Fu and Yang claim their newly designed drill bit can drill 6000 holes instead of 4000 holes before the drill bit becomes useless. [64] Moreover, Banda et al. suggest an alternative for improving the drillability of PCBs by adding toughener. With the use of different loadings (3.75 wt % and 7.5 wt%) of toughener, fiber pullout, debonding, and brittle

failures were absent. [65] Unfortunately, the researchers did not disclose the chemical compositions of the toughener.

Alternative to mechanical drilling, high density interconnect (HDI) technology using laser drilling has proven to be reliable and reduce production cost. It allows production of vias as small as 50 µm, a pad size of 150 to 200 µm, and low via aspect ratios. [11] This allows the thickness of the metal layer to be reduced to 15 µm and the width of copper trace to be decreased to between 40 to 70 µm. Nonetheless, there are still some challenges to laser drilling. For example,

1. It is difficult to drill anisotropic materials.
2. It is hard to clean the microvias and to electroplate Cu on the vias. [28]
3. It is limited to drilling laminate of thickness of 400 µm [29]

Unfortunately, there are only limited studies demonstrating the effects of laser drilling on CAF formation. Nonetheless, hypothetically, laser drilled microvias should be less susceptible to CAF formation due to minimal damage to the glass fibers.

2.10 CAF resistance materials

Early studies done by Rudra and Pecht had shown that both bismaleimide triazine (BT) and cyanate esters (CE) were less susceptible to CAF formation than traditional FR-4 materials. They concluded that there were two main reasons for the superior properties of BT and CE. One of the reasons was the moisture uptake at a specific relative humidity was lower for BT and CE than FR-4 materials. For example, at temperature of 50 °C and 70% RH, moisture absorption was 0.65%, 0.85%, and 1.15% for BT, CE, and FR-4 respectively. Another reason was the higher glass transition temperature T_g for CE and BT. For example, T_g for CE, BT, and FR-4 were around 240 °C, 195 °C, and 120 °C. Unfortunately, there were insufficient data to distinguish the susceptibility of BT and CE. [30]

Welsher *et al.* from Bell Labs also compared Triazine A and FR-4 materials using hole-to-hole and hole-to-land configurations. Test results showed that insulation resistance for Triazine A with H-H configuration was at least 20 to 30 times higher than FR-4 materials. Even though there were some electrical failures in the H-L configuration with conductor spacing of 127 µm, the overall performance of Triazine A material was still better than any of the FR-4 materials tested. [49]

2.11 Summary

This chapter has summarized the first discovery of CAF by the researchers at AT&T Bell Laboratory and Raytheon in mid 1970's, and described the studies that have been conducted to understand the chemical and microstructure of CAF and the two step model for CAF formation. Details of mean-time-to-failure models as a function of temperature, RH, conductor spacing, voltage supply, and conductor configuration have been discussed, and the IPC standard CAF test and its limitations were also mentioned. Finally, material and manufacturing related factors that accelerate CAF formation were covered.

The next chapter will provide details about the composition, structure, and dimension of the test coupons, the procedures for sample preparation, parameters for equipment setup, data collection and analysis methods, and CAF site identification and chemical composition verification.

Chapter 3

Experimental Procedures

This chapter describes the details of the structures, dimensions, and compositions of the test coupons, followed by listing the parameters for setting up equipments, the procedures for sample preparations, and the methods for verifying the failure mode.

3.1 Test coupon structures and dimensions

The test coupon contained two different test sites - surface laser-drilled microvias (SLDM) in Layers (1, 2, and 3) or (8, 9, and 10), and buried mechanically drilled vias (BMDV) in Layers (4 to 7) as shown in Figure 3-1.

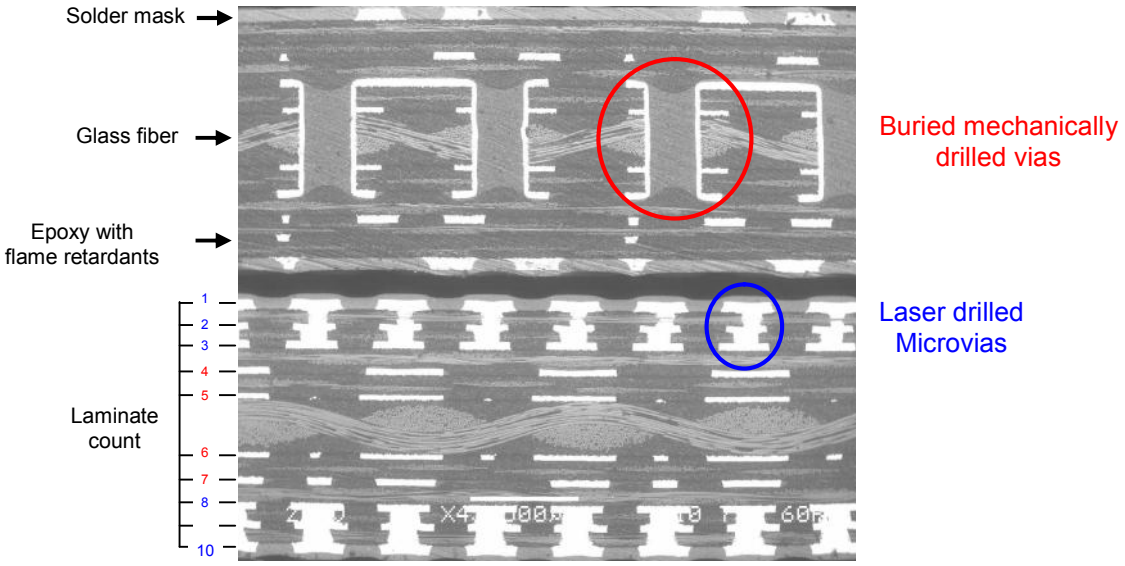

Figure 3-1: SEM picture of the cross-section of a test coupon. Top picture illustrates the BMDV between Layer 4 to 7, and bottom picture shows the SLDM in Layers (1, 2, and 3) and (8, 9, and 10).

3.1.1 Surface laser-drilled microvias (SLDM)

As shown in Figure 3-2, the two layer stacked microvias have a tapered shape; therefore, a via diameter of 80 µm indicates the average dimension of the tapered microvia. The wall-to-wall distance of 320 µm indicates an average distance between the walls of two adjacent microvias. Moreover, the pad-to-pad distance was 150 µm with pad diameter of 250 µm.

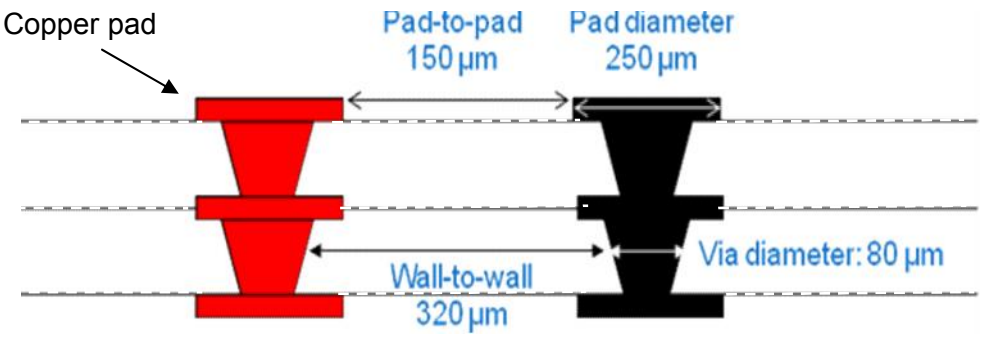

Figure 3-2: Dimension of SLDM.

These SLDM were located on the top three layers (Layer 1, 2, and 3 in Figure 3-1) and bottom three layers (Layer 8, 9, and 10 in Figure 3-1) of a multi-layer PCB. Each anode and cathode is daisy chained so that the SLDM are connected linearly. As shown in Figure 3-3, there are seven vias in each row of anode/cathode and a total of 74 rows of anodes/cathodes in a test coupon; therefore, a total of 518 vias were positioned along the anode/cathode in a daisy chain style.

The anode of the test coupon was connected to the positive side of the power supply; the cathode of the test coupon was connected to the negative side of the power supply as shown in Figure 3-3.

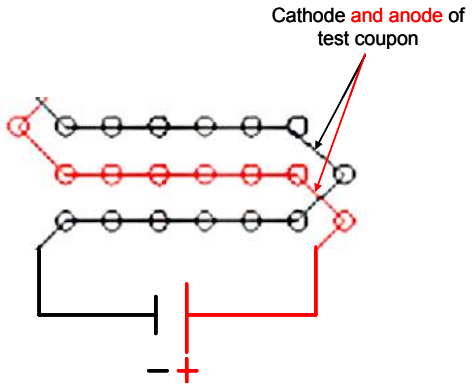

Figure 3-3: Electrical layout of SLDM

The anode and cathode were running parallel to each other in a test coupon across the surfaces. This design ensured that the vias were equally spaced (320 µm). Moreover, each anode or cathode was running in a zigzag pattern as shown in Figure 3-3.

Because of the layout of the vias on the test coupon, there could be multiple sites/orientations for CAF formation. Figure 3-4 illustrates the possible sites for CAF formation. For example, Site A could only grow CAF towards the two adjacent rows of cathodes, but Site B could grow CAF to the cathode on the same row and on the adjacent row. The sites for CAF formation are based on the fact that CAF grows from the anode to the cathode. There were 518 vias on one anode; therefore, there were 1036 possible sites to find CAF because each anode was surrounded by two cathodes.

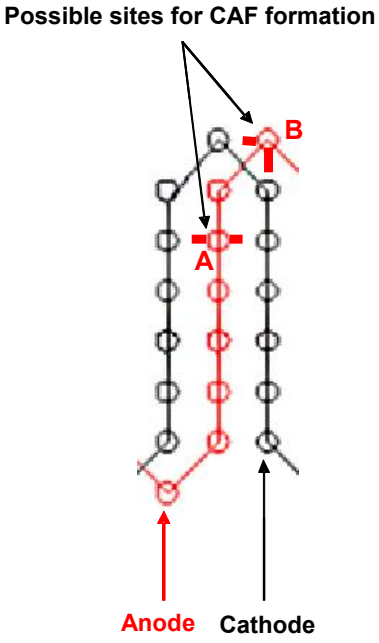

Figure 3-4: Possible CAF formation sites (A and B).
CAF grows from anode (red) to cathode (black)

3.1.2 Buried mechanically drilled vias (BMDV)

The BMDV penetrated four layers of laminates (Layer 4 to 7 in Figure 3-1) in the test coupon. The dimensions related to BMDV are shown in Figure 3-5. The via diameter was 200 µm, and the wall-to-wall distance was 500 µm. The pad diameter was 500 µm, and pad-to-pad distance was 300 µm. These vias have a straight wall unlike the tapered shape as the SLDM.

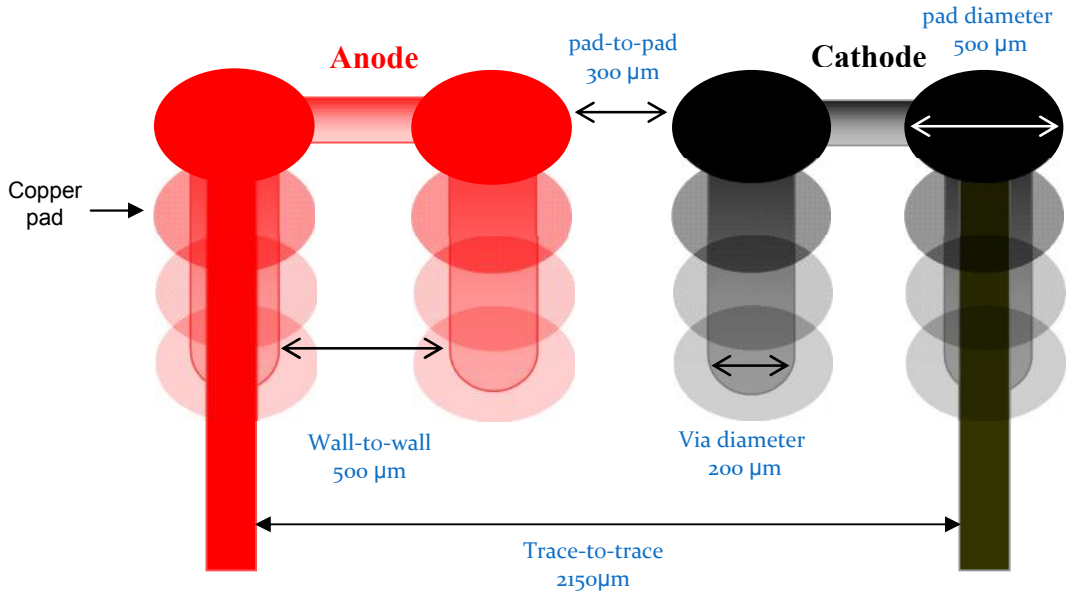

Figure 3-5: Dimensions of BMDV

Because all the BMDV were electrically connected in a daisy chain format in the original test coupon, a modification was required to accommodate the circuit for a CAF test.

First, the end of the test coupon had to be ground off to disconnect the daisy chain, in order to create two daisy chains with buried vias that are oppositely charged as shown in Figure 3-6. Because the vias were constructed in a zigzag fashion, CAF would likely grow in the shortest distance between the vias as illustrated in Figure 3-7. There were a total of 36 possible sites for CAF formation in each coupon.

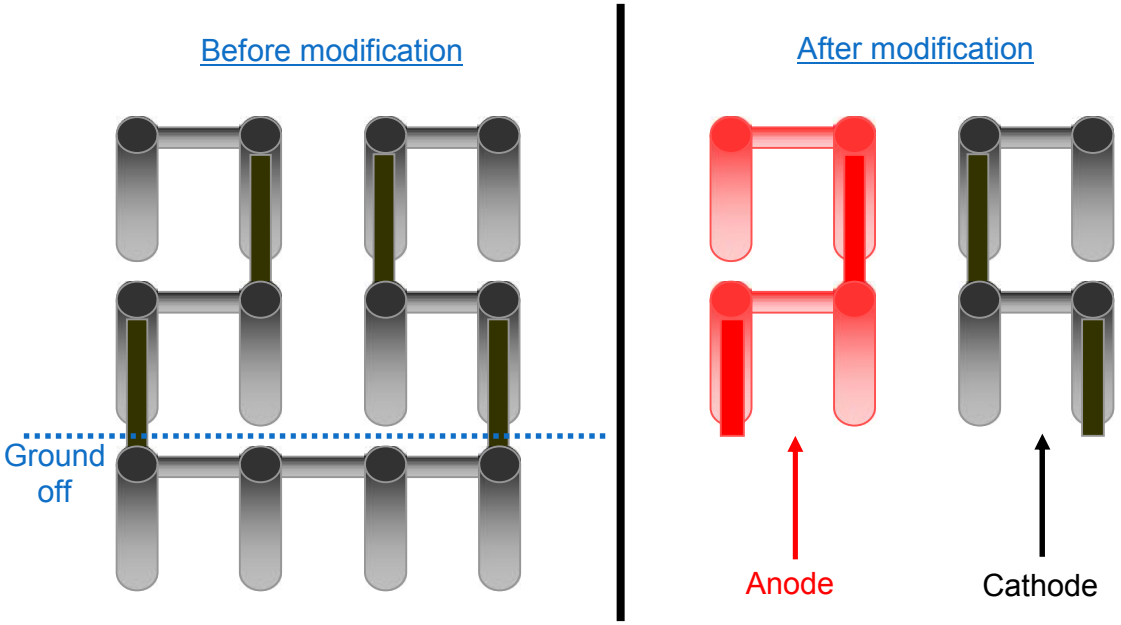

Figure 3-6: Illustration of reconstructing a test coupon for CAF test (simplified). One daisy chain was cut and formed separate daisy chains. One was anode, and one was cathode

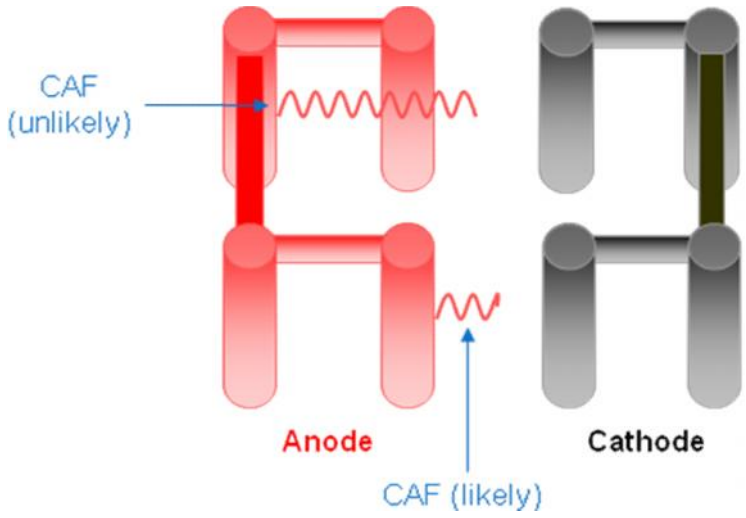

Figure 3-7: Sites for CAF formation.

CAF grows from the anode to the cathode at the shortest distance.

Secondly, the ends of all test coupons were coated with conformal coating (Hysol PC18M). The purpose of applying the conformal coating was to protect the ground ends from exposure to the humid environment during the accelerated temperature-humidity test.

The conformal coating was applied twice on each sample. The first coating was applied using a Q-tip to brush the coating solution on the sample, followed by air drying for 40 minutes and curing at 60ºC and 30% RH for three hours in the environmental chamber (SL-2CA). The second coating was applied by dipping the end of the sample into the coating solution, and then air drying and curing using the same settings.

3.2 Material compositions and properties

There were two main types of materials evaluated in this study: DICY-cured epoxy and phenolic-cured epoxy. The details of material compositions and properties provided by the supplier are listed in Table 3-1. In each test, thirty DICY-cured SLDM/BMDV test coupons would be tested with thirty phenolic-cured SLDM/BMDV test coupons. Ideally, each of the thirty coupons should have the same material obtained from the same production date and reflowed at the manufacturing facility.

Unfortunately, due to supply limit, there were two lots of materials obtained for the phenolic-cured test coupons with SLDM. One lot (Phenolic-SLDM-Lot 1) contained ten test coupons that were reflowed at the lab facility and had a different date code than the other twenty coupons (Phenolic-SLDM-Lot 2) which were reflowed at the manufacturing facility.

Table 3-1: List of materials properties for DICY-cured and phenolic-cured test coupon

	DICY-cured	Phenolic-cured
Resin system	Phosphorus doped, SiO_2, and $Al(OH)_3$	Phosphorus doped, SiO_2, and $Al(OH)_3$
T_g (°C, DSC)	149	150
z-CTE before T_g (ppm/°C)	38-46	30-50
z-CTE after T_g (ppm/°C)	206-238	200-230
T-260 (min)	7	>60
T-280 (min)	0.3	>40
T_d (°C, TGA)	339 (1%) 359 (2%) 394 (5%)	350 (% n.a.)

3.3 Equipment set-up

Four major pieces of equipment were needed for a test run: an environmental chamber (SL-2CA), a power supply/electrometer (Keithley 6517A Electrometer / High Resistance Meter), a switch system (Keithley 7002 Switch System), and a computer installed with LabView and Microsoft Access, as shown in Figure 3-8.

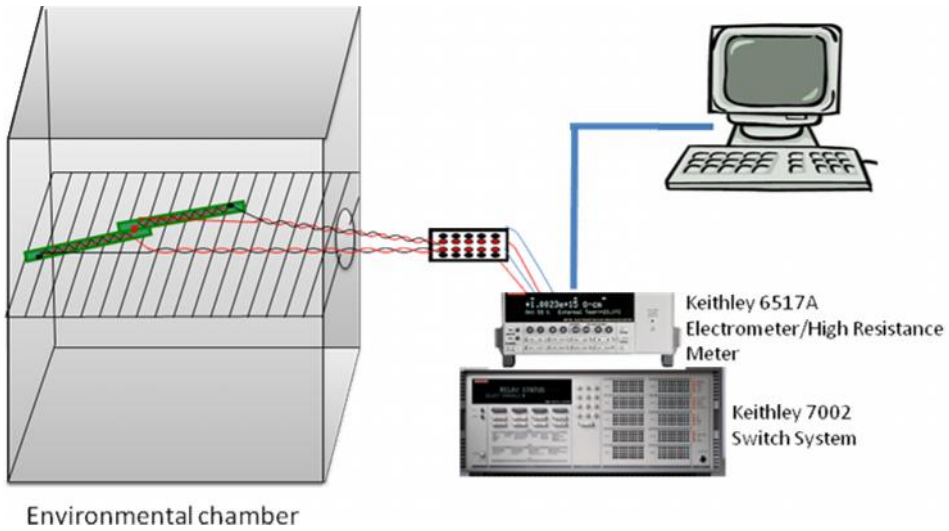

Figure 3-8: Illustration of main equipments setup for CAF test.

Once the test coupons were wired to the switch boxes (details of the wiring process is explained in Section 3.5), the coupons were placed inside an environmental chamber, and an electrical continuity test was run to ensure that the test coupons were properly connected to the CAF tester (the Keithley 6517A Electrometer/High Resistance Meter and Keithley 7002 Switch System).

The coupons were pre-conditioned in the chamber for 4 hours at a temperature of 85 °C and RH of 85% for stabilization, with no voltage applied. These temperature and RH setups were maintained during the entire test. After the pre-conditioning process, a bias voltage (128V for SLDM, and 200V for BMDV) was supplied to all test coupons for 30 minutes using a Keithley 6517A Electrometer/High Resistance Meter. After 30 minutes the voltage supply would be terminated temporarily and followed by a measurement phase that used the Keithley 7002 Switch System to switch one coupon/reference resistor at a time for 20 seconds to obtain a resistance reading.

At this measurement phase, a LabView software program analyzed the resistance readings. If the measured resistance was above 10^{14} ohms or below 10^{6} ohms, it would terminate the bias voltage to that particular coupon (failed) for the rest of the test period. A voltage supply period would be resumed after the measurement phase and so on for passing coupons. Details of the equipments and parameters used are shown in Table 3-2.

Because the rate of failures were different for the SLDM and BMDV, the total measurement time would vary depending on the number of the surviving coupons. For example, on the tenth day of the test, 50 SLDM coupons survived and 20 BMDV coupons, the total measurement time would be about 17 minutes for SLDM and 7 minutes for BMDV.

Due to the difference in measurement time, the analysis for time-to-failure will only account for the total bias voltage supplied time but not the total bias voltage supplied time plus the measurement time. At the end of the test run, the power supply was terminated and the environmental chamber was dehumidified and then was cooled down gradually to prevent condensation on the samples.

Unfortunately, while testing coupons with SLDM, there was a power outage that lasted for about 22 hours on the 41th day of experiment. All the equipment shut down at the bias time of 504.5 hours. The test coupons were inspected inside the chamber, and

no abnormalities were observed. The CAF test was restarted with the same initial settings such as pre-conditioning, bias and measurement cycles, 85 ºC and 85% RH, and the cooling down cycle mentioned earlier.

Table 3-2: Details of parameters set up for the equipments (environmental chamber, Keithley 7002 Switch System, Keithley 6517A Electrometer/High Resistance Meter, and Computer) for CAF test.

Equipments	Parameters/settings
Environmental Chamber (SL-2CA)	1. Before the test started to run, test coupons were electrically wired to the test equipment and then placed inside the chamber for 4 hours to reach the equilibrium condition of 85 °C and RH of 85% 2. 85 °C and RH of 85% were maintained until all the samples failed or 60 days was reached 3. After each test was finished, the chamber was gradually cycled down to a % RH of 25% and 25 °C before removing the samples to avoid water condensation on the samples
Keithley 7002 Switch System	1. Switched the power supply on/off to the test coupons a. Based on a pre-set measurement sequence, the Switch System would turn power on for a given test coupon for a 20 second resistance measurement b. Permanently terminated test coupons that had a resistance detected to be above 10^{14} ohms or less than 10^{4} ohms 2. Currently a maximum of 80 coupons can be connected
Keithley 6517A Electrometer/High Resistance Meter	1. During the measurement cycle: 100 V was applied to measure each test coupon every 20 seconds. The total measurement time would vary during testing based on the number of coupons that survived to that particular point 2. While not measuring resistance: 128 V was applied to laser-drilled microvias, and 200 V for mechanically drilled vias for thirty minutes to induce CAF formation
Computer/interface	1. Parameters setup in LabView: a. Lower resistance limit: 10^{4} ohms b. Upper resistance limit: 10^{14} ohms c. Bias: 128 V for laser-drilled vias, and 200V for mechanically drilled vias d. Bias duration: 30 minutes e. Measurement voltage: 100 V f. Measurement duration: 20 seconds for each test coupon 2. Data analysis using Microsoft Access

Since surface dendrite formation is a competing mechanism with CAF formation in the test coupons; condensation of water vapor on the surface had to be avoided. Three methods were used for preventing dendrite formation. The first method was to ensure that the coupons were placed above the wires; thus, no water droplets flowed back to the test coupons. The second method was to tape K-Pak bags on the window (for monitoring the chamber) with thermal tape, so that water could not splash from the chamber window to the coupons. The final method was implemented once all the samples failed/reached 60 days. This included terminating the bias voltage supply, and gradually cooled down the environmental chamber to RH of 25% and a temperature of 25 °C, never going below the dew point.

Table 3-3 summarizes the materials, coupon structure, and parameters used for testing the SLDM and BMDV. Most of the settings for the two tests were the same, except that the bias voltage was 128 V for the SLDM and 200 V for the BMDV. This difference in voltage supply ensured that the same voltage gradient (0.4 V/μm) was applied to both via structures. For example, the laser-drilled vias with a wall-to-wall spacing of 320 μm and an applied voltage of 128 V will generate a voltage gradient of 0.4 V/μm for testing. At the same time, a 200 V applied to a wall-to-wall distance of 500 μm would provide the same voltage gradient 0.4 V/μm for BMDV.

Table 3-3: List of test coupon dimensions and testing conditions.

Tests	Samples	Via structure	Dimension	Conditions/testing parameters
1st test	30 DICY-cured	Surface laser-drilled microvia (SLDM)	• Center to center: 400 µm • Via diameter: 80 µm • Pad diameter: 250 µm • Edge to edge (pad): 150 µm • Edge to edge (drill): 320 µm	• Pre-conditioning: 4 hours • Temperature: 85 °C • RH: 85% • Duration for bias supply: 30 mins • Voltage bias: 128 V for laser drilled vias, and 200 V for mechanically drilled vias • Voltage gradient of 0.4V/µm was maintained for both SLDM and BMDV • Measurement voltage: 100V at a rate of 20 seconds for each test coupon/reference resistor • Measurement time: 20 seconds / coupon • After 60 days, the chamber was slowly cooled down to RH of 25% and temperature of 25 °C
	30 phenolic-cured			
2nd test	30 DICY-cured	Buried mechanically drilled via (BMDV)	• Center to Center: 800 µm • Via diameter: 200 µm • Pad diameter: 500 µm • Edge to Edge (pad): 300 µm Edge to Edge (drill): 500 µm	
	30 phenolic-cured			
Note: 1. Four reference resistors were used in each run.				

3.4 Tester verification process

In addition to the 60 coupons that were tested in each run, four reference resistors were used as controls. There were two 2.8 M ohm resistors, one 28 M ohm resistor, and one 2.8 G ohm standard resistor used while running the test for SLDM to test the stability and functionality of the tester during the entire testing period (60 days). Three 2.8 M ohm resistors and one 2.8 G ohm resistor were used for the BMDV samples.

These resistors were wired the same way as the test coupons, and they were measured in sequence with the testing coupons but were not placed inside the environmental chamber. If the resistance readings were consistent and did not have a dramatic increase or decrease, the tester was functioning properly.

3.5 Sample preparations

Before the test coupons were placed into the environmental chamber for testing, they were wired to the CAF tester (the Keithley 6517A Electrometer/High Resistance Meter and Keithley 7002 Switch System). Figure 3-9 illustrates the wiring process.

All test coupon boards were reflowed before evaluation, and then cut into separate 0.6 cm x 6.5 cm coupons using the ALLIED Electrical Saw. The samples were then cleaned with deionized water to remove dirt from the cutting process. Finally, a desktop heater was used to dry the samples for 30 mins.

Two twisted wires were used to electrically connect a test coupon to the switch on the switch box using lead-free solder (SAC 305), and two shielded wires connected the same switch to the CAF tester. During soldering, a K-pak bag was used to cover the top surface of a test coupon, in order to avoid flux contamination.

One twisted wire (colored red) was electrically connecting the anode of the test coupon to the banana plug (positive charge) of the switch. Another twisted wire (colored black) was connecting the cathode of the test coupon to the BNC connector (negative charge) of the same switch. The banana plug was the positive electrode of the power supply, and the BNC connector was the negative charge of the power supply as explained in Section 3.1. The twisted wires used for connections were single-strand ALPHA WIRE (22 AWG SOLID). Moreover, each switch box was wired with a 1 mega-ohm resistor to limit the maximum current of the circuit.

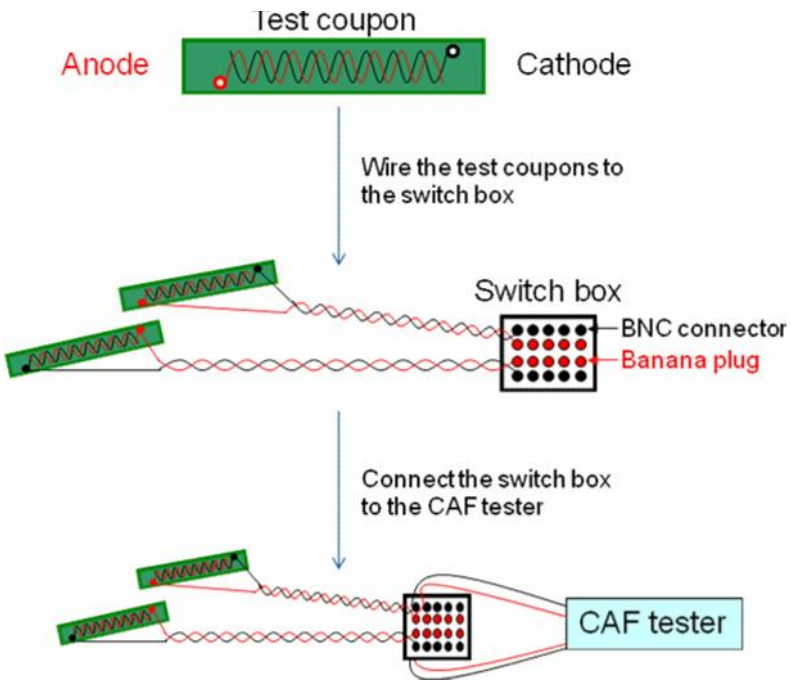

Figure 3-9: Simplified sample preparation procedures.

The wires used to connect the coupons to the switch box were twisted, and the wires that connected to the CAF tester were shielded. The purpose of twisting and shielding the wires was to achieve minimal electrical interference. This practice was important because a high insulation resistance (low current signal) was being measured during the test, and the measurements would be sensitive to noise. After the samples were connected to the CAF tester, an electrical continuity test using a multi-meter was used to verify that all coupons were connected electrically to the CAF tester before starting a 60 day CAF test.

In the above setup, a maximum of ten coupons could be connected to one switch box which contained ten switches. The current CAF tester could accommodate up to eight switch boxes, which was equivalent to 80 test coupons. However, this system is able to expand to accommodate up to 400 test coupons if additional equipment is installed.

3.6 Data analysis

In order to compare the reliability of the tested materials and structure, a few statistics tools such as mean-time-to-failure (MTTF) and Weibull distribution were used.

MTTF is a commonly used reliability parameter for non-repairable test coupons in the electronics industry. The formula for MTTF is

$$\text{MTTF} = \frac{\text{total number of samples tested * bias time}}{\text{total number of failed samples}} \quad \text{.....(3.1)}$$

Since the failure rates were not constant for the test coupons, a Weibull function [66 and 67]

$$\ln\left[\ln\left(\frac{1}{1 - F(t)}\right)\right] = \beta \cdot \ln t - \beta \cdot \ln\alpha \quad \text{.....(3.2)}$$

was used to study the distribution of failure time. t is the time-to-failure (bias time) for each coupon, β is the slope or the shape parameter and α is the scale parameter of the Weibull plot. β and α can be calculated using the Analysis ToolPak Add-In function in Excel. The cumulative distribution function (cdf), F(t), can be estimated by median rank using the formula

$$F(t) = \frac{i - 0.3}{N + 0.4} \quad \text{.....(3.3)}$$

where i is the ranking of the failures, N is the total number of tested samples. [66] If the data are fitted into a straight line in the Weibull probability graph, it indicates that the failure follows a Weibull distribution. Details of the calculation can be found in Appendix A.

3.7 Verification of failure modes

In order to find out the causes of failures, it is important to identify the location of failure sites and then verify the compositions. The failure sites were identified through electrical continuity tests using a microprobing machine (Suss Micro Tech with test system GmbH), an optical microscopy (Olympus SZx7 with image analysis software Leica Application Suite), and cross-sectioning using standard metallographic methods for grinding and polishing.

The compositions of the failure sites were verified by using a Scanning Electron Microscopy (SEM), model JEOL JSM-6460LV, equipped with Energy-dispersive X-ray spectroscopy (EDX). The procedures for CAF detection in laser-drilled microvias and buried mechanically drilled vias were not the same due to the differences in via layout.

3.7.1 Surface laser-drilled microvias

Due to the large number of vias on a daisy chain (anode/cathode) and the use of a multi-layer PCB; it was a challenge to locate CAF. An alternative method was adopted to detect CAF.

This alternative method required that the solder mask to be removed so that the probes of a microprobing machine could reach the vias (copper pad) directly and measure the electrical resistance. The solder mask remover used in this research was Magnastrip 600 HF. The solution was heated up to 75 °C and test coupons were then placed in the solution for 35 minutes. The coupons were then rinsed with deionized water to remove the solder mask residues on the surface.

The adopted method included the use of a microprobing machine and careful cutting out of certain copper traces on the daisy chain to identify the specific CAF location. The sample was then mounted using Struers SpeciFix Resin and SpeciFix-40 Curing Agent for cross-sectioning in order to allow the use of SEM and EDX to verify the chemical composition.

Since the vias were located linearly along a daisy chain, individual vias could be isolated by disconnecting the copper traces between vias. For example, as shown in Figure 3-10, copper traces on point A, B, and C were removed first, and then followed by point D and E. This procedure could allow fast identification of CAF sites among 1036 possible CAF sites.

By using a microprobing machine connected with a mega ohmmeter, the resistance between AC and CB were measured, and AC would indicate a lower resistance (CAF site) than the resistance between BC. In order to narrow down the search for the CAF site, copper traces at E and D were disconnected. The resistance between CE would be lower than ED. The same method would be applied until the exact CAF location was identified.

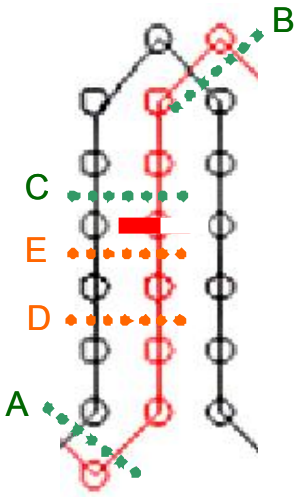

Figure 3-10: Direction of cross-sectioning a test coupon with SLDM to identify CAF grown from the anode.

After the CAF site was identified, cross-sectioning was required. Since CAF grows from the anode to the cathode, the direction for polishing the cross-section should be from the cathode towards the anode as shown in Figure 3-11. After cross-sectioning, SEM with EDX would be used to identify the compound as containing Cu, Cl, and O.

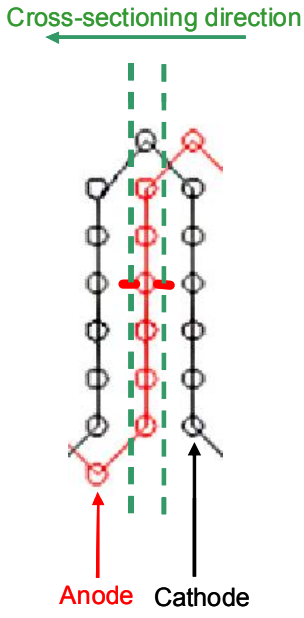

Figure 3-11: Cross-sectioning direction for SLDM. Based on the fact that CAF grows from anode to cathode.

3.7.2 *Buried mechanically drilled vias*

Since the buried vias were located between layer 4 to 7 and CAF was predicted to form between the closest distance between a pair of vias, the cross-sectioning procedure was relatively easier. As shown in Figure 3-12, the cross-section plane would be sufficient to capture any CAF formation among the 36 via pairs.

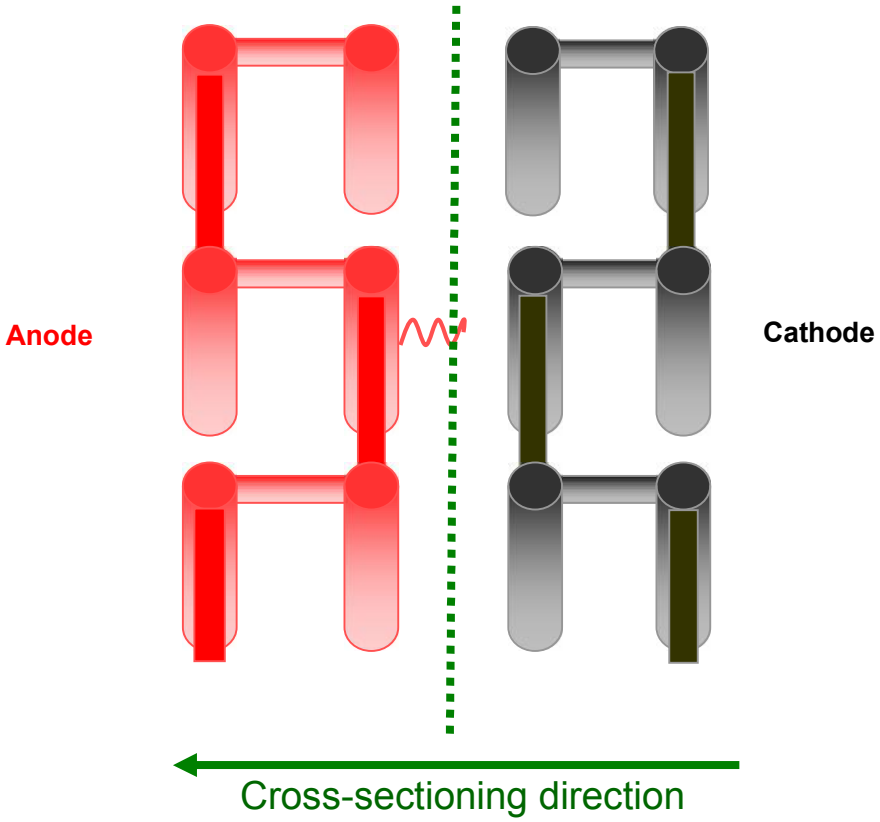

Figure 3-12: Directions of cross-sectioning a test coupon with BMDV. Based on the fact that CAF grows from anode to cathode

3.8 Summary

This chapter has detailed descriptions of the procedures for testing the coupons, the parameters used for equipment setup, the tester verification method, the data collection and analysis methods, and the failure sites identification and chemical composition verification techniques etc. The next chapter will present the results such as insulation resistance measurements, SEM-EDX images of CAF, and Weibull plots obtained from the experiment.

Chapter 4

Results

This chapter will summarize the insulation resistance readings obtained from electrical testing of four materials and test structure combinations: DICY-SLDM, Phenolic-SLDM, DICY-BMDV, and phenolic-BMDV. Moreover, it will present the optical and SEM-EDX images of the failure site for CAF verification purposes.

For naming convenient, the following abbreviations will be used for a combination of curing agent and drilling method system.

Abbreviations		Descriptions
DICY-SLDM	--	DICY-cured test coupons with SLDM
DICY-BMDV	--	DICY-cured test coupons with BMDV
Phenolic-SLDM	--	Phenolic-cured test coupons with SLDM
Phenolic-BMDV	--	Phenolic-cured test coupons with BMDV

4.1 Tester verification

4.1.1 Surface laser drilled microvias (SLDM)

Four reference resistors (two 2.8 M ohm resistors, one 28 M ohm resistor, and one 2.8 G ohm resistors) were tested at the same time when the test coupons with surface laser drilled microvias were tested. The average resistance readings and % difference from standard indicated by the manufacture are shown in Table 4-1.

Table 4-1: Resistance readings from reference resistors before and after power outage at t_B = 504.5 hours for SLDM in units of ohms.

Resistors	Standard resistance (ohms)	Average resistance measured before t = 504.5 hrs (ohms)	% difference from standard	Average resistance measured after t = 504.5 hrs (ohms)	% difference from standard
Ref. box - 1	2.8 M	2.76 ± 0.000 M	-1.4 %	2.96 ± 0.000 M	5.7 %
Ref. box - 2	2.8 M	2.96 ± 0.000 M	5.7 %	2.94 ± 0.000 M	5.0 %
Ref. box - 3	2.8 G	2.85 ± 0.000 G	1.8 %	3.08 ± 0.001 G	10 %
Ref. box - 4	28 M	27.9 ± 0.003 M	0.4 %	29.9 ± 0.002 M	6.9 %

The resistance readings for all reference resistors were stable during the entire test period (t = 681 hours) except at bias time equal to 504.5 hours when the resistance readings showed a small increase in value. This event corresponded to the time of power outage that occurred during the test on the 41th day and lasted for about 22 hours. Nonetheless, the % differences of resistance readings from the standards indicated by the manufacturer for all the reference resistors were all within 10% tolerance.

4.1.2 Buried mechanically drilled vias (BMDV)

Four reference resistors (three 2.8 M ohm resistors and one 2.8 G ohm resistor) were tested at the same time when the test was running for test coupons with BMDV. Table 4-2 indicates the average resistance measured and % difference from standard.

The reference resistors also had a stable insulation resistance readings over the entire test period of 60 days. Finally, for both the SLDM and the BMDV test, the % difference was the highest (10%) for the highest reference resistor (2.8 G). This was expected as the highest the resistance the more susceptibility it is to electrical interferences.

Table 4-2: Resistance readings from reference resistors for BMDV in units of ohms

Resistors	Standard resistance as indicated by the manufacturer	Average resistance measured	% difference from standard
Ref. box - 1	2.8 M	2.96 ± 0.000 M	5.7 %
Ref. box - 2	2.8 M	2.99 ± 0.000 M	6.8 %
Ref. box - 3	2.8 G	3.08 ± 0.001 G	10 %
Ref. box - 4	2.8 M	2.98 ± 0.000 M	6.4 %

4.2 Analysis for insulation resistance readings

For convenience, Table 4-3 summarizes the numbering system for each test coupon to differentiate the test structure and curing agents used. Coupons #101 to #110 were obtained from a different board lot (phenolic-SLDM-Lot 1) than Coupons #111 to #130 (phenolic-SLDM-Lot2). Figures 4-1 to 4-4 illustrate the insulation resistance (IR) readings for DICY-cured and phenolic-cured test coupons with SLDM and BMDV.

There were two coupons (Coupon #26 and #126) labelled in red in Figure 4-3 and Figure 4-4 that needed to be excluded in data analysis as the initial IR readings were too high (10^{12} ohms) or too low (10^{6} ohms). These abnormal IR readings indicate that there were defects in these coupons and they should not be used for CAF testing. The y-axis in the figures are the Log values of resistance and the x-axis is the bias time (t_B) in hours. The total bias time for SLDM was 680 hours which was less than the 1116 hours for BMDV.

The difference in total t_B was due to the variation in measurement time (t_M) during the 60 day test period even though each bias time was constant (30 mins). There were a total of fifty samples with SLDM that survived in comparison to only seventeen that survived for BMDV at t_B = 500 hours. Therefore, t_M was decreased from 18 mins for SLDM to 7 mins for BMDV (including four reference resistors).

The failed samples had a sudden drop of resistance to below 10^{6} ohms or increased above 10^{14} ohms. The sudden drops of resistance (short circuits) were anticipated, because CAF is a semi-conductive salt and the resistance decreased as CAF grew closer to the cathode. On the other hand, the open circuits occurred only on the test coupons with BMDV were not expected at the time of testing. However, by analyzing the test

coupons using optical microscopy and SEM-EDX, it was then verified that all the open circuits were also caused by CAF formation.

In discussions with the equipment supplier, it was noted that there was a pre-set maximum current allowance (10 mA) for each test coupon to prevent damage to the CAF filament. Using Ohm's Law, the lowest resistance that could be measured was 10 k ohms; therefore, if the insulation resistance was lower than 10 k ohms but not shorted, the current supply to that particular test coupon would be terminated and read as an open circuit instead of a short circuit. This inaccurate resistance display is being modified currently.

Table 4-3: Numbering system for all test coupons.

Coupon #101-110 were from a different board lot and were reflowed at the laboratory facility.

Surface laser drilled microvias (SLDM)		Buried mechanically drilled vias (BMDV)	
DICY-cured	Phenolic-cured	DICY-cured	Phenolic-cured
#1	**#101**	B1	B101
#3	**#102**	B2	B102
#4	**#103**	B3	B103
#5	**#104**	B4	B104
#6	**#105**	B5	B105
#7	**#106**	B6	B106
#10	**#107**	B7	B107
#11	**#108**	B8	B108
#13	**#109**	B9	B109
#14	**#110**	B10	B110
#15	#111	B11	B111
#16	#112	B12	B112
#17	#113	B13	B113
#18	#114	B14	B114
#19	#115	B15	B115
#20	#116	B16	B116
#22	#117	B17	B117
#24	#118	B18	B118
#25	#119	B19	B119
#26	#120	B20	B120
#27	#121	B21	B121
#28	#122	B22	B122
#29	#123	B23	B123
#30	#124	B24	B124
#31	#125	B25	B125
#34	#126	B26	B126
#35	#127	B27	B127
#36	#128	B28	B128
#37	#129	B29	B129
#38	#130	B30	B130

4.2.1 Graphic illustration of insulation resistance readings

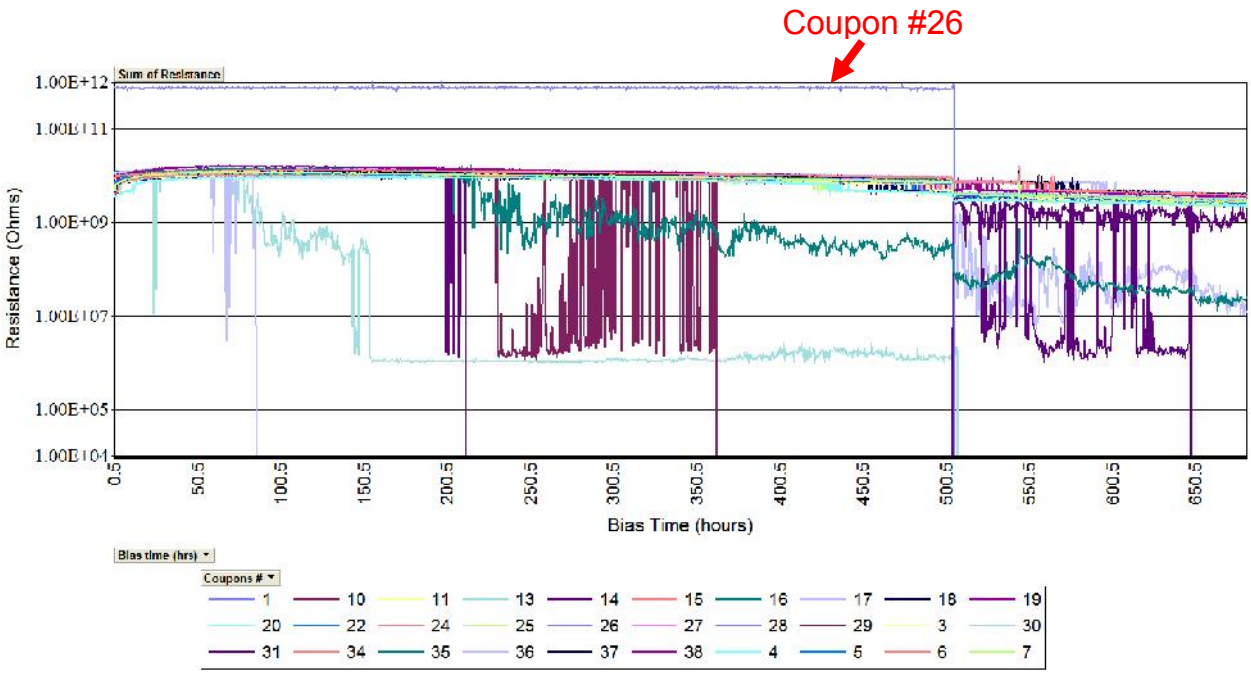

Figure 4-1: Resistance readings for the thirty DICY-cured test coupons with SLDM.

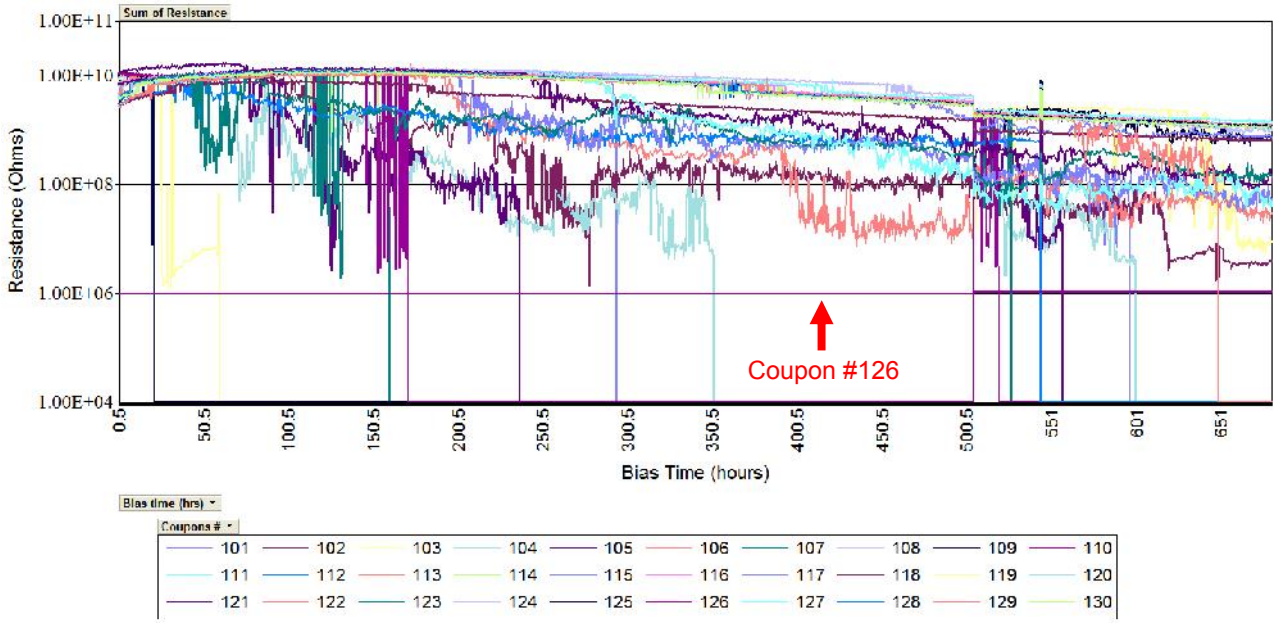

Figure 4-2: Resistance readings for the thirty phenolic-cured test coupons with SLDM

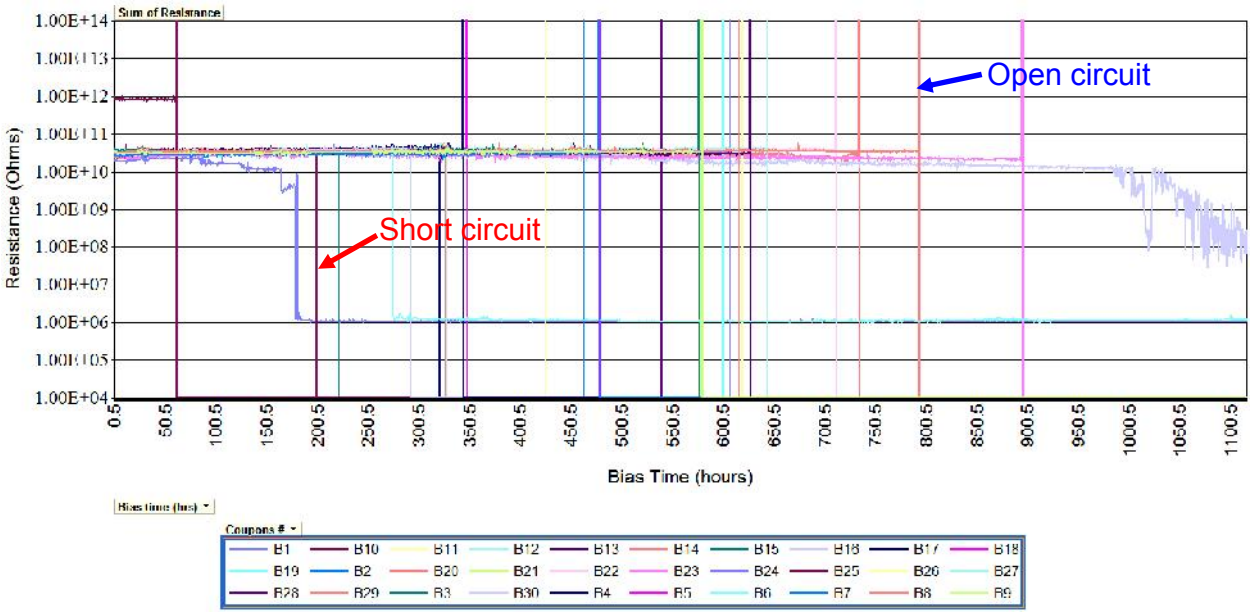

Figure 4-3: Resistance readings for the thirty DICY-cured test coupons with BMDV.

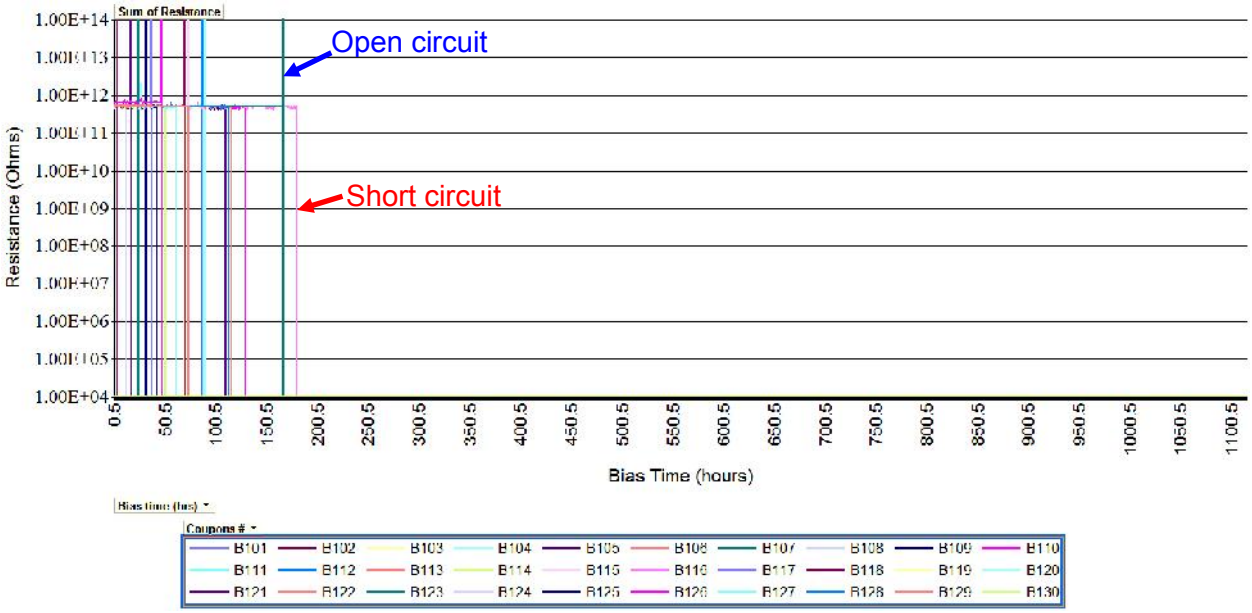

Figure 4-4: Resistance readings for the thirty phenolic-cured test coupons with BMDV.

It was noted that most of the failures (seven) for phenolic-SLDM were concentrated on one lot of the test coupons (Coupon#101 - #110) as shown in Figure 4-5, and only two failed in another lot of test coupons (Coupon#111-#130) as shown in Figure 4-6, therefore two set for data analysis were obtained for the phenolic-SLDM.

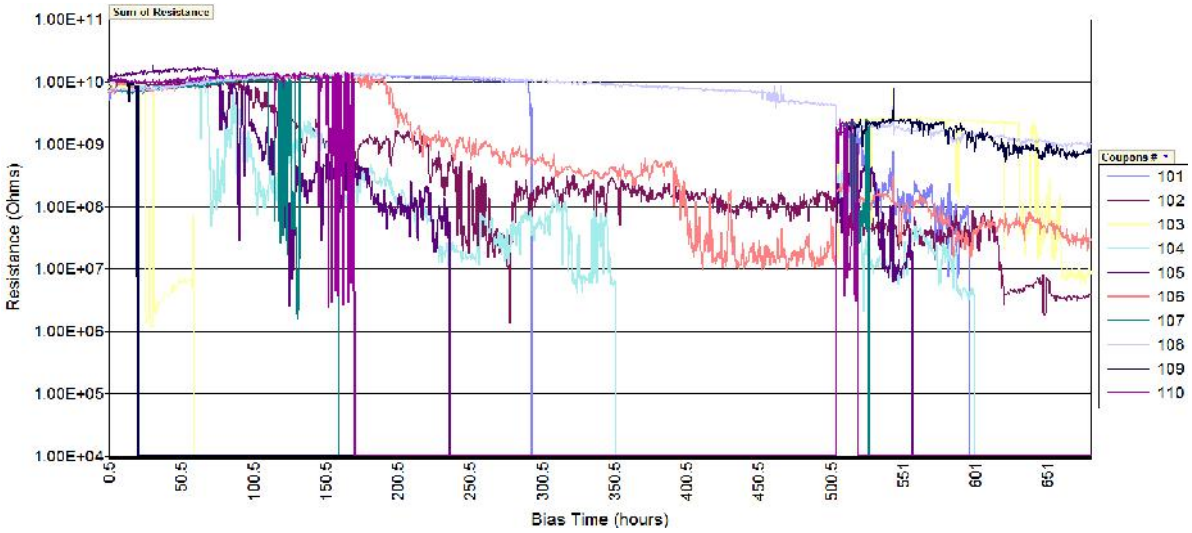

Figure 4-5: IR readings for ten phenolic - SLDM - Lot 1 test coupons #101-110

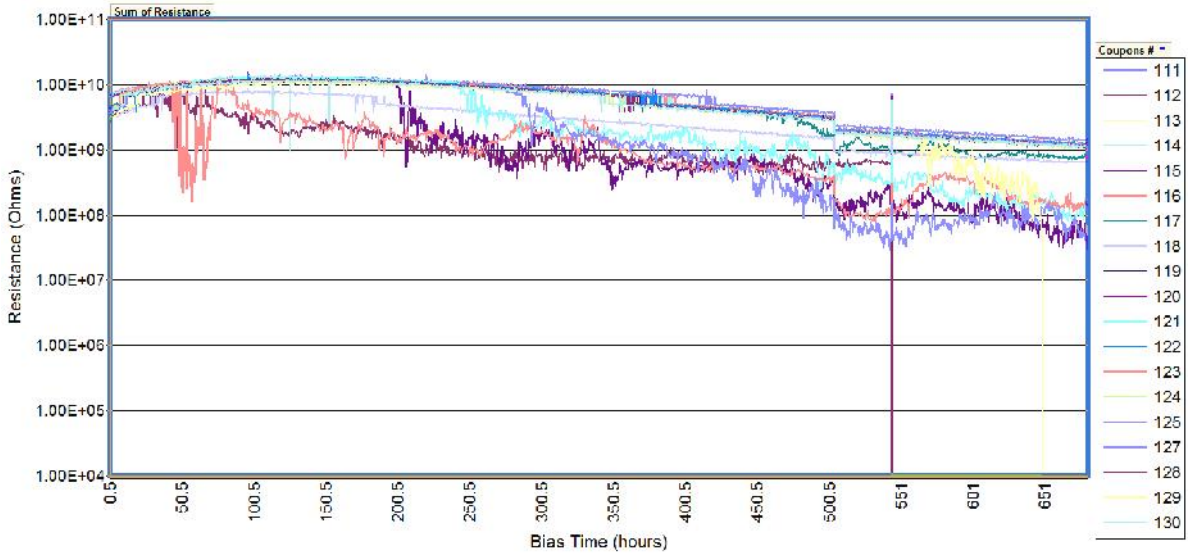

Figure 4-6: IR readings for twenty phenolic - SLDM - Lot 2 test coupons (Coupon #111-130)

4.2.2 Mean time-to-failure

On the 41th day of testing (t_B = 504.5 hrs) the coupons with SLDM, an unpredicted power outage lasting 22 hours occurred. There was a built-in backup power supply of 15 mins for the CAF tester after which it powered down, but no backup power supply for the environmental chamber.

Since the power outage was longer than 15 mins, to reinitiate the test, the environmental chamber was bought up to 85 ºC and 85% RH and allowed to stabilize. All the test coupons including the failed ones were tested again. Some of the originally failed coupons failed again after the test restarted but some did not. Table 4-4 summarizes the breakdowns of the numbers of failures that occurred before and after power outage for SLDM.

As shown in Table 4-4, the test coupons that failed before the power outage did not immediately fail again when the power was re-supplied. For example, for the three coupons (Coupon #17, 29, 31) that failed before the power outage, only coupon #31 failed again until the end of the test. The same phenomenon occurred for phenolic-cured coupons. Of the seven samples that failed before the power outage only five failed again.

Moreover, the order of failure was also not the same before and after the power outage. Table 4-5 summaries the number of failures for both SLDM and BMDV, first time-to-failure, and mean time-to-failure etc.

Table 4-4: Summary of coupons shorted/failed before and after power outage which occurred at t = 504.5 hrs for SLDM

	DICY-cured	Phenolic-cured
Coupons shorted Before t = 504.5 hrs	#17 ***#31*** #29	#109 #103 ***#107*** ***#110*** ***#105*** ***#101*** ***#104***
Coupons shorted after t = 504.5 hrs	#26 #13 ***#31***	***#110*** ***#107*** #112 ***#105*** ***#101*** ***#104*** #129
Coupons shorted before and after power outage	***#31***	***#107*** ***#110*** ***#105*** ***#101*** ***#104***
Total no. of shorts (eliminating repeated ones)	**5**	**9**

Table 4-5: Summary of failures as resistance dropped below 10^6 or above 10^{14} by analysing insulation resistance tested electrically

	Surface laser drilled microvias (SLDM)			Buried mechanically drilled vias (BMDV)	
	DICY-cured	Phenolic-cured (Lot 1)	Phenolic-cured (Lot 2)	DICY-cured	Phenolic-cured
Shorted @ t = 0	0	0	0	0	5
Shorts during testing	4	7	2	9	13
Opens during testing	0	0	0	20	12
Total Failed (electrically)	4	7	2	29	25
Total survived	25	3	17	1	0
First time-to-failure (hrs) (electrically)	86 (Coupon #17)	21 (Coupon #109)	544.5 (Coupon 112)	62 (Coupon B10)	3.5 (Coupon B102)
Mean time-to-failure (hrs)	4937	973	6470	1154	1116
Total bias time (hrs)	681	681	681	1116	1116
Total testing time	1440 hrs				
Total valid test coupons	29 (eliminating Coupon #26)	10	19 (eliminating Coupon #126)	30	25 (disregard five samples that were failed at t = 0)

4.2.3 *Weibull distribution*

Since the failure rate for CAF test was not constant; Weibull analysis was used to determine the distribution of failures instead of an exponential distribution model. A few criteria have to be considered for the Weibull analysis:

1. The time used for the analysis should be the total bias time (hours).
2. The sample set should only include coupons that had an initial resistance around 10^9 ohms.
3. The failed samples should exclude coupons that were found containing CAF but had not failed electrically.

Invalid coupons:

1. Coupon #26 (DICY-cured) had relatively high initial IR measurement of around 10^{12} ohms,
2. Coupon #126 (phenolic-cured) had exceptionally low initial IR readings of about 10^6 ohms,
3. Coupon B103, B104, B111, B113, and B130 (phenolic-cured) were shorted at t=0, but no CAF was found, and
4. Coupon B16 was not considered as a failed sample even though CAF was found, because the IR measurements were not below 10^6 ohms.

Four Weibull plots were constructed to compare the effect of curing agents and drilling methods on CAF formation. The plots are listed as follow:

1. Figure 4-7: demonstrates the effect of DICY-cured epoxy on SLDM vs. BMDV,
2. Figure 4-8: compares the effect of phenolic-cured epoxy on SLDM vs. BMDV,
3. Figure 4-9: shows the effect of DICY- vs phenolic-cured epoxy on SLDM,
4. Figure 4-10: illustrates the effect of DICY- vs. phenolic-cured epoxy on BMDV.

Finally, the total failed coupons and tested coupons for Weibull plot are shown in Table 4-6 with the Beta and Alpha values.

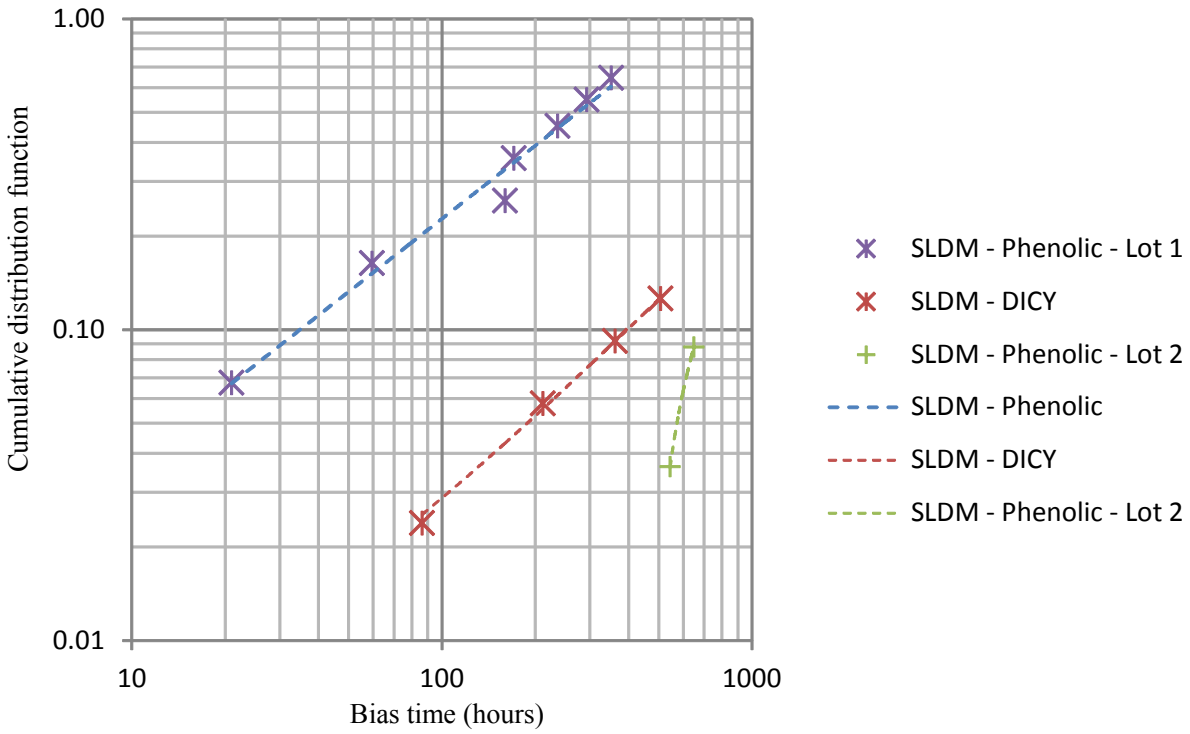

Figure 4-7: Weibull plot for DICY-cured (red) vs. phenolic cured (blue and green) test coupons with SLDM

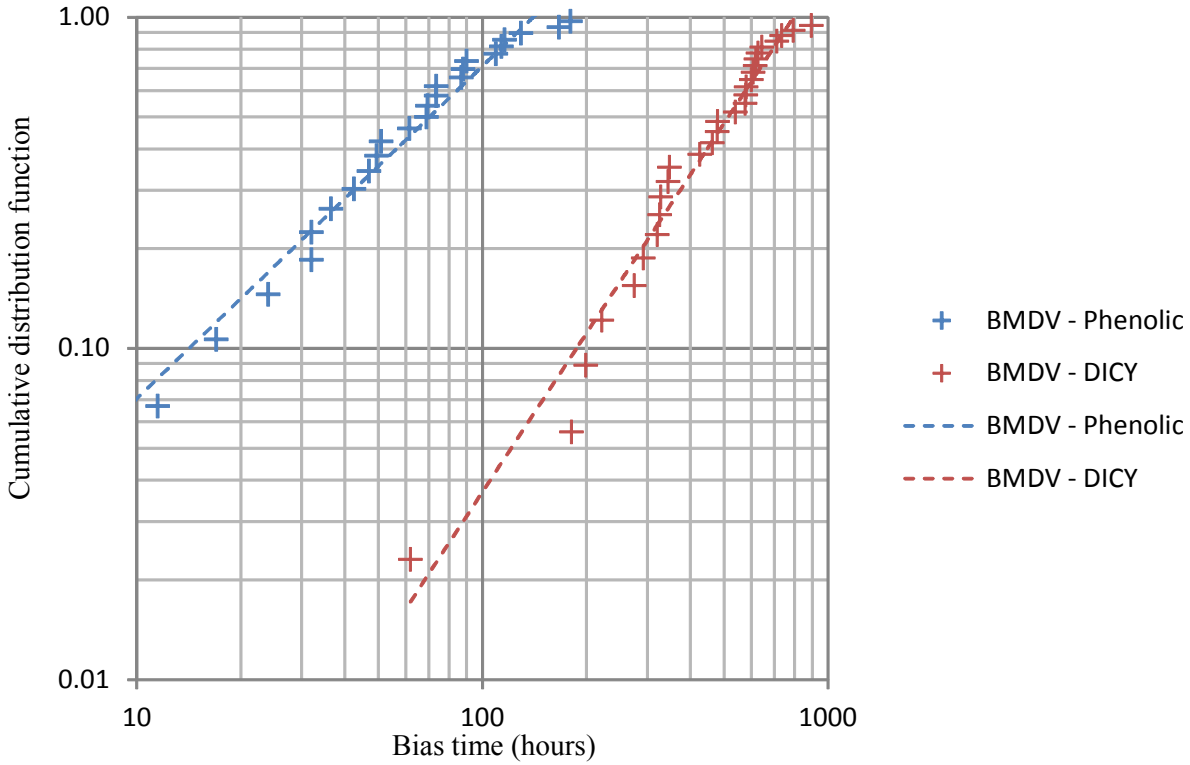

Figure 4-8: Weibull plot for DICY-cured (red) vs. phenolic-cured (blue) test coupons with BMDV

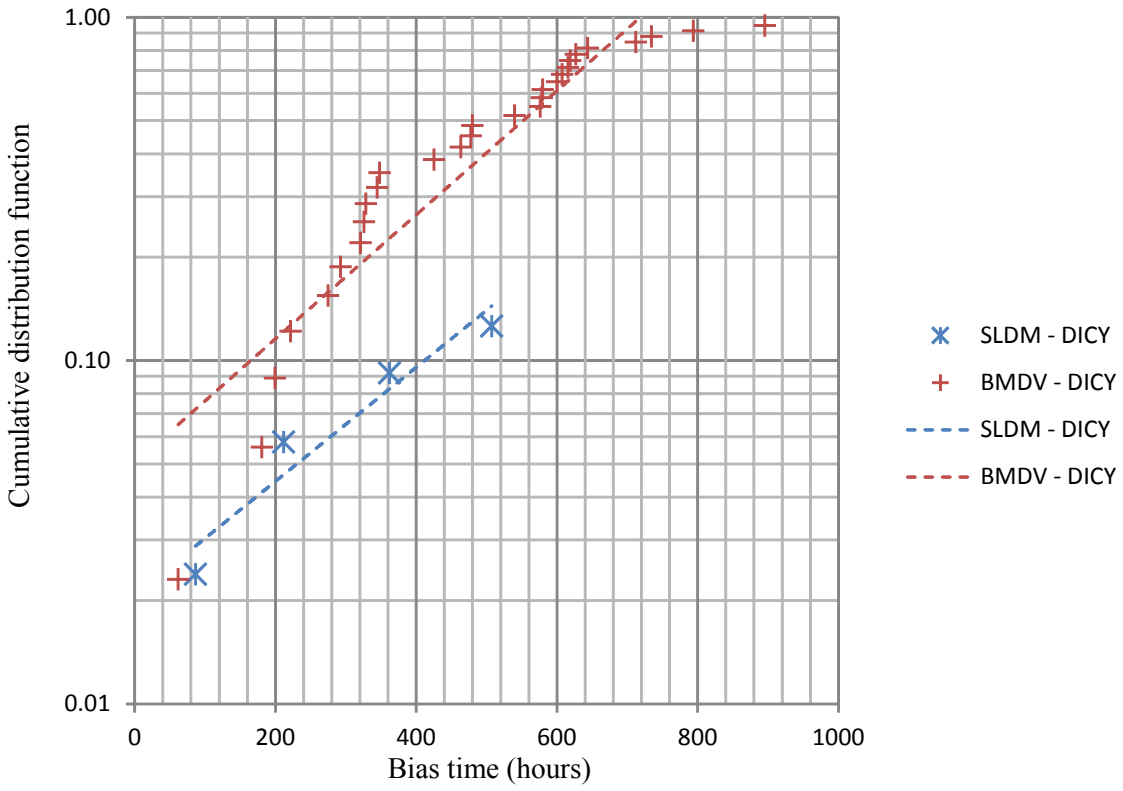

Figure 4-9: Weibull plot for DICY-cured test coupons with SLDV (blue) vs. BMDV (red)

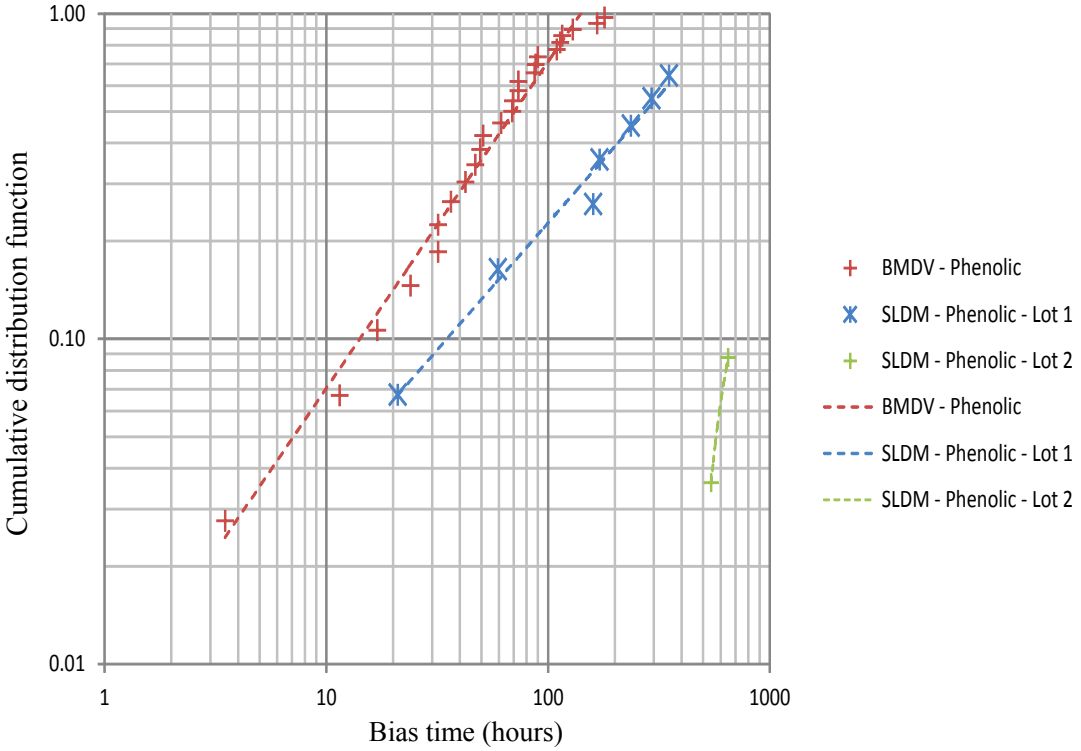

Figure 4-10: Weibull plot for phenolic-cured test coupons with SLDM (blue and green) vs. BMDV (red)

Table 4-6: Summary of beta and alpha values from Weibull analysis

	DICY - SLDM	Phenolic - SLDM		DICY - BMDV	Phenolic - BMDV
No. of tested coupons	29	10 (Lot 1)	19 (Lot 2)	30	25
No. of failed coupons	4	7	2	29	25
Beta	0.97	0.92	5.2	2.0	1.3
Alpha	4018	410	1030	576	4.4

4.3 Chemical compositions and via structure

The solder mask for DICY-cured test coupons (dark green) looked different from phenolic-cured solder mask (light green), therefore, Fourier transform infrared spectroscopy (FTIR) was used to identify its chemical compositions as shown in Figure 4-11. Both solder masks appeared to have the same chemical compositions. It was concluded that the difference in color could be due to the different in the thickness and/or the % of dye use in the solder mask.

Coupon B25 (DICY-BMDV) was used to illustrate the percentage of Cl and Cu around a CAF site. The highest Cl concentration (5.57 at%) was found right at the site where corrosion started, but decreased in the direction toward the cathode copper trace and conformal coating as shown in Figure 4-12 a, b and Table 4-7. In addition, Figure 4-13 is an EDX analysis for CAF found in Coupon B25 that contained elements (Cu, O, and Cl).

The interaction between the vias and glass fibers is an important parameter for contributing to CAF formation; therefore, cross-sections (top view) images of the SLDM and BMDV with glass fibers were taken as shown in Figure 4-14 and Figure 4-15. It is noted that SLDM have less glass fiber contact than BMDV, as the microvias have smaller diameter and do not directly align with the glass/fibers. On the other hand, BMDV have larger diameter and were directly drilled into the glass fibers.

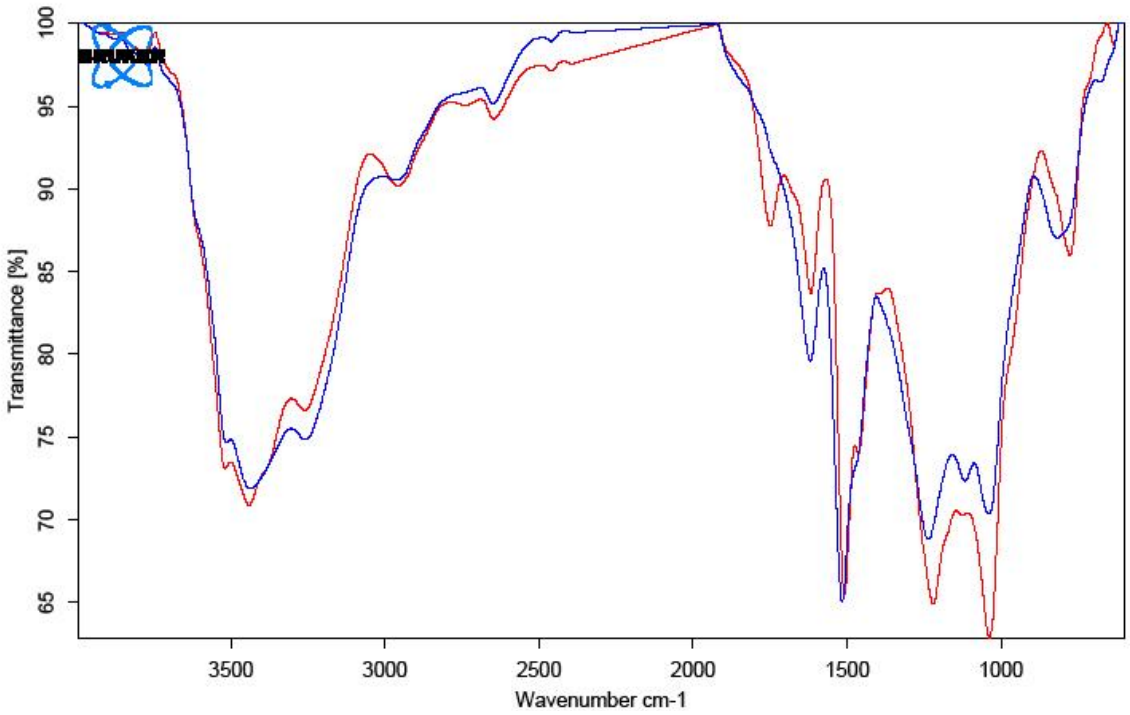

Figure 4-11: FTIR image of the solder mask used for DICY-cured test coupons. Solder mask on DICY-cured epoxy is highlighted in red; Solder mask on phenolic-cured epoxy is highlighted in blue.

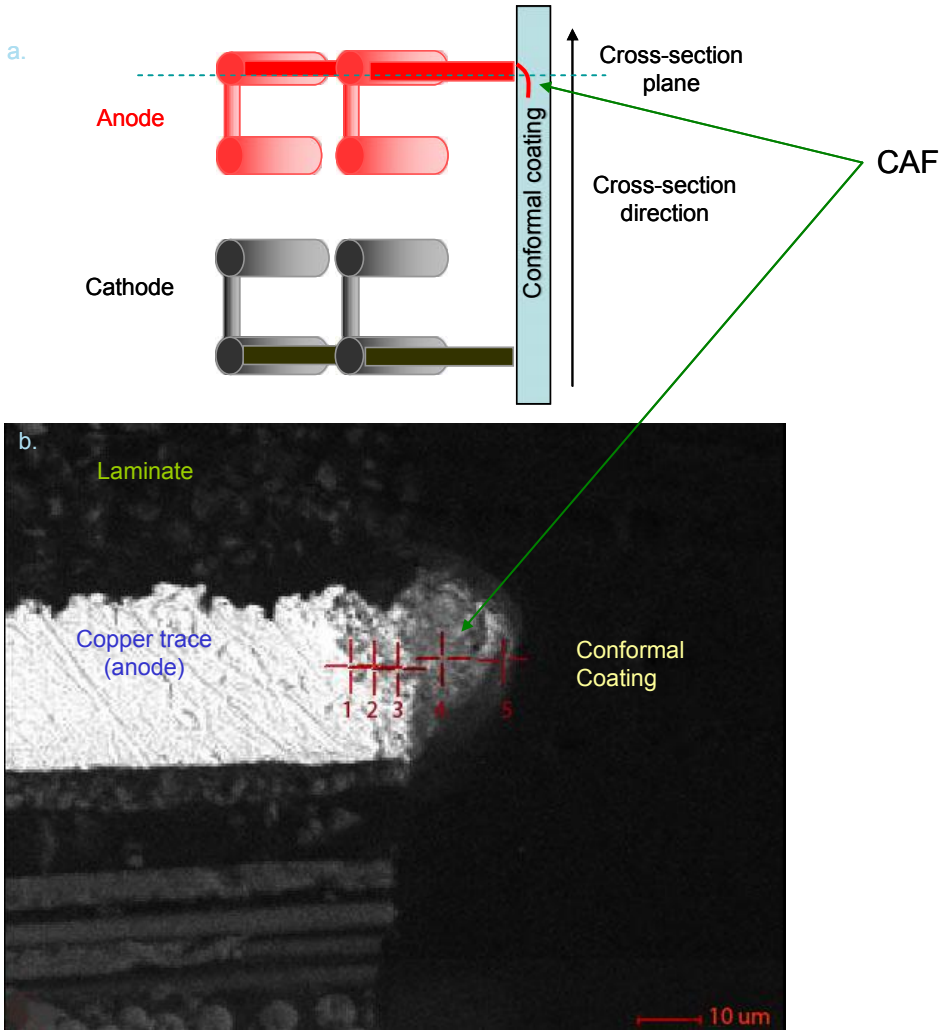

Figure 4-12: CAF site found in Coupon B25- CAF (a) top view and (b) side view.

Table 4-7: At% of Cu and Cl near the end of the copper trace (anode)

	Cl at%	Cu at%
1	1.13	29.86
2	4.68	21.93
3	5.57	18.19
4	4.84	16.72
5	0.51	6.96

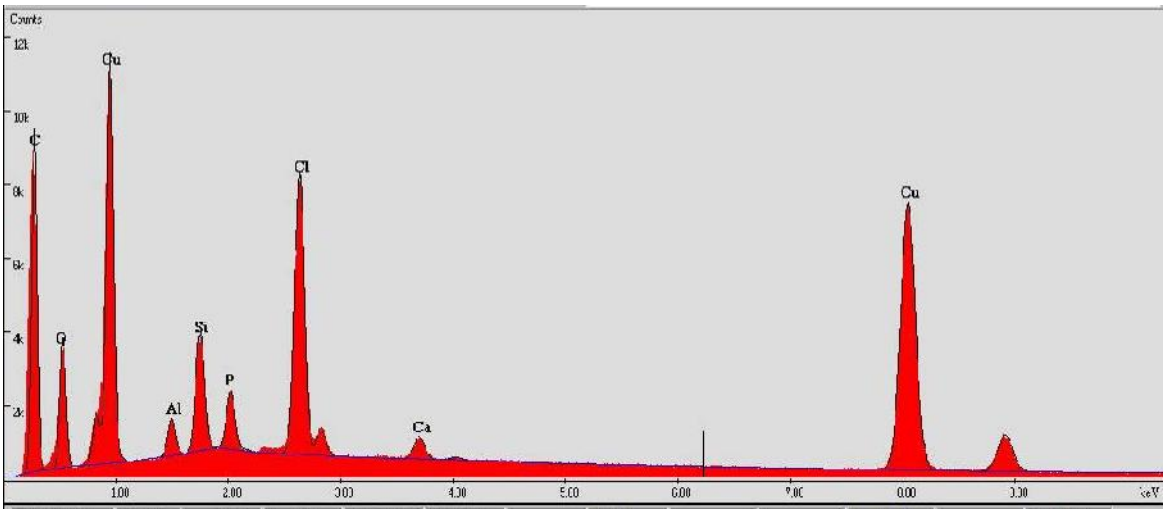

Figure 4-13: EDX spectra of test coupon B25 for identifying CAF containing (Cl, Cu, and O)

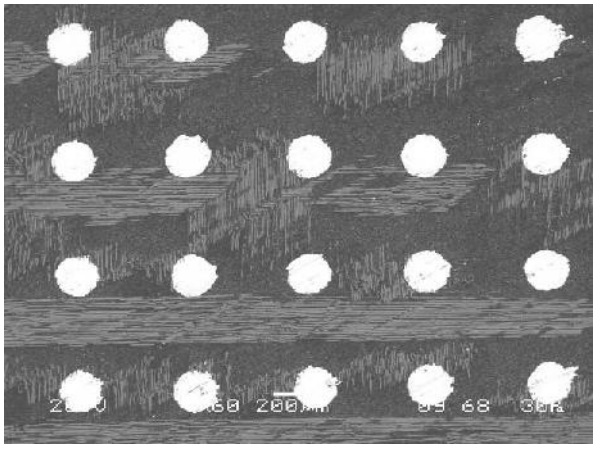

Figure 4-14: Cross-section of the SLDM (top view).

SLDM have less glass fiber contact, because some of the vias were located on the epoxy not the glass fibers.

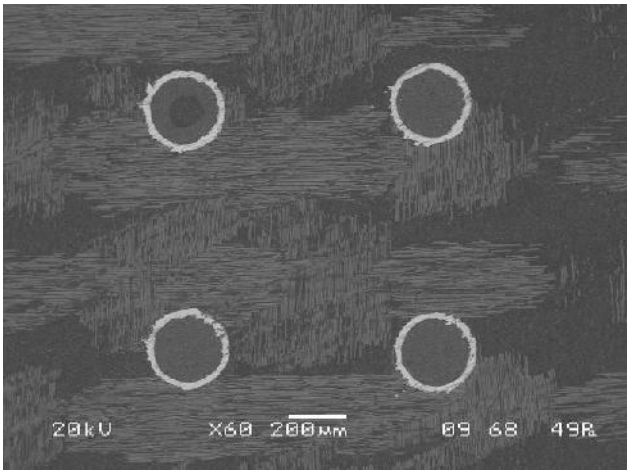

Figure 4-15: Cross-section of the BMDV (top view).

BMDV were drilled on the glass fibers; therefore, had more glass fiber contact.

4.4 Failure verifications

As stated in the IPC standard for testing CAF formation, insulation resistance readings only are not enough to verify the failures are caused by CAF. In order to verify the failures were caused by CAF, SEM-EDX was used to determine the chemical compositions of the failure sites.

4.4.1 SEM images of surface laser drilled microvias

Figure 4-16 and Figure 4-17 illustrate the possible CAF sites in DICY-SLDM using SEM-EDX; Figure 4-18 and Figure 4-19 for phenolic-SLDM. The Cl peaks were relatively small so it might indicate the CAF was found further away from the corroding anode. Moreover, not all of the test coupons that failed electrically showed CAF using SEM-EDX. This is not unexpected due to the large number of potential CAF sites on a given coupon.

4.4.1.1 DICY-cured test coupons

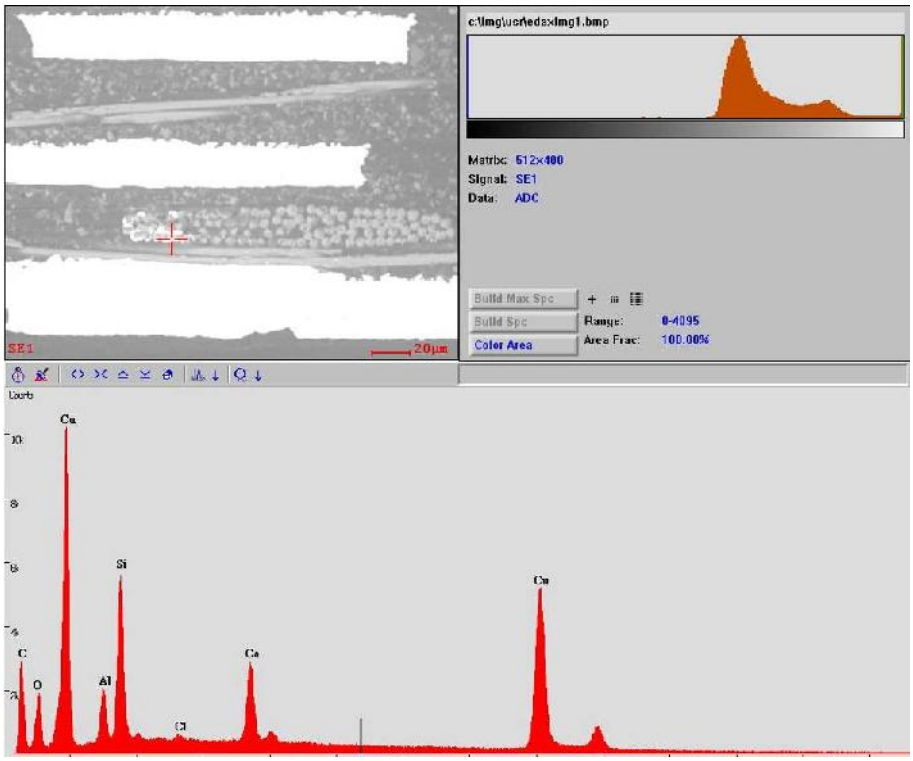

Figure 4-16: SEM-EDX image of test coupon #29

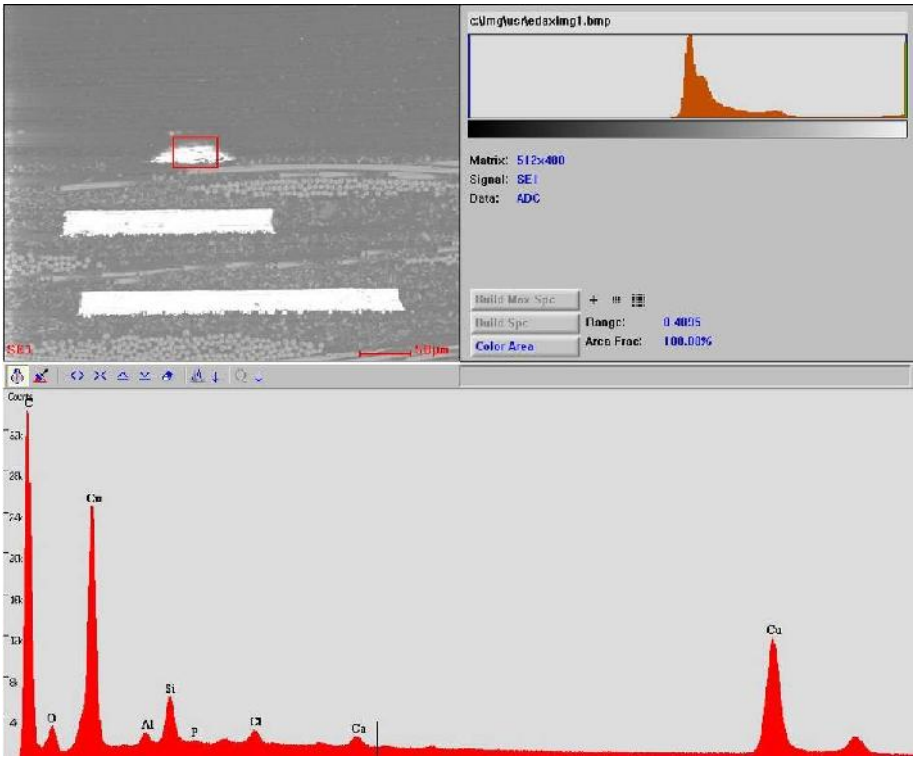

Figure 4-17: SEM-EDX image of test coupon #31

4.4.1.2 *Phenolic-cured test coupons*

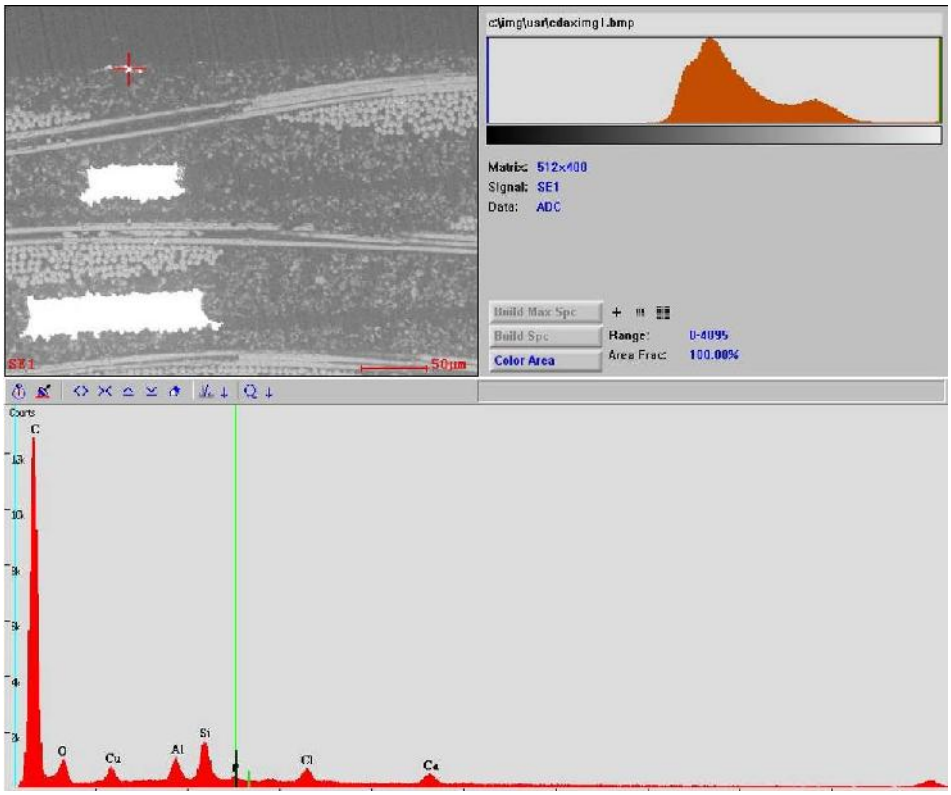

Figure 4-18: SEM-EDX image of test coupon #104

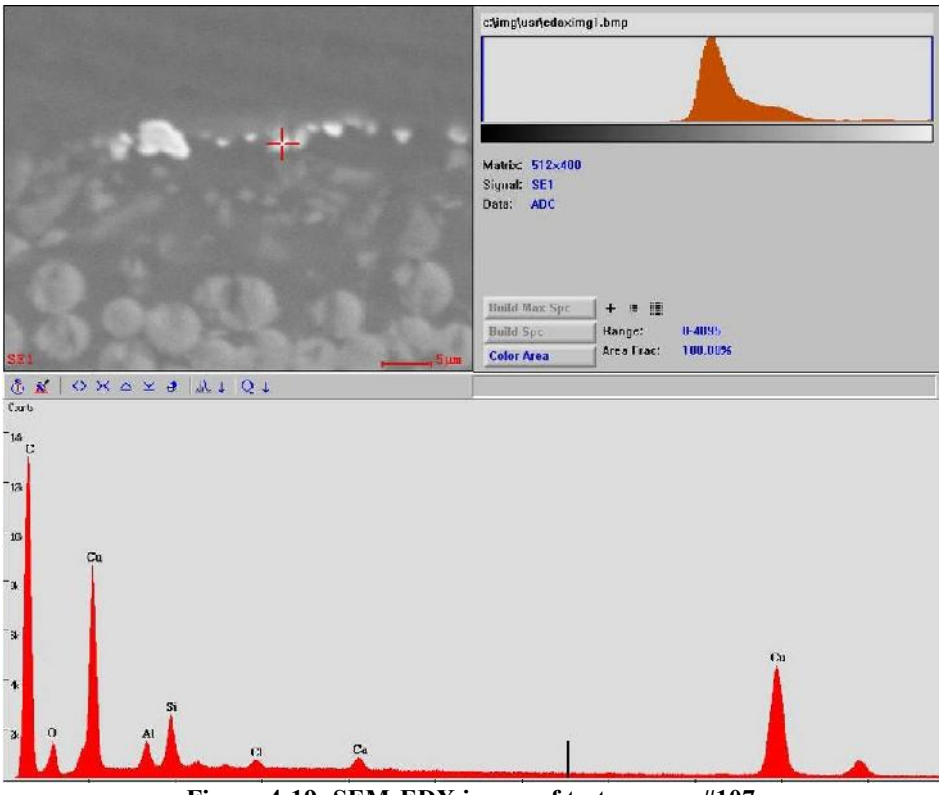

Figure 4-19: SEM-EDX image of test coupon #107

4.4.2 *Optical images and SEM images of buried mechanically drilled vias at the coating surfaces*

Because there were sixty samples tested for BMDV, only some representative test coupons are shown in Section 4.4.2.1 (DICY-cured) and Section 4.4.2.2 (phenolic-cured). Table 4-8 summarized the Coupon #, Figure #, time-to-failure, and reasons for showing the images.

Table 4-8: Summary of representative failed and survived coupons for DICY- and phenolic-cured epoxy using test coupons with BMDM.

DICY-cured epoxy			
Figure #	Coupon	Time-to-failure	Description
4-21 4-22	B17	321 hrs	Short circuit
4-23 4-24	B24	607.5 hrs	Open circuit
4-25 4-26	B16	681 hrs	Not failed survived until end of test
Phenolic-cured epoxy			
4-29 4-30	B125	42.5 hrs	Short circuit
4-31 4-32	B118	69.5 hrs	Open circuit
4-33 4-34	B116	180 hrs	Last short circuit

Optical microscopy was used for BMDV due to the clear color of the conformal coating at the modified end. Figure 4-21 to Figure 4-26 indicate the optical and SEM-EDX images of DICY-cured test coupons, while Figure 4-27 to Figure 4-34 show the optical and SEM-EDX images of the CAF sites for phenolic-cured epoxy. By comparing the optical images with the SEM-EDX images, the dark substances at the anode was identified as CAF.

The anode and cathode (copper traces) are highlighted in the optical images as shown in Figure 4-20. The SEM-EDX images only shown the end of the copper trace

(anode) where the conformal coating was applied. The direction of CAF formation is perpendicular to the copper trace plane and pointing towards the reader (Figure 4-20).

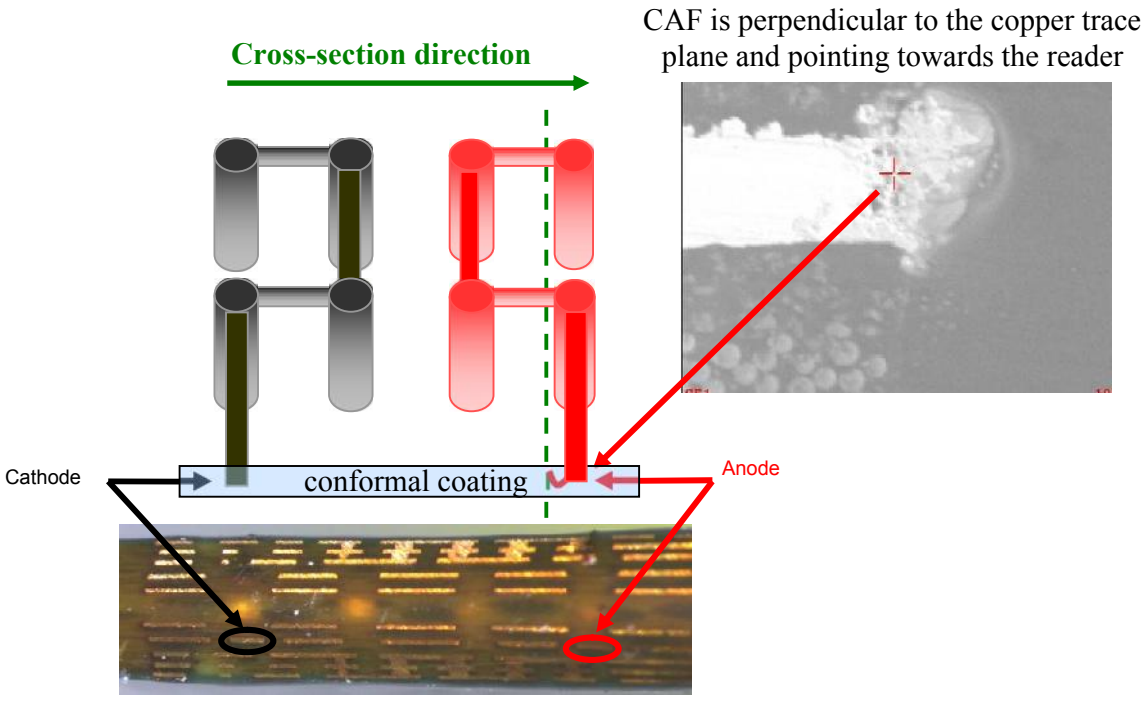

Figure 4-20: Schematic diagram for the anode and cathode corresponding to the optical and SEM-EDX images.

As mentioned in Section 4.2, a sudden increase in insulation resistance (open circuit) of a test coupon did not indicate an actual open circuit. Instead CAF formation had occurred and was identified using SEM-EDX technique. To demonstrate, optical and SEM-EDX images of BMDV with open circuits are provided as shown in Figure 4-23 and 4-24 for Coupon B24, and Figure 4-31 and 4-32 for Coupon B118.

In addition, all the samples with shorted circuits were identified to contain CAF. This can be illustrated by observing the optical and SEM-EDX images of the shorted test coupons as shown in Figure 4-21 and 4-22 for Coupon B17, and Figure 4-29 and 4-30 for Coupon B125.

As shown in Figure 4-25 and 4-26, test coupon B16 that still survived until the end of the test period (60 days) was found to have CAF at the copper trace / coating

interface, but did not fail electrically as the IR measurement did not drop below 10^6 ohms.

Finally, by cross-section from the cathode to the anode, there was no CAF found between the BMDV. Instead, all the CAF formed in the test coupons were found at the end of the copper trace where the conformal coating was applied.

4.4.2.1 DICY-cured test coupons

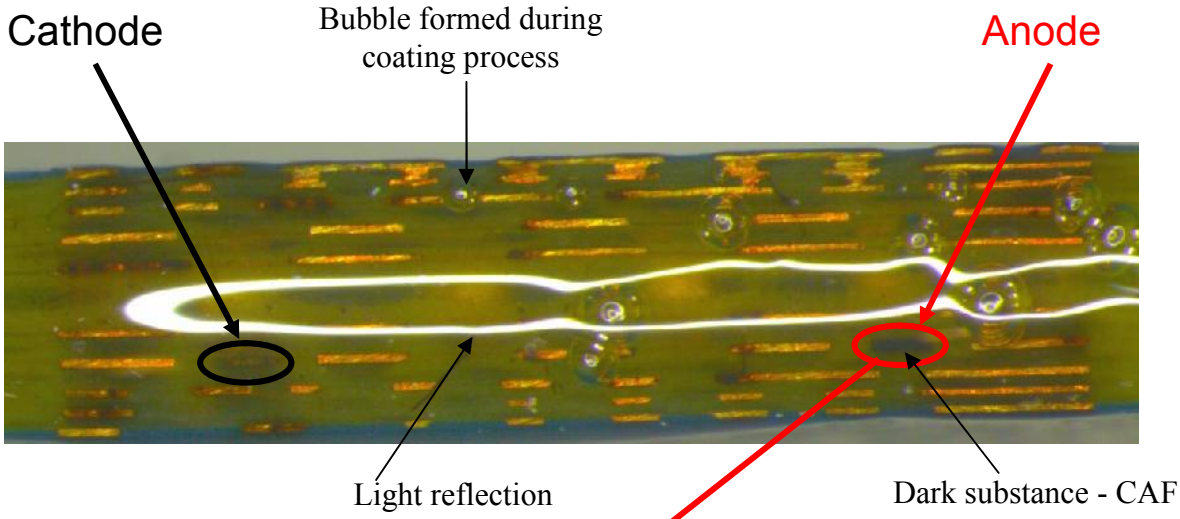

Figure 4-21: Optical image of test coupon B17 (short circuit) at t_B = 321 hrs

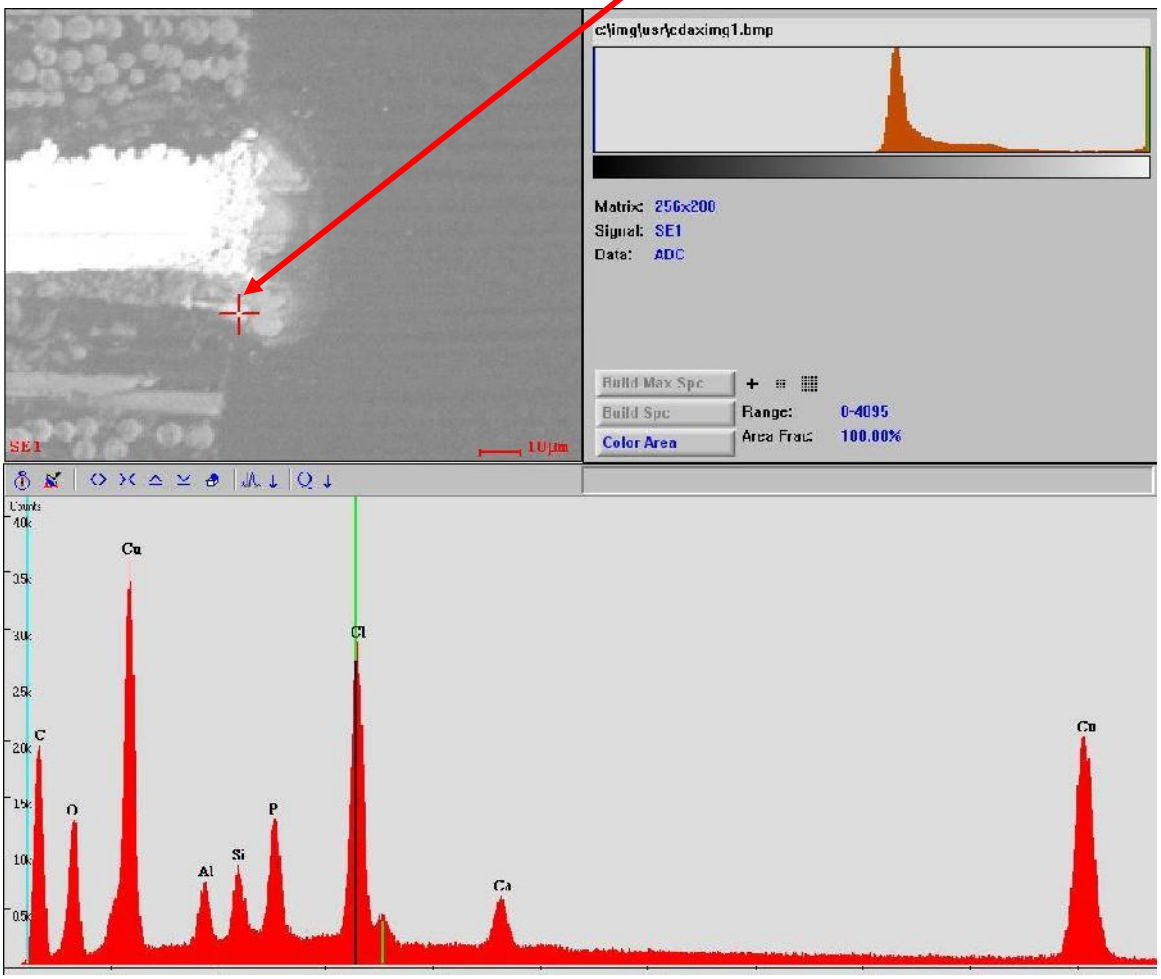

Figure 4-22: SEM-EDX of test coupon B17 (short circuit) at t_B = 321 hrs, cross-section from the coating end

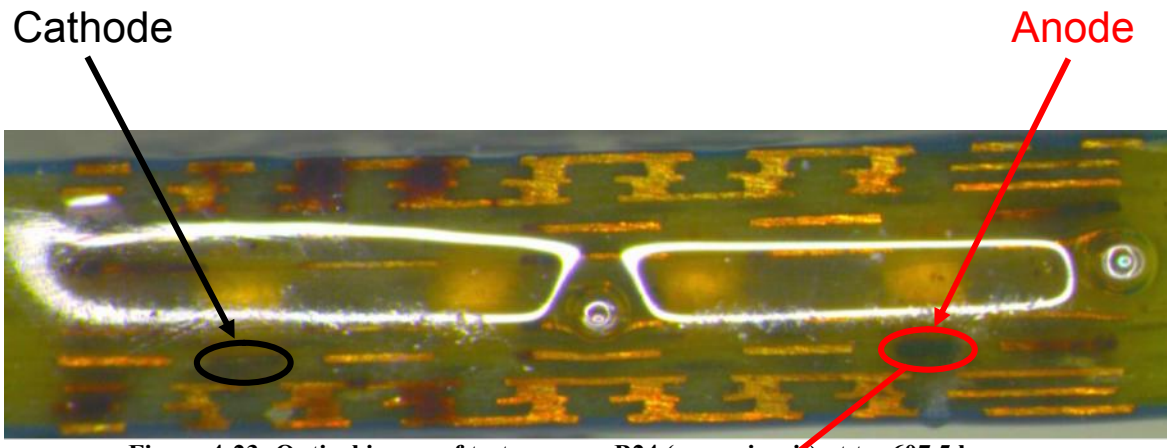

Figure 4-23: Optical image of test coupon: B24 (open circuit) at t = 607.5 hrs

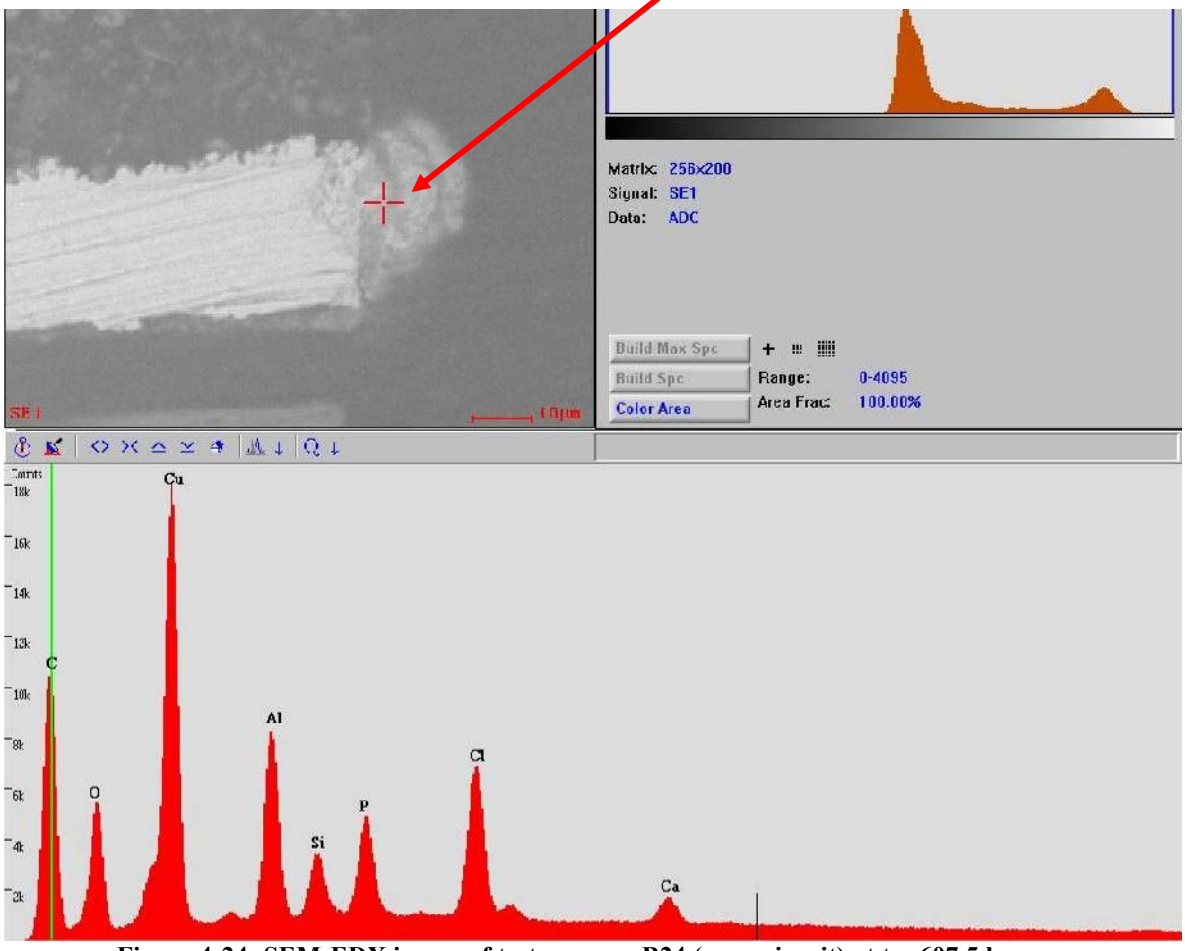

Figure 4-24: SEM-EDX image of test coupon: B24 (open circuit) at t = 607.5 hrs

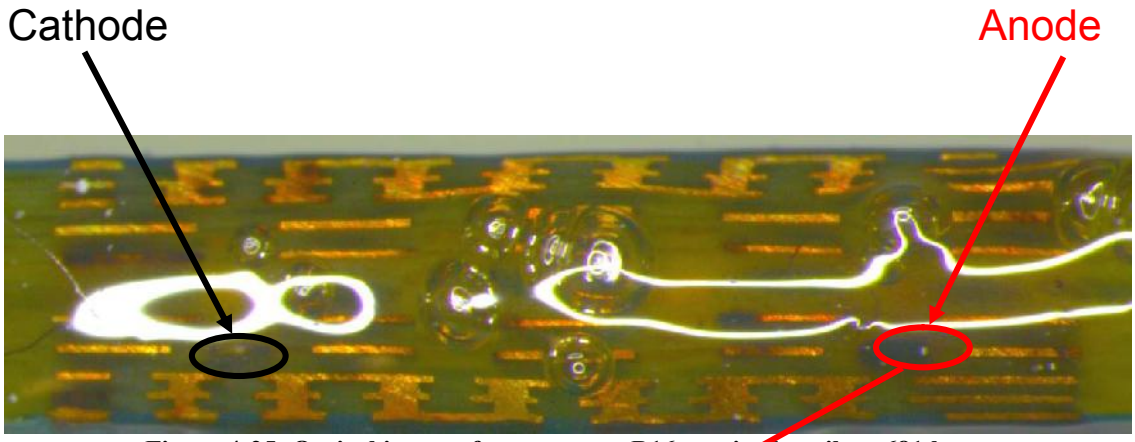

Figure 4-25: Optical image of test coupon: B16 survived until t = 681 hrs

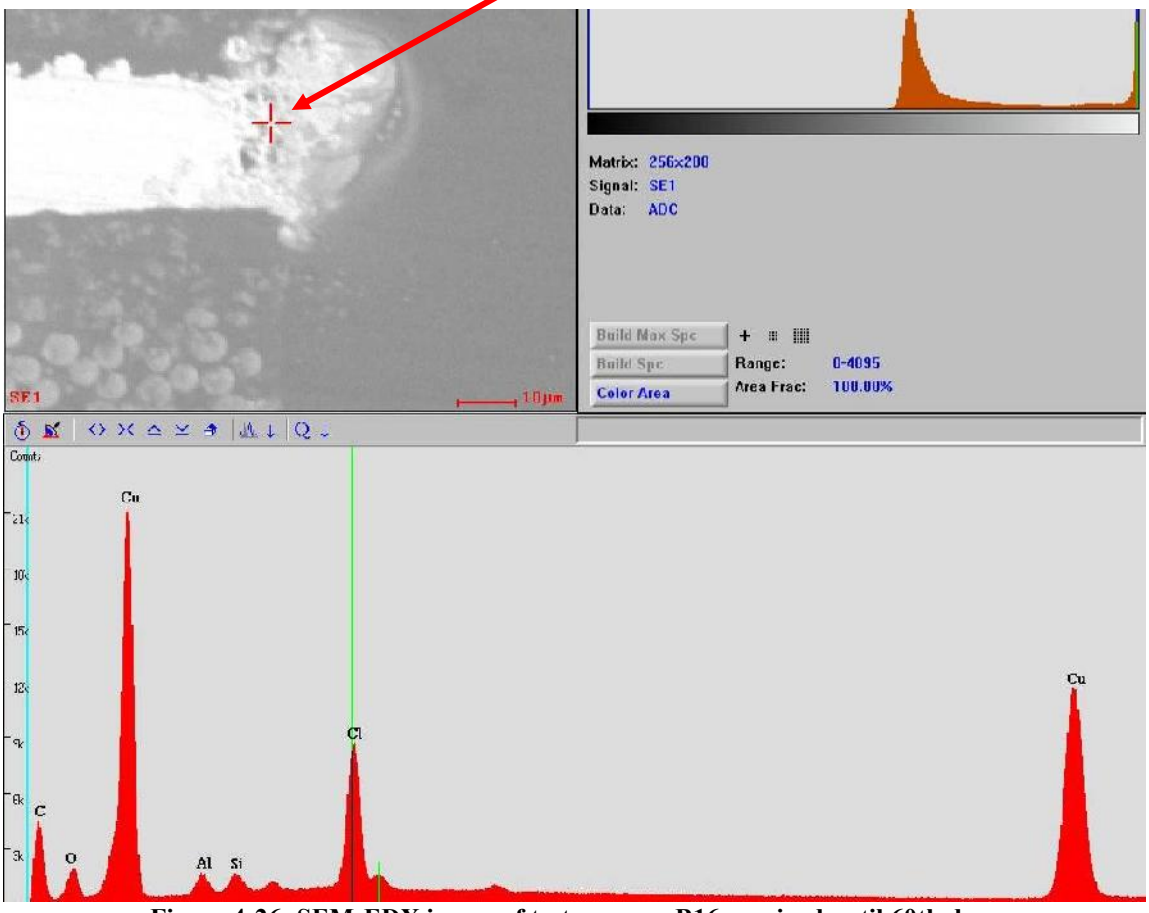

Figure 4-26: SEM-EDX image of test coupon: B16 survived until 60th day

4.4.2.2 Phenolic-cured test coupons

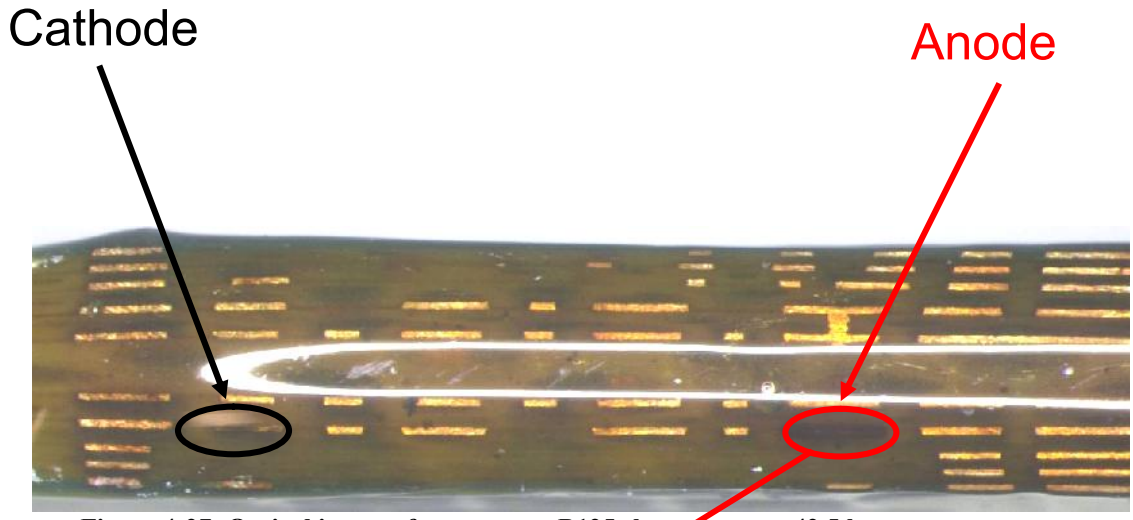

Figure 4-27: Optical image of test coupon B125 shorted at t_B= 42.5 hrs

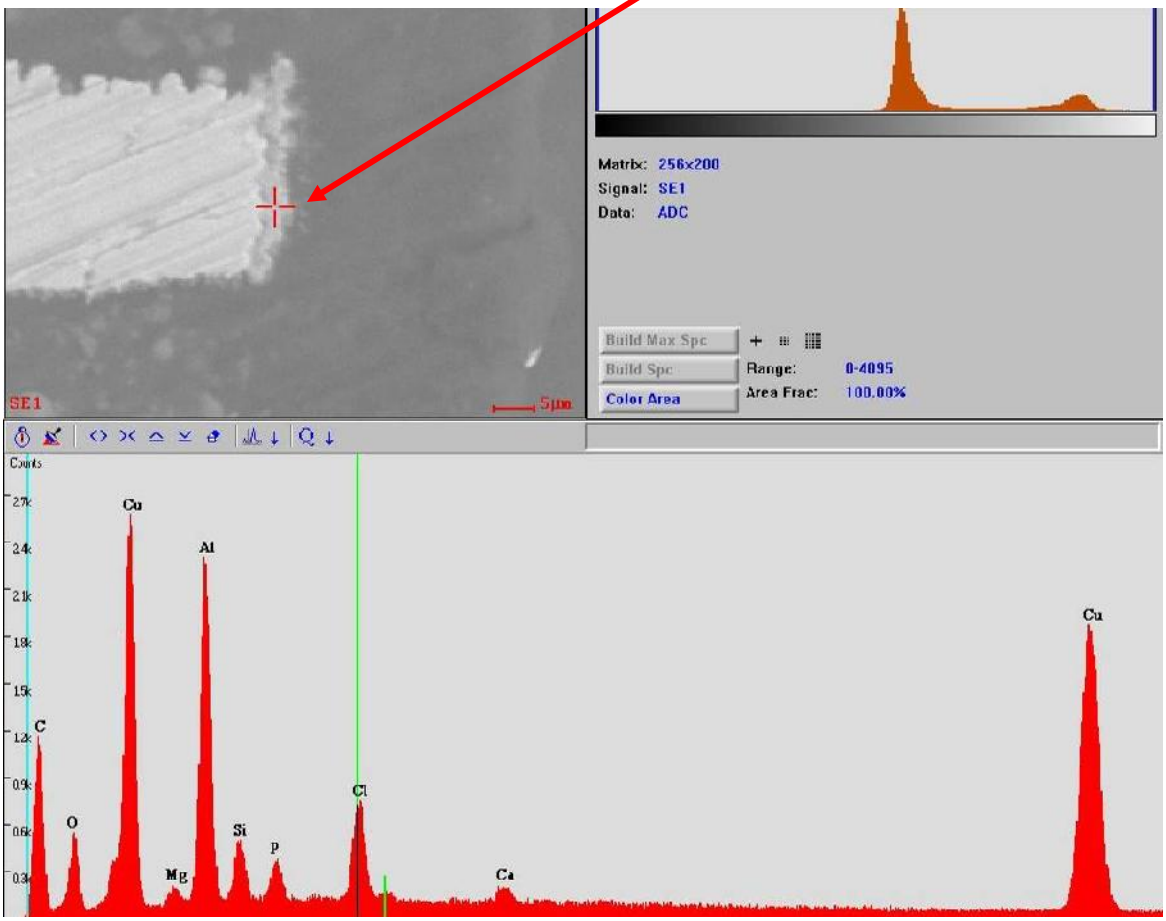

Figure 4-28: SEM-EDX image of test coupon B125 shorted at t_B = 42.5 hrs

Figure 4-29: Optical image of test coupon B118 (open circuit) at t_B = 69.5 hrs

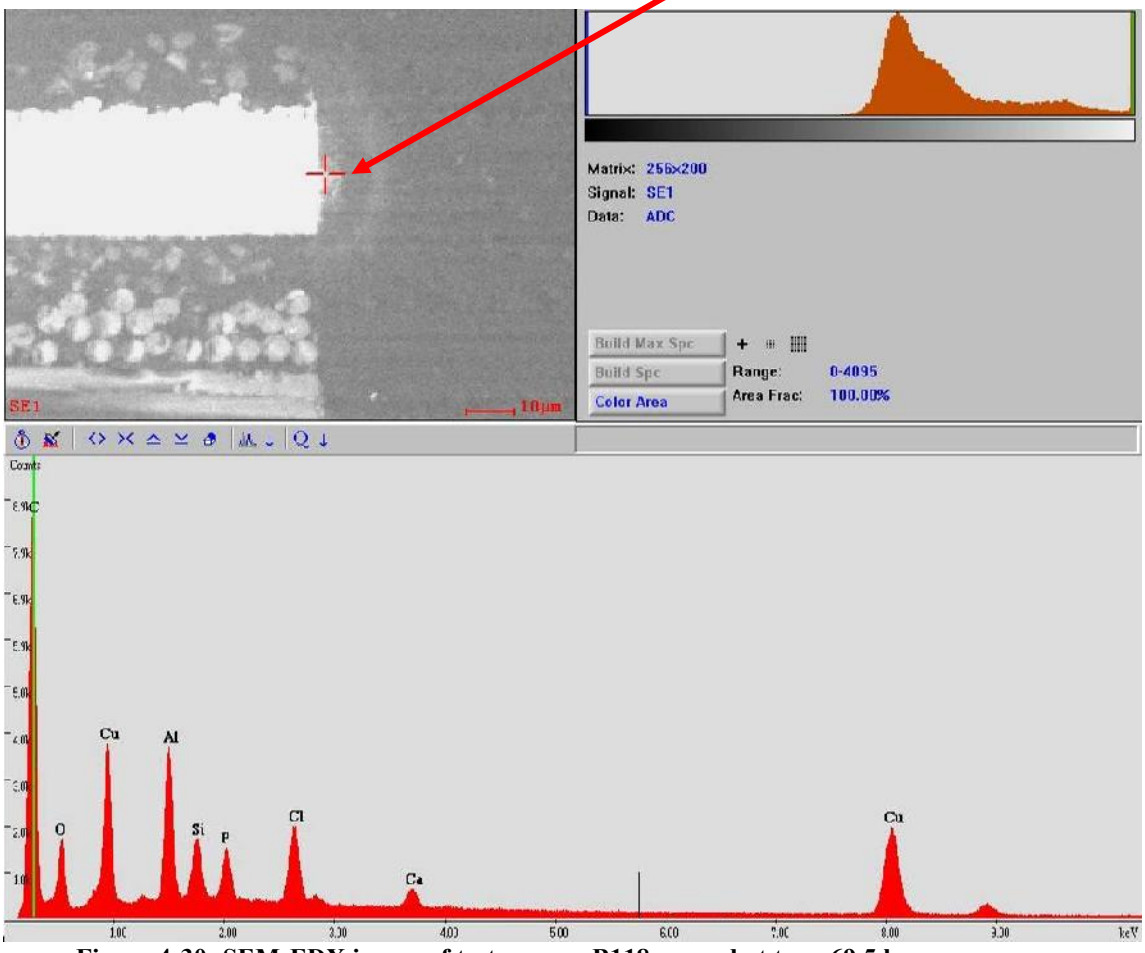

Figure 4-30: SEM-EDX image of test coupon B118 opened at t_B = 69.5 hrs

Figure 4-31: Optical image of test coupon B116 shorted at t_B = 180 hrs

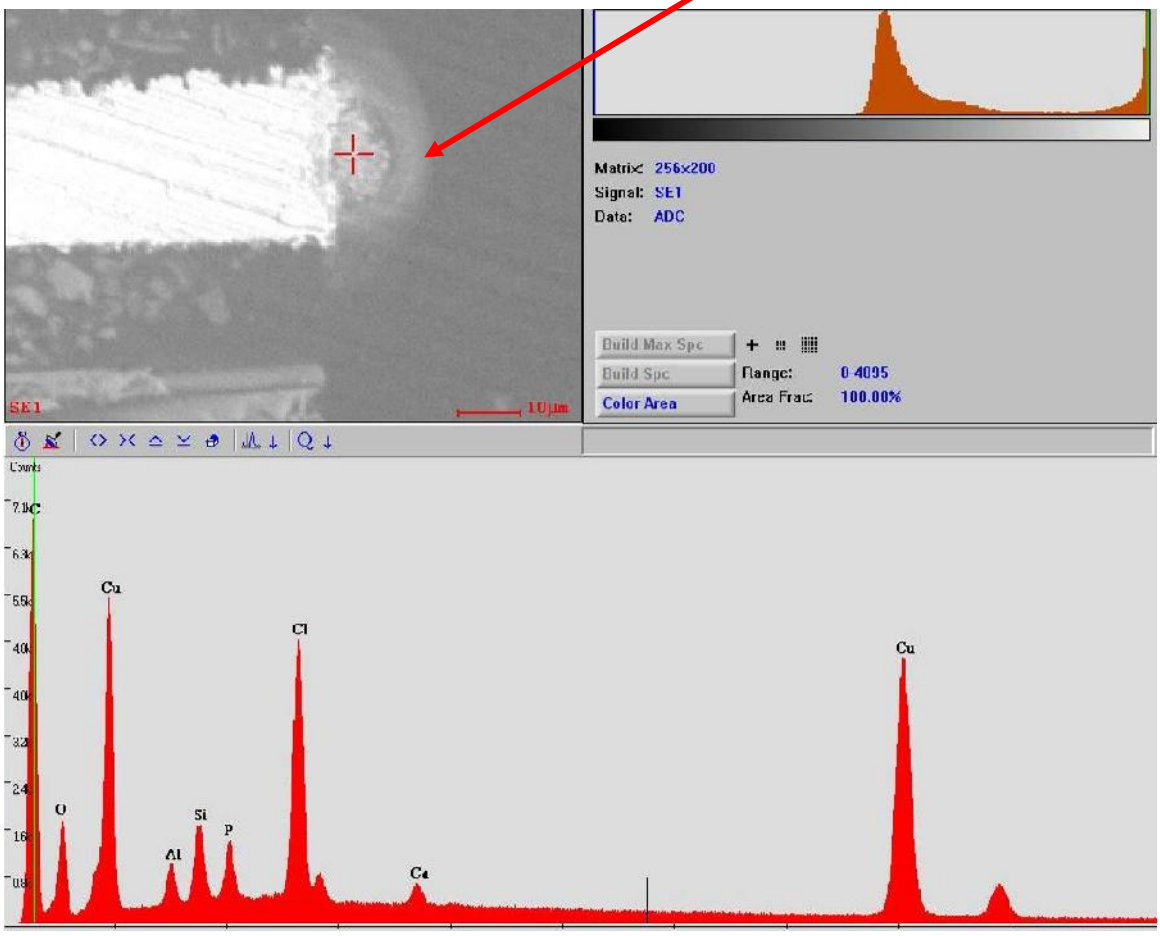

Figure 4-32: SEM-EDX image of test coupon B116 shorted t_B = 180 hrs (last failed sample)

4.5 Summary

This chapter has illustrated the insulation resistance readings obtained for DICY-SLDM, phenolic-SLDM, DICY-BMDV, and phenolic-BMDV. It also summaries the number of failures and time-to-failure in a table, and compared the Weibull distribution between different curing agents and drilling methods. Finally the electrical readings were also verified with cross-sectioning and elemental analysis using SEM-EDX. The next chapter will explain the results obtained from this research, sources of errors, and suggest future research to improve the techniques for CAF detection and verification.

Chapter 5

Discussion and Conclusion

Before going into the discussion of the test results as shown in Chapter 4, it is important to recap and summarize the following:

1. Research objective:
    a. Compare DICY- vs. phenolic-cured epoxy on CAF formation.
    b. Compare laser vs. mechanical drilling on CAF formation.
2. Standardizing of failure criteria:
    a. The coupon is considered a failure if the resistance reading is below 10^6 ohms. The failure should be verified with SEM-EDX when it is possible.
    b. Test coupons which failed electrically are considered failures, even though CAF was not identified by cross-sectioning and SEM-EDX.
    c. Coupons that were found to contain CAF but did not fail electrically are still considered to have survived.
3. The commonalities between SLDM and BMDV test:
    a. The same voltage gradient (0.4 V/ μm) was used.
    b. The test was run for a total of 60 days, with measurements taken after each 30 minutes of bias time.
4. The variations between SLDM and BMDV tests:
    a. No modification to the test coupons was needed for the SLDM, but the BMDV coupons required that the ends of the test coupons be ground off to remove the electrical connection between the buried vias to create two daisy chains.
    b. There were thirty test coupons for each material, the phenolic-SLDM had twenty test coupons from one lot, and ten from another lot.
    c. SLDM were located on the top two layers of the test coupons, whereas, BMDV were located on the inner core layers.
    d. Pad-to-pad distance for SLDM was 320 μm, but 500 μm for BMDV.

e. Most BMDV were drilled on top of the glass fibers, while the SLDM in the HDI layer were drilled on glass fibers and/or epoxy.
f. The more coupons that failed, the shorter the IR measurement time for the remaining coupons; therefore, the total bias time for BMDV (1116 hours) was longer than SLDM (681 hours).

5.1 Failure analysis

Weibull analysis is a powerful tool to compare the reliability of different materials. The analysis is used in this research because failure rate caused by CAF is not constant. The general form for the cumulative distribution function F (t) for the Weibull distribution is:

$$F(t) = 1 - e^{-(\frac{t}{\alpha})^{\beta}} \quad \text{..... (5.1)}$$

This function includes two important parameters: Alpha (α) - the scale factor in hours and Beta (β) - the shape factor that is dimensionless. The value of α corresponds to the failure time at which 63.2% of the test samples fail in a Weibull plot as shown in Figure 5-1. [68] Moreover, at a constant β, the further the best-fit-line lies to the right in the graph the better the material it is, because α will be greater.

The value of β corresponds to the slope of the best-fit-line in a Weibull plot. Alternatively, β can be found by drawing a line that intercepts the y-axis and parallel to the best-fit-line for the data points as shown in Figure 5-1. In this research the parameters were estimated using the analysis tool in MS Excel. The calculations to obtain α and β can be found in Appendix A.

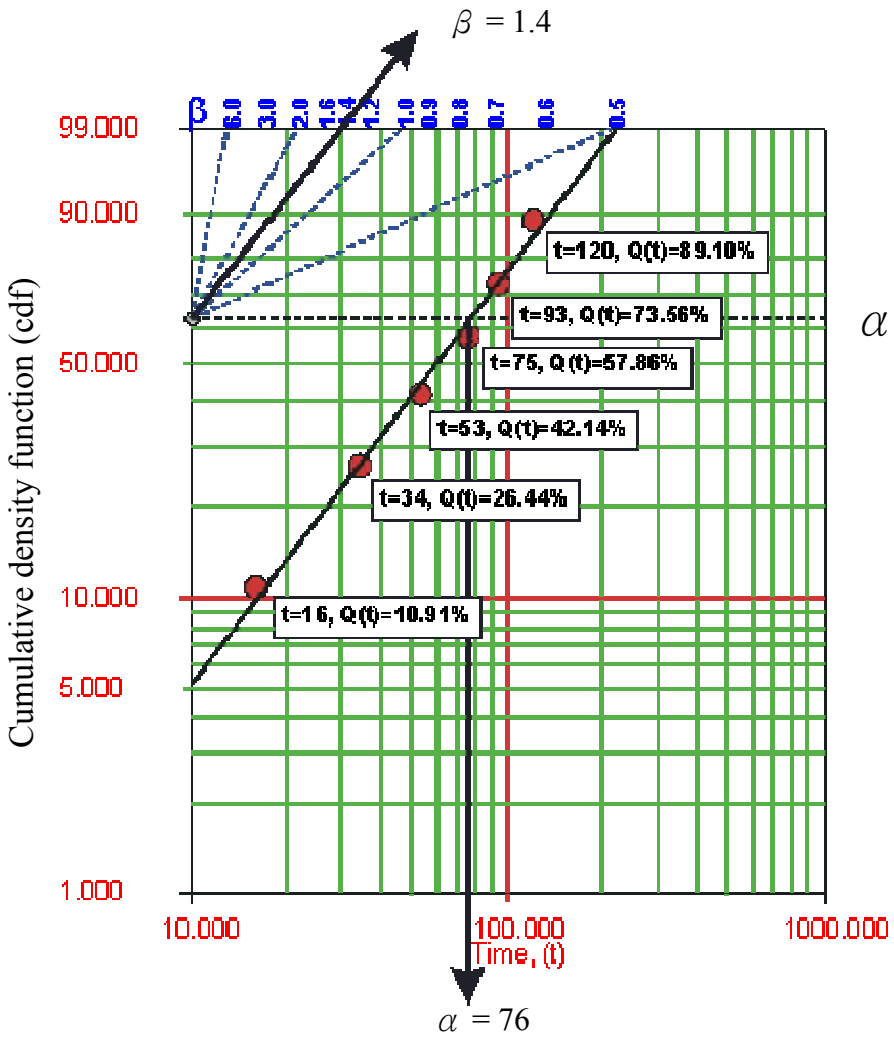

Figure 5-1: Typical Weibull plot [69]

Beta (β) also indicates the types of failure modes of the test coupons. When $0 < \beta < 1$, the failure rate decreases as time increases and represents an infant mortality failure. When $\beta = 1$, the failure mode follows an exponential distribution. It indicates that failures occur randomly and the failure rate is constant. On the other hand, when $\beta > 1$, the failure rate increases as time increases and indicates a wear-out type failure. [70] Figure 5-2 illustrates the three failure modes in the famous Bathtub curve.

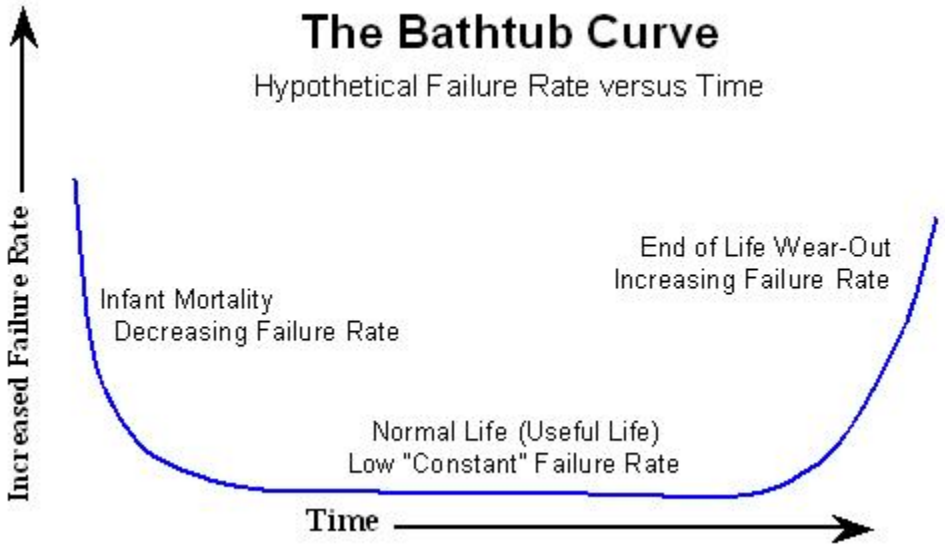

Figure 5-2: Bathtub curve for different failure modes. [71]

5.1.1 Comparison of DICY- vs. phenolic-cured epoxy on CAF formation

5.1.1.1 Surface laser drilled microvias (SLDM)

In this research, it is noted that α follows the following order for DICY- and phenolic-cured epoxy:

DICY-SLDM (4018 hrs)
↓
Phenolic-SLDM Lot 2 (1030 hrs)
↓
Phenolic-SLDM Lot 1 (410 hrs)

Moreover, β is less than one for both DICY-SLDM and phenolic-SLDM Lot 1; this indicates that the failure mode is an infant-mortality failure. However, β for phenolic-SLDM-Lot 2 is 5.2, which indicates that the failure rate increases as time increases and is a wear-out type failure. The test results also indicate that the failure mode varies from lot-to-lot of the same material.

This variation in failure rate for the same material could be due to manufacturing defects or the difference in the reflow profile at the laboratory and manufacturing facilities. It could be the reflow temperature and reflow duration were higher during the reflow process at the laboratory facility that lead to the infant-mortality failure for phenolic-SLDM-Lot 1 material. However, the above observations for phenolic-cured epoxy for Lot 1 and 2 were based on a sample size of 10 and 19 coupons. This might

lead to statistical errors. Table 5-1 summarizes α and β for DICY-SLDM, phenolic-SLDM-Lot 1 and phenolic-SLDM-Lot 2 materials.

Table 5-1: Summary of the Alpha and Beta values for SLDM.

	DICY - SLDM	Phenolic - SLDM	
No. of tested coupons	29	10 (Lot 1)	19 (Lot 2)
Alpha (hours)	4018	410	1030
Beta	0.97	0.92	5.2

5.1.1.2 Buried mechanically drilled vias (BMDV)

The same trend was observed for BMDV. DICY-cured test coupons had better CAF resistance than phenolic-cured epoxy, as α was 576 hours for DICY-cured epoxy versus 4.4 hours for phenolic-cured epoxy The Beta values for both curing agents were above one; and hence, they were experiencing wear-out type failures. Table 5-2 summarizes α and β for DICY-BMDV and phenolic-BMDV materials.

Table 5-2: Summary of the Alpha and Beta values for BMDV.

	DICY - BMDV	Phenolic - BMDV
No. of tested coupons	30	30
Alpha (hours)	576	4.4
Beta	2.0	1.3

5.1.1.3 Summary

The wear-out failure mode is anticipated as CAF formation is a wear-out type failure. As time passes, detrimental CAF will grow more substantially; and hence, failure will occur more easily. The infant-mortality failure for phenolic-SLDM-Lot 1 and DICY-SLDM might be due to slightly different reflowing processes and/or manufacturing defects. Unfortunately, there was no standard or proper burn-in test to exclude defective coupons except the instant electrical continuity test. Alternatively, there might be insufficient time for the test coupons with SLDM to reach a wear-out type failure mode, because failure modes vary as time passes as shown in the Bathtub curve.

Theoretically, DICY-cured epoxy should have lower CAF resistance as it consists of a strong polar aliphatic alky bond which has higher affinity for water molecules than the non-polar ring structure of the phenolic-cured epoxy. However, test results have shown that phenolic-cured epoxy was more susceptible to CAF. This result indicates that factors other than water resistance are more prominent to induce CAF formation.

It is believed that once the RH% reaches a particular point, the water content in the material will be saturated for both materials. On the other hand, the brittleness of phenolic-cured materials appears to be the more critical effect for CAF formation than the water resistance property.

If the material is more brittle, it will experience more damage at the epoxy/glass interface during the drilling process; and hence, accelerate subsequent CAF formation. Unfortunately, this research did not compare the brittleness of the DICY-cured vs. phenolic-cured epoxy. It is important to study the brittleness of these test coupons, because some companies have claimed to develop phenolic-cured materials that have significantly improved the drillability of the PCBs.

5.1.2 Comparison of laser vs. mechanical drilling on CAF formation

5.1.2.1 DICY-cured epoxy

Applying the same analytical procedure, it was concluded that test coupons with BMDV were more prone to CAF formation than SLDM. The α value for the SLDM is 4018 hours versus 576 hours for BMDV. In addition, the Beta value for SLDM is 0.97 but 2.0 for BMDV. This indicates that SLDM experienced infant-mortality failure mode, but BMDV experienced wear-out type failure. Table 5-3 summarizes α and β for DICY-SLDM and DICY-BMDV materials.

Table 5-3: Summary of the Alpha and Beta values for DICY-cured epoxy.

	DICY - SLDM	DICY - BMDV
No. of tested coupons	30	30
Alpha (hours)	4018	576
Beta	0.97	2.0

5.1.2.2 Phenolic-cured epoxy

For phenolic-cured epoxy, the same trend was observed. BMDV were more susceptible than SLDM and follows this order:

Phenolic-SLDM Lot 2 (1030)
↓
Phenolic-SLDM Lot 1 (410)
↓
Phenolic-BMDV (4.4)

However, β was the highest for phenolic-SLDM-Lot 2 as shown in Table 5-4.

Table 5-4: Summary of the Alpha and Beta values for phenolic-cured epoxy.

	Phenolic - SLDM		Phenolic - BMDV
No. of tested coupons	10 (Lot 1)	19 (Lot 2)	29
Alpha	410	1030	4.4
Beta	0.92	5.2	1.3

5.1.2.3 Summary

The test results showed that BMDV were more prone to CAF formation than SLDM, and it could be explained by following:

1. The effect of modifying the end of the test coupon might have had an effect on CAF formation, because all the CAF were found at the end of the anodic copper trace. The grinding of the end of the test coupons with BMDV probably caused more mechanical damage at the epoxy/glass interface.
2. All BMDV were drilled on top of the glass fibers versus only some of the SLDM were drilled on the glass fibers. Hence, BMDV had more glass fibers to facilitate CAF formation.
3. Defects such as copper wicking might occur due to improper mechanical drilling and copper plating process, but no evidence was detected.

5.1.3 Summary of the effects of curing agents and drilling methods on CAF formation

Because there were only two data points for the phenolic-SLDM-Lot 2, this lot of material is excluded in a summary analysis. Figure 5-3 shows the Weibull distribution for all the test coupons including DICY-SLDM, DICY-BMDV, phenolic-SLDM-Lot 1, phenolic-SLDM -Lot 2, phenolic-BMDV.

As summarised in Section 5.1.1 and 5.1.2, DICY-cured epoxy is better than phenolic-cured epoxy and SLDM is better than BMDV. In addition, the test results also show that the curing agent (DICY) had a more profound effect on reducing CAF formation than drilling method as both DICY-SLDM and DICY-BMDV are located further to the right in the Weibull plot (Figure 5-3).

DICY - SLDM (α = 4018 hrs)

↓

DICY - BMDV (576 hrs)

↓

phenolic - SLDM-Lot 1 (410hrs)

↓

phenolic-BMDV (4.4 hrs)

As shown in the Weibull plot (Figure 5-3), the DICY-cured and phenolic-cured epoxy with BMDV are relatively parallel and have steep slopes (β = 2 and 1.3) that indicate wear-out type failure. On the other hand, DICY-cured and phenolic-cured epoxy with SLDM are parallel to each other and have slopes that are less than one (β = 0.92 and 0.97) representing infant mortality failures. This observation indicates that drilling method is significant in determining the failure mode of the test coupons.

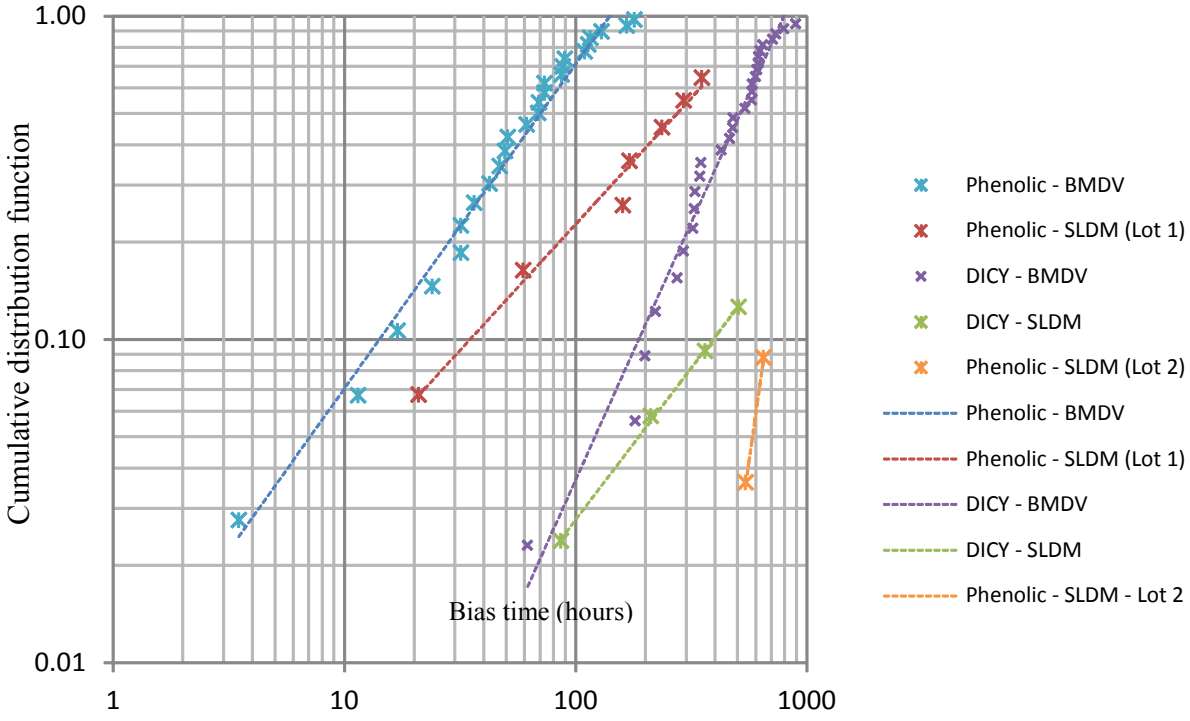

Figure 5-3: Weibull plots for all the test coupons.

5.2 Study of CAF formation

5.2.1 Concentration gradient of CAF

It was challenging to identify CAF sites for the test coupons with SLDM by cross-sectioning, because there were 1036 possible sites where CAF could have formed and damage to CAF could have taken place during cross-sectioning.

On the other hand, CAF was easily identified in test coupons with BDMV. The highest concentration of Cl was found at location 3 where the anodic copper trace met the conformal coating, but decreased as CAF grew into the conformal coating and toward the cathode copper trace.

As shown in Figure 5-4, it is suggested that copper was slowly corroded from the copper trace and moved toward the conformal coating and the cathode copper trace due to the voltage gradient by consuming the copper from the anodic copper trace.

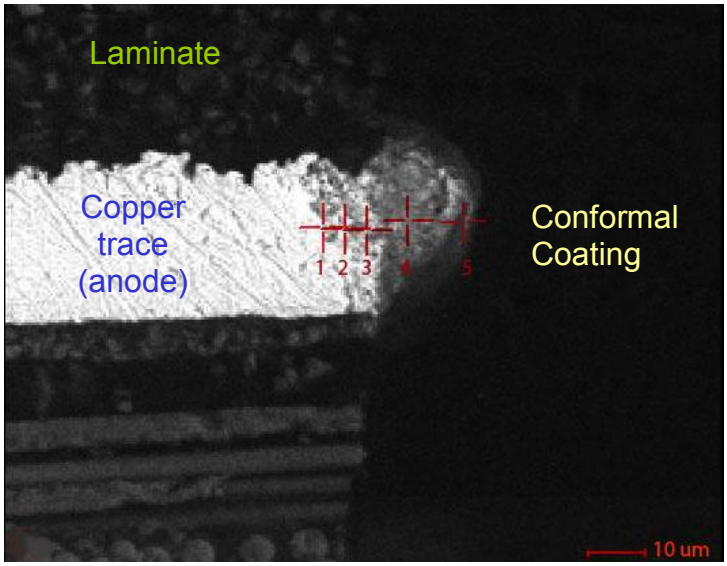

Figure 5-4: SEM image of test coupon B25 (DICY-BMDV)

5.2.2 *Atypical CAF formation site*

Since it was unknown where CAF could be found in between the anode and the cathode, serial cross-sectioning and SEM-EDX analysis were carried out as shown in Figure 5-5. There was no CAF found in cross-section planes A and B but only C. This finding was not predicted as it was assumed that:

1. CAF would form within the closest spacing between two PTHs. It is because two oppositely charged PTHs were 300 µm apart from each other, whereas the cathode and anodic copper traces were 2150 µm away from one another.
2. PTH would be more susceptible to CAF formation than copper traces because of the weakening of the glass fibers during the drilling process.

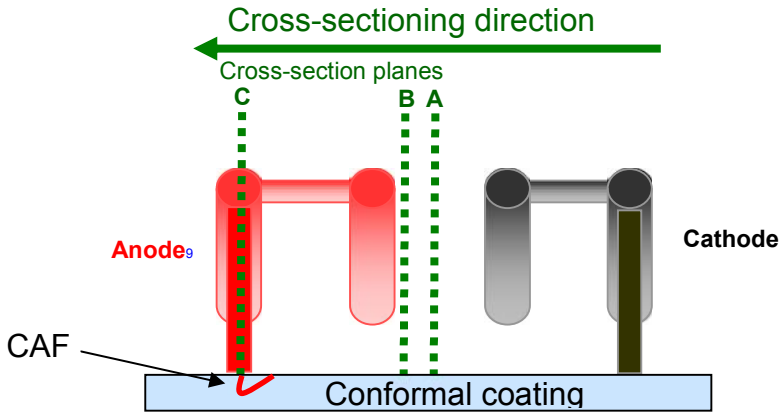

Figure 5-5: Serial cross-sectioning of BMDV.

Some explanations are attempted to explain the observed phenomenon:

1. Grinding off the end of the test coupon could have exerted mechanical stress on the glass fibers/epoxy interface, and decreased the activation energy needed for CAF formation at this end site.

In summary, the test results indicate the ends of the anodic copper traces were more susceptible to CAF formation than the mechanically drilled vias because of more mechanical stress exerted on the copper traces. Instead of expecting CAF along the glass fibers, CAF was discovered at the substrate/coating interface and within the coating. This failure mode is similar to the covercoat-related failure or interface-related failure that Boddy, Delaney, and Lahti *et al.* discovered in 1976. [36]

5.2.3 IR readings for CAF

It was observed that during the CAF verification process (cross-sectioning) CAF was found in coupons that did not fail the THB test. For example Coupon B16 was detected to have a significant amount of CAF at the end of the copper trace, but did not fail the electrical test as shown in Figure 5-6. Moreover, the IR readings were fluctuating at 1116 hours > t_B > 1000 hours.

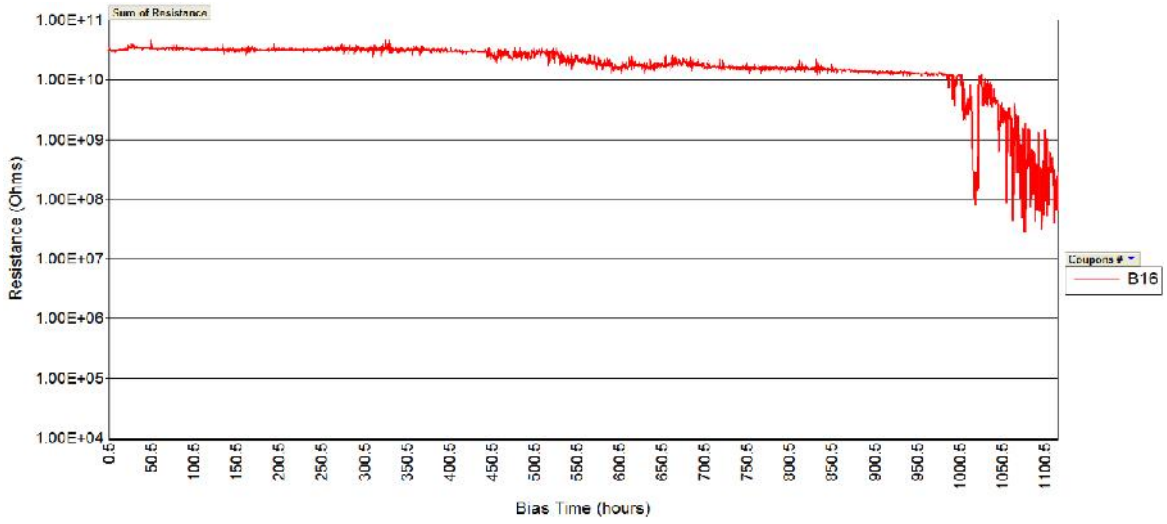

Figure 5-6: IR readings for phenolic-BMDV coupons (Coupon B16)

These observations suggested that as CAF grew closer to the cathode, a temporary electrical discharge might have occurred and reduced the resistance between oppositely charged conductors. If CAF eventually grows too close to the cathode, the high energy carried with electrical discharge will cause catastrophic failure by burning and charring the epoxy.

Fortunately, the equipment setup has stopped this type of catastrophic failure by terminating a particular test coupon that had resistance below 10^6 ohms. This can preserve the test coupon for further failure analysis. Nonetheless, when analyzing the results one should consider that CAF might have already formed without failing electrically. It has just not come close enough to the cathode to reduce the IR below 10^6 ohms.

5.2.4 CAF dissolution

After the unexpected power outage at t_B = 504.5 hours, the test for SLDM was restarted with the original settings for all the test coupons. It was surprising that the failed samples that had failed electrically before power outage did not fail immediately as shown in the IR readings in Figure 5-7. CAF will dissolve while the bias is withdrawn. When the power is terminated, water is no longer oxidized to form hydrogen ions to maintain the acidity at the anode; this causes partial CAF dissolution to occur because CAF is soluble above pH4.

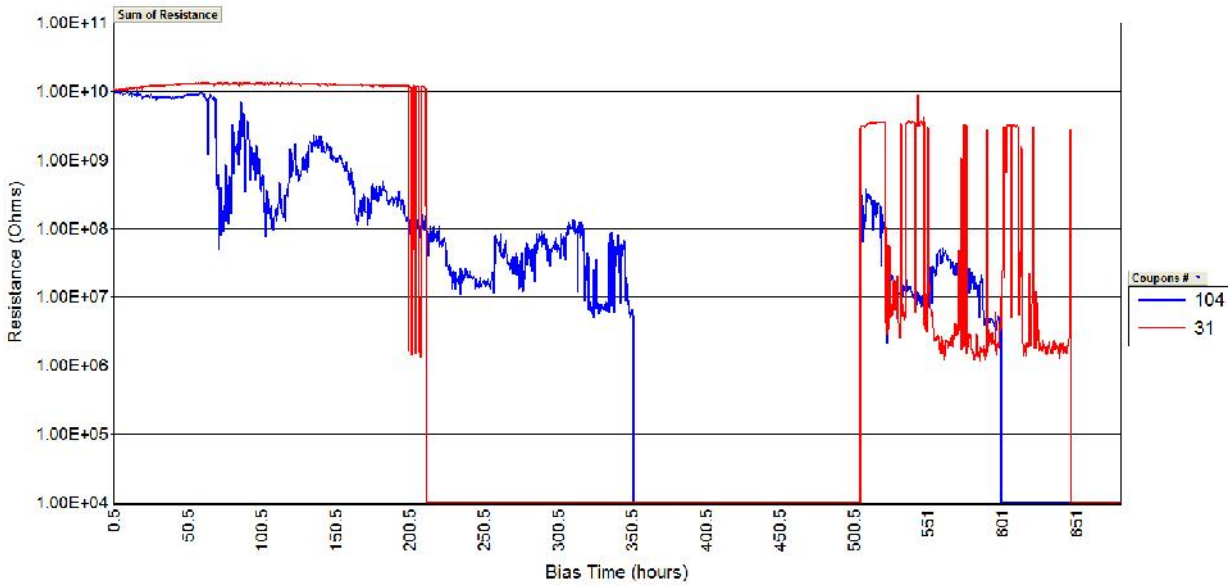

Figure 5-7: IR readings for Coupon #31 and Coupon #104 before and after power outage at t_B = 504.5 hours.

5.3 Suggestions for improving CAF testing

5.3.1 Modify the switching system

Because of the CAF tester setup, the measurement time varied depending on the number of test coupons that survived to a particular time. This will change the total bias time for different set of samples during the same testing period (60 days). For example, the total bias time was 681 hours for SDMV but 1116 hours for BMDV within 60 days. This phenomenon led to incomplete data collections for Weibull analysis for the SLDM vs. BMDV that had a longer total bias time. However, in an industrial setting, CAF

testing will not have a limited time frame as in this research (60 days), and all the samples would be tested to failure.

Nonetheless, the lengthy measurement time would delay the collection of data. If there were two parallel switching systems, simultaneous measurements of two different samples could be obtained. The total measurement time can be reduced by half. However, when there are two systems in place, equipment errors and variances needed to be considered. In order to reduce the errors and variances, regular maintenance, calibration, and random order of measurements are recommended. A drawback of the parallel switching system is cost.

5.3.2 Simplify test coupon design

Due to the damage on the originally designed test coupons by the PCB manufacturer and the lengthy time to order new materials, a different designed test coupon design that was available in the research lab was used for testing. Unfortunately, these test coupons with SLDM and BMDV used in this research were not ideal.

For example, the coupons with SLDM are too complicated and difficult to locate CAF sites by electrical testing and cross-sectioning. Even though electrical testing was some what useful in identifying the CAF sites, most of the time, the insulation resistance was still so high that a mega-ohmmeter was not capable of definitively identifying CAF sites electrically.

In order to find evidence of CAF formed between vias more easily, a test board containing a simplified test pattern and fewer via pairs is desired. For example, test patterns containing ten rows of cathodes intermeshed with ten rows of anodes would be a better design as the via pairs are reduced and the complicated zigzag pattern that imposed a challenge for cross-sectioning would be eliminated.

5.3.3 Adjust the data display criteria for the CAF tester

As mentioned in Chapter 4, the abnormal IR measurements (open circuits) for phenolic-cured test coupons with BMDV were caused by CAF formation as already verified by SEM-EDX. The IR appeared as an open circuit when resistance was below 10^4 ohms but above 0 ohm (shorted). This was caused by the default setting (the

maximum current allowance of 10 mA) that was trying to limit excessive current flowing through the test coupon when the resistance is too low.

By discussing with the equipment supplier, it was found possible to measure the resistance and display the actual readings in the future, even though the resistance are below 10k ohms.

5.3.4 Improve data collection

The time for test initiation, data collection, test termination, and power termination should all be recorded in a *txt* document and imported into some database program such as MS Access. This will enable one to track the exact time for power outages; and hence, facilitate data analysis.

5.3.5 Study new materials and new interconnect structures on CAF formation

Concerns about the impact of the electronic industry on the environment have pushed the implementation of lead-free soldering and the use of halogen-free materials. The higher processing temperature and newly developed halogen-free materials needed to be fully examined for CAF formation. Moreover, new laminate materials without glass fibres should also be studied because it might be a solution to CAF reduction as CAF usually grows along glass fibres.

In the present study, only the two layer stacked microvias were examined. However, as the HDI technology becomes more mature and the PCB circuits get denser, microvias drilling will become more popular and be used more frequently. It is important to evaluate the effects of different microvia structures (Figure 5-8) on CAF formation.

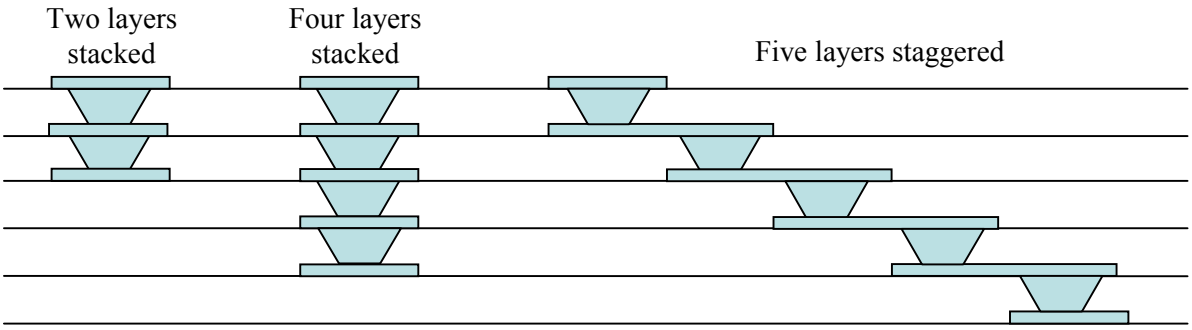

Figure 5-8: Types of microvias

5.3.6 Study CAF formation in a range of conditions

In this research, the tests were focusing on comparing the effect of curing agents and drilling methods on CAF formation; however, this does not provide sufficient information on how the time-to-failure changes as temperature, RH, and voltage gradient varies. It is important to study the effects of these parameters as it will provide a mathematical model that can predict the time-to-failure for different conditions.

5.4 Conclusion

The objective of the research was to evaluate the effects of curing agents and drilling methods on CAF formation, and test results have proven the following:

1. DICY-cured epoxy is a better CAF resistant material than phenolic-cured epoxy.
2. Laser drilled microvias have are better CAF resistance than mechanically drilled vias.
3. Effect of curing agents on CAF resistance is more significant than drilling methods.

References

[1] G. Nevison. "The Lead-free Directive and the Distributor." *Electronics Weekly,* pp. 20, 2003.

[2] Susanna Pelzel, Minna Juuti, Yukio Sugimoto. "Chapter 4. Environmental stewardship with regional perspectives and drivers of the lead-free issue," in *Handbook of Lead-Free Solder Technology for Microelectronic Assemblies*, New York: Marcel Dekker, Inc. 2004, pp. 115-148.

[3] B. H. Robinson. "E-waste: An Assessment of Global Production and Environmental Impacts." *Sci. Total Environ.,* vol. 408, pp. 183-191, 2009.

[4] V. J. Biancomano. "Lead-free Solders Remain a Hard Sell." *Electronic Engineering Times,* pp. 40.

[5] L. J. Turbini, G. C. Munie, D. Bernier, J. Gamalski and D. W. Bergman. "Examining the Environmental Impact of Lead-free Soldering Alternatives." *IEEE Transactions on Electronics Packaging Manufacturing,* vol. 24, pp. 4-9, 2001.

[6] A. S. G. Andrae, N. Itsubo and A. Inaba. "Global Environmental Impact Assessment of the Pb-free Shift." *Soldering & Surface Mount Technology,* vol. 19, pp. 18-28, 2007.

[7] Anonymous. " IPC - Environmental and health issues" 2011." Internet: http://www.ipc.org/ContentPage.aspx?pageid=Environment-and-Health-Issues, 2011 [Oct. 12, 2011]

[8] J. D. Boysère and A. Beard. "Halogen-free Laminates: Worldwide Trends, Driving Forces and Current Status." *Circuit World,* vol. 32, pp. 8-11, 2006.

[9] N. Patton. "Lead/halogen-free Laminates and Their Effect on Desmearing and Metallisation," *Circuit World,* vol. 33, pp. 28-35, 2007.

[10] David Yuk Ho Lau. "Evaluation of Halogen-free Laminate Used in Handheld Electronics." MASc thesis, University of Waterloo, Canada, 2009.
Waterloo.

[11] A. Caputo, L. Turbini and D. Perovic. "Design Limitations Related to Conductive Anodic Filament Formation in a Micro-world." *Microsystem Technologies,* vol. 15, pp. 39-44, 2009.

[12] Charles A. Harper. *Electronic Assembly Fabrication: Chips, Circuit Boards, Packages, and Components*. New York: The McGraw-Hill, 2002.

[13] G. L. Gary Brist. "Advanced print circuit board materials," in *Materials for Advanced Packaging*, Daniel Lu, C. P. Wong, Ed. New York: Springer Science and Business Media, 2009, pp. 273-306.

[14] R. S. Khandpur. *Printed Circuit Boards: Design, Fabrication, Assembly and Testing.* New York: The McGraw-Hill, 2006.

[15] S. Siau, J. D. Baets, A. V. Calster, L. Heremans and S. Tanghe. "Processing Quality Results for Electroless/electroplating of High-aspect Ratio Plated Through Holes in Industrially Produced Printed Circuit Boards." *Microelectronics Reliability,* vol. 45, pp. 675-687, 2005.

[16] Augis, J.A., DeNure, D.G., LuValle, M.J., Mitchell, J.P., Pinnel, M.R., and Welsher, T.L. "A humidity threshold for conductive anodic filaments in epoxy glass printed wiring board," in *Proceedings of 3rd International SAMPE Electronics Conference,* 1989, pp. 1023-1030.

[17] K. Karavakis and S. Bertling. "Conductive Anodic Filament (CAF): the Threat to Miniaturization of the Electronics Industry." *CircuiTree,* vol. 17, pp. 70.

[18] H. Kimura, A. Matsumoto, and K. Ohtsuka. "New Type of Phenolic Resin - The Curing Reaction of Bisphenol A Based Benzoxazine with Bisoxazoline and the Properties of the Cured Resin. III. The Cure Reactivity of Benzoxazine with a Latent Curing Agent." *Journal of Applied Polymer Science,* vol. 107, pp. 710-718.

[19] S. Ehrler. "The Compatibility of Epoxy-based Printed Circuit Boards with Lead-free Assembly." *Circuit World,* vol. 31, pp. 3-13.

[20] Yih-Rern Peng, Xiaolong Qi and Christos Chrisafides. "The Influence of Curing Systems on Epoxide-based PCB Laminate Performance." *Circuit World,* vol. 31, pp. 14-20, 2005.

[21] B. Sood, R. Sanapala, D. Das, M. Pecht, C. Y. Huang and M. Y. Tsai. "Comparison of Printed Circuit Board Property Variations in Response to Simulated Lead-Free Soldering." *IEEE Transactions on Electronics Packaging Manufacturing,* vol. 33, pp. 98-111, 2010.

[22] M. H. David Bedner. "Halogen-free Materials with Improved Thermal and Electrical Properties." *Circuit World,* vol. 35, pp. 3-7, 2009.

[23] L. Ying Ling. "Flame-retardant Epoxy Resins from Novel Phosphorus-containing novolac." *Polymer,* vol. 42, pp. 3445-3454, 4, 2001.

[24] P. R. Hornsby and C. L. Watson. "A Study of the Mechanism of Flame Retardance and Smoke Suppression in Polymers Filled with Magnesium Hydroxide." *Polymer Degradation and Stability,* vol. 30, pp. 73-87, 1990.

[25] John H. Lau and Chris Chang. "An Overview of Microvia Technology." *Circuit World,* vol. 26, pp. 22-32, 2000.

[26] A. Kestenbaum, J. F. D'Amico, B. J. Blumenstock and M. A. DeAngelo. "Laser Drilling of Microvias in Epoxy-glass Printed Circuit Boards." *IEEE Transactions on Components, Hybrids, and Manufacturing Technology,* vol. 13, pp. 1055-1062, 1990.

[27] B. Birch. "Reliability Testing for Microvias in Printed Wire Boards." *Circuit World,* vol. 35, pp. 3-17.

[28] R. De Oliveira, D. Berthet and E. Van der Bij. "State of the art technologies for front-end hybrids," in *12th Workshop on Electronics for LHC and Future Experiments,* Valencia, Spain, 2006, pp. 64-68.

[29] C. Cohn and H. Kimbara. "Via to via isolation vs. quality of via formation in organic substrates," in *Electronics Packaging Technology Conference,* 2007, pp. 86-93.

[30] B. Rudra, M. Pecht and D. Jennings. "Assessing Time-to-failure due to Conductive Filament Formation in Multi-layer Organic Laminates." *IEEE Transactions on Components, Packaging, and Manufacturing Technology, Part B: Advanced Packaging,* vol. 17, pp. 269-276, 1994.

[31] W. Ready and L. J. Turbini. "The Effect of Flux Chemistry, Applied Voltage, Conductor Spacing, and Temperature on Conductive Anodic Filament Formation." *Journal of Electronic Materials,* vol. 31, pp. 1208-1224, 2002.

[32] A. DeMarderosian. "Raw material evaluation through moisture resistance testing." in Proceedings of the IPC Fall Meeting 1976, pp. 708.

[33] D. J. Lando, J. P. Mitchell and T. L. Welsher. "Conductive anodic filaments in reinforced polymeric dielectrics: formation and prevention," in *17th International IEEE Reliability Physics Symposium,* vol. 1979, pp. 51-63.

[34] Laura J. Turbini, Westin R. Bent and W. Jud Ready. "Impact of Higher Melting Lead-free Solders on the Reliability of Printed Wiring Assemblies." *Journal of SMT,* vol. 13, 2000.

[35] A. Caputo, L. Turbini and D. Perovic. "Conductive Anodic Filament Formation Part II: Electrochemical Reactions Leading to CAF." *Journal of Electronic Materials,* vol. 39, pp. 92-96, 2010.

[36] P. J. Boddy, R. H. Delaney, J. N. Lahti, E. F. Landry, and R. C. Restrick. "Accelerated life testing of flexible printed circuits," in *14th Annual IEEE Reliability Physics Symposium,* 1976, pp. 108-117.

[37] G. Parry, P. Cooke, A. Caputo, and L. J. Turbini. “The effect of manufacturing parameters on board design on CAF evaluation,” in *Proceedings of the International Conference on Lead-free Soldering,* May 26, 2005.

[38] W. J. Ready, B. A. Smith, L. J. Turbini, and S. R. Stock. "Analysis of Catastrophic Field Failures due to Conductive Anodic Filament (CAF) Formation," *Electronic Packaging Materials Science X,* vol. 515, 1998.

[39] Laura J. Turbini and W. J. Ready. "Conductive anodic filament failure: A materials perspective," in *Proceedings of the Third Pacific Rim International Conference on Advanced Materials and Processing,* 1998, pp. 1977-1982.

[40] W. J. Ready, S. R. Stock, G. B. Freeman, and L. J. Turbini. "Microstructure of Conductive Anodic Filaments Formed during Accelerated Testing of Printed Wiring Boards." *Circuit World,* vol. 21, pp. 5-9, 1995.

[41] Dean Kossives. "Conductive Anodic Filament Formation." *The National Electronics Manufacturing Center of Excellence,* vol. 2011, 2007.

[42] H. C. Lichtenegger, T. Schoberl, M. H. Bartl, H. Waite and G. D. Stucky. "High Abrasion Resistance with Sparse Mineralization: Copper Biomineral in Worm Jaws." *Science,* vol. 298, pp. 389.

[43] S. R. Stock and L. J. Turbini. "Atacamite in Jaws and Printed Wiring Boards. (Letter to the Editor)." *Science,* vol. 298, pp. 1892.

[44] Tarun Amla. "Conductive anodic filament growth failure," in *IPC Printed Circuits Expo,* 2002.

[45] J. N. Lahti, R. H. Delaney and J. N. Hines. "The characteristic wearout process in epoxy-glass printed circuits for high density electronic packaging," in *IEEE Transactions on Reliability Physics Symposium, 1979. 17th Annual*, pp. 39-43.

[46] Pourbaix M. "Lectures on electrochemical corrosion." *Plenum Press,* pp. 299-302, 1973.

[47] W. Ready and L. J. Turbini. "A Novel Test Circuit for Automatically Detecting Electrochemical Migration and Conductive Anodic Filament Formation." *Journal of Electronic Materials,* vol. 28, pp. 1158-1163.

[48] John O'M. Bockris, Amulya K. N. Reddy, and Maria Gamboa-Aldeco. *Modern Electrochemistry: Fundamentals of Electronics, Volume 2.* New York: Kluwer Academic / Plenum Publishers, 2000.

[49] T. L. Welsher, J. P. Mitchell and D. J. Lando. "CAF in composite printed-circuit substrates: Characterization, modeling and a resistant material," in *18th Annual IEEE Reliability Physics Symposium,* 1980, pp. 235-237.

[50] M. Pecht and A. Dasgupta. "Physics-of-failure: An approach to reliable product development," in *Integrated Reliability Workshop,* 1995, pp. 1-4.

[51] Anonymous. "IPC-TM-650 Test Methods Manual - Conductive Anodic Filament (CAF) Resistance Test: X-Y Axis--11/03." Internet: http://www.ipc.org/4.0_Knowledge/4.1_Standards/test/2-6-25.pdf, 2003 [Sep. 9, 2011].

[52] J. Clyde and F. Coombs. *Printed Circuits Handbook.* New York: McGraw-Hill, 2008.

[53] Bob Neves. "Setup, Procedures, and Patterns for CAF and ECM Testing." PC FAB, pp. 46, 2002.

[54] W. J. Ready. "A Comparison of Hourly Versus Daily Testing Methods for Evaluating the Reliability of Water Soluble Fluxes," *IEEE CPMT Advanced Packaging,* vol. 23, pp. 285-292.

[55] Anonymous. "IPC-TM-650 Test Methods Manual - Surface Insulation Resistance." Internet: http://www.ipc.org/4.0_Knowledge/4.1_Standards/test/2-6-3-7.pdf, 2007 [Sep. 4, 2011]

[56] L. A. Knauss, A. B. Cawthorne, N. Lettsome, S. Kelly, S. Chatraphorn, E. F. Fleet, F. C. Wellstood, W. E. Vanderlinde. "Scanning SQUID Microscopy for Current Imaging." *Microelectronics Reliability,* vol. 41, pp. 1211-1229.

[57] K. L. Rogers. "An Analytical and Experimental Investigation of Filament Formation in Glass/epoxy Composites." PhD Thesis, University of Maryland, United States, 2005.

[58] Erik J. Bergum. "CAF Resistance of Non-DICY FR-4." *PC FAB,* 2002.

[59] P. Johander, P. Tegehall, A. A. Osman, G. Wetter and D. Andersson. "Printed Circuit Boards for Lead-free Soldering: Materials and Failure Mechanisms." *Circuit World,* vol. 33, pp. 10-16, 2007.

[60] M. Li, M. Pecht, and L. Wang. "The physics of conductive filament formation in MCM-L substrates," in *Proceedings of the International Electronic Packaging Conference,* 1995, pp. 517-527.

[61] K. L. Rogers and M. G. Pecht. "A Variant of Conductive Filament Formation Failures in PWBs with 3 and 4 mil Spacings." *Circuit World,* vol. 32, pp. 11-18, 2006.

[62] Karl J. Puttlitz, and Kathleen A. Stalter. *Handbook of Lead-Free Solder Technology for Microelectronic Assemblies.* New York: Marcell Dekker, Inc.: 2004.

[63] C. Navarro. "Development of a Standard Test Method for Evaluating Conductive Anodic Filament (CAF) Growth Failure in PCBs." *Circuit World,* vol. 28, pp. 14-18, 2002.

[64] Fu L, and Yang F. "Development of micro drill bit for drilling environment-friendly PCB." in *IPC Printed Circuits Expo, and the Designers Summit,* 2008.

[65] Lameck Banda, Mark Wilson, Robert Hearn, and Michael Mullins. "Toughened laminates for printed circuit boards: Correlation of drillability to material properties," in *IPC Printed Circuit Expo, APEX & Designer Summit Proceedings,* 2010.

[66] William W. Dorner. "Using Microsoft Excel for Weibull analysis." Internet: http://www.qualitydigest.com/jan99/html/body_weibull.html, 1999 [Oct. 19, 2011]

[67] E. E. Lewis, *Introduction to Reliability Engineering.* New York: J. Wiley, 1996.

[68] Anonymous. "Calculating the Parameters of the Weibull Distribution." Internet: http://www.weibull.com/AccelTestWeb/calculating_the_parameters_of_the_weibull_distribution.htm, 1998 [Oct. 1, 2011]

[69] Anonymous. "Estimation of the Weibull Parameters." Internet: http://www.weibull.com/LifeDataWeb/estimation_of_the_weibull_parameter.htm, 2011 [Oct. 28, 2011].

[70] Anonymous. "Characteristics of the Weibull Distribution." Internet: http://www.weibull.com/LifeDataWeb/characteristics_of_the_weibull_distribution.htm, 2011 [Oct. 28, 2011].

[71] Dennis J. Wilkins, "The Bathtub Curve and Product Failure Behaviour Part Two - Normal Life and Wear-out", *Reliability HotWire eMagazine,* vol. 22, Dec 2002.

Appendix A

Calculation for Weibull distribution for DICY-SLDM

DICY - SLDM (29 tested coupons)					
Rank	time-to-failure (hrs)	median rank	1/(1-MR)	ln(ln(1/(1-MR))	ln(t)
1	86.5	0.02	1.02	-3.73	4.46
2	212	0.06	1.06	-2.82	5.36
3	362.5	0.09	1.10	-2.34	5.89
4	507.5	0.13	1.14	-2.01	6.23

Regression Statistics	
Multiple R	1.00
R Square	1.00
Adjusted R Square	1.00
Standard Error	0.02
Observations	4

ANOVA

	df	*SS*	*MS*	*F*	*Significance F*
Regression	1	1.67	1.67	3434.40	0.00
Residual	2	0.00	0.00		
Total	3	1.68			

	Coefficients	*Standard Error*	*t Stat*	*P-value*	*Lower 95%*	*Upper 95%*	*Lower 95.0%*	*Upper 95.0%*
Intercept	-8.0	0.1	-88.0	0.0	-8.4	-7.6	-8.4	-7.6
ln(t)	1.0	0.0	58.6	0.0	0.9	1.0	0.9	1.0
Beta	1.0							
Alpha	4017.6							

Calculation for Weibull distribution for phenolic-SLDM-Lot 1

Phenolic – SLDM – Lot 1 (10 tested coupons)					
Rank	time-to-failure (hrs)	median rank	1/(1-MR)	ln(ln(1/(1-MR))	ln(t)
1	21	0.07	1.07	-2.66	3.04
2	59.5	0.16	1.20	-1.72	4.09
3	160	0.26	1.35	-1.20	5.08
4	171	0.36	1.55	-0.82	5.14
5	236.5	0.45	1.82	-0.51	5.47
6	293.5	0.55	2.21	-0.23	5.68
7	351.5	0.64	2.81	0.03	5.86

Regression Statistics	
Multiple R	1.0
R Square	1.0
Adjusted R Square	1.0
Standard Error	0.2
Observations	7

ANOVA

	df	*SS*	*MS*	*F*	*Significance F*
Regression	1	5.1	5.1	162.1	0.0
Residual	5	0.2	0.0		
Total	6	5.3			

	Coefficients	*Standard Error*	*t Stat*	*P-value*	*Lower 95%*	*Upper 95%*	*Lower 95.0%*	*Upper 95.0%*
Intercept	-5.5	0.4	-15.3	0.0	-6.5	-4.6	-6.5	-4.6
ln(t)	0.9	0.1	12.7	0.0	0.7	1.1	0.7	1.1
Beta	0.9							
Alpha	409.6							

Calculation for Weibull distribution for phenolic-SLDM-Lot 2

Phenolic – SLDM – Lot 2 (19 tested coupons)					
Rank	time-to-failure (hrs)	median rank	1/(1-MR)	ln(ln(1/(1-MR))	ln(t)
1	544.5	0.04	1.04	-3.30	6.30
2	649.5	0.09	1.10	-2.39	6.48

Regression Statistics	
Multiple R	1
R Square	1
Adjusted R Square	65535
Standard Error	0
Observations	2

ANOVA

	df	*SS*	*MS*	*F*	*Significance F*
Regression	1	0.4	0.4	N.A.	N.A.
Residual	0	0.0	65535.0		
Total	1	0.4			

	Coefficients	*Standard Error*	*t Stat*	*P-value*	*Lower 95%*	*Upper 95%*	*Lower 95.0%*	*Upper 95.0%*
Intercept	-36.0	0.0	65535.0	N.A.	-36.0	-36.0	-36.0	-36.0
ln(t)	5.2	0.0	65535.0	N.A.	5.2	5.2	5.2	5.2
Beta	5.2							
Alpha	1029.6							

Calculation for Weibull distribution for DICY-BMDV

DICY - BMDV (30 tested coupons)					
Rank	Time-to-failure (hrs)	median rank	1/(1-MR)	ln(ln(1/(1-MR))	ln(t)
1	62	0.02	1.02	-3.76	4.13
2	181	0.06	1.06	-2.86	5.20
3	199.5	0.09	1.10	-2.38	5.30
4	221.5	0.12	1.14	-2.04	5.40
5	275	0.15	1.18	-1.78	5.62
6	292.5	0.19	1.23	-1.57	5.68
7	321	0.22	1.28	-1.39	5.77
8	326	0.25	1.34	-1.23	5.79
9	328.5	0.29	1.40	-1.09	5.79
10	344.5	0.32	1.47	-0.96	5.84
11	348	0.35	1.54	-0.84	5.85
12	425.5	0.38	1.63	-0.72	6.05
13	463.5	0.42	1.72	-0.61	6.14
14	478	0.45	1.82	-0.51	6.17
15	480	0.48	1.94	-0.41	6.17
16	540	0.52	2.07	-0.32	6.29
17	576.5	0.55	2.22	-0.23	6.36
18	578.5	0.58	2.39	-0.14	6.36
19	580	0.62	2.60	-0.05	6.36
20	600.5	0.65	2.84	0.04	6.40
21	607.5	0.68	3.13	0.13	6.41
22	616	0.71	3.49	0.22	6.42
23	619	0.75	3.95	0.32	6.43
24	627	0.78	4.54	0.41	6.44
25	644	0.81	5.33	0.52	6.47
26	712	0.85	6.47	0.62	6.57
27	734.5	0.88	8.22	0.74	6.60
28	794	0.91	11.26	0.88	6.68
29	895.5	0.94	17.88	1.06	6.80

Calculation for Weibull distribution for DICY-BMDV (cont'd)

Regression Statistics	
Multiple R	1.0
R Square	1.0
Adjusted R Square	1.0
Standard Error	0.2
Observations	30

ANOVA

	df	*SS*	*MS*	*F*	*Significance F*
Regression	1	39.9	39.9	677.4	0.0
Residual	28	1.6	0.1		
Total	29	41.5			

	Coefficients	*Standard Error*	*t Stat*	*P-value*	*Lower 95%*	*Upper 95%*	*Lower 95.0%*	*Upper 95.0%*
Intercept	-12.9	0.5	-27.1	0.0	-13.9	-11.9	-13.9	-11.9
ln(t)	2.0	0.1	26.0	0.0	1.9	2.2	1.9	2.2
Beta	2.0							
Alpha	576.0							

Calculation for Weibull distribution for phenolic-BMDV

Phenolic - BMDV (25 tested coupons)					
Rank	Time-to-failure (hrs)	median rank	1/(1-MR)	ln(ln(1/(1-MR))	ln(t)
1	3.5	0.03	1.03	-3.58	1.25
2	11.50	0.07	1.07	-2.67	2.44
3	17.00	0.11	1.12	-2.19	2.83
4	24.00	0.15	1.17	-1.85	3.18
5	32.00	0.19	1.23	-1.59	3.47
6	32.00	0.22	1.29	-1.37	3.47
7	36.50	0.26	1.36	-1.18	3.60
8	42.50	0.30	1.44	-1.02	3.75
9	47.00	0.34	1.52	-0.87	3.85
10	49.50	0.38	1.62	-0.73	3.90
11	51.00	0.42	1.73	-0.60	3.93
12	61.50	0.46	1.85	-0.48	4.12
13	69.00	0.50	2.00	-0.37	4.23
14	69.50	0.54	2.17	-0.25	4.24
15	73.50	0.58	2.37	-0.15	4.30
16	73.50	0.62	2.62	-0.04	4.30
17	87.00	0.66	2.92	0.07	4.47
18	88.00	0.70	3.30	0.18	4.48
19	90.00	0.74	3.79	0.29	4.50
20	109.50	0.78	4.46	0.40	4.70
21	113.50	0.81	5.40	0.52	4.73
22	116.00	0.85	6.86	0.66	4.75
23	129.50	0.89	9.41	0.81	4.86
24	166.50	0.93	14.94	0.99	5.11
25	180.00	0.97	36.29	1.28	5.19

Calculation for Weibull distribution for phenolic-BMDV (cont'd)

Regression Statistics	
Multiple R	1.0
R Square	1.0
Adjusted R Square	1.0
Standard Error	0.2
Observations	25

ANOVA

	df	*SS*	*MS*	*F*	*Significance F*
Regression	1	32.9	32.9	909.2	0.0
Residual	23	0.8	0.0		
Total	24	33.8			

	Coefficients	*Standard Error*	*t Stat*	*P-value*	*Lower 95%*	*Upper 95%*	*Lower 95.0%*	*Upper 95.0%*
Intercept	-5.8	0.2	-32.5	0.0	-6.2	-5.5	-6.2	-5.5
ln(t)	1.3	0.0	30.2	0.0	1.2	1.4	1.2	1.4
Beta	1.3							
Alpha	4.4							